Journal of Paleontology, Volume 96, Memoir 90, 2022, p. 1–39

0022-3360/22/1937-2337 doi: 10.1017/jpa.2022.49

JOURNAL OF PALEONTOLOGY
A PUBLICATION OF THE Paleontological SOCIETY

Puercosuchus traverorum n. gen. n. sp.: a new malerisaurine azendohsaurid (Archosauromorpha: Allokotosauria) from two monodominant bonebeds in the Chinle Formation (Upper Triassic, Norian) of Arizona

Adam D. Marsh,[1]* William G. Parker,[1] Sterling J. Nesbitt,[2] Ben T. Kligman,[1,2] and Michelle R. Stocker[2]

[1]Division of Science and Resource Management, Petrified Forest National Park, 1 Park Road #2217, Petrified Forest, AZ 86028, USA <adam_marsh@nps.gov><william_parker@nps.gov>
[2]Department of Geosciences, Virginia Tech, Blacksburg, VA 24061, USA <sjn2104@vt.edu><bkligman@vt.edu><stockerm@vt.edu>

Abstract.—Non-archosaur archosauromorphs are a paraphyletic group of diapsid reptiles that were important members of global Middle and Late Triassic continental ecosystems. Included in this group are the azendohsaurids, a clade of allokotosaurians (kuehneosaurids and Azendohsauridae + Trilophosauridae) that retain the plesiomorphic archosauromorph postcranial body plan but evolved disparate cranial features that converge on later dinosaurian anatomy, including sauropodomorph-like marginal dentition and ceratopsian-like postorbital horns. Here we describe a new malerisaurine azendohsaurid from two monodominant bonebeds in the Blue Mesa Member, Chinle Formation (Late Triassic, ca. 218–220 Ma); the first occurs at Petrified Forest National Park and preserves a minimum of eight individuals of varying sizes, and the second occurs near St. Johns, Arizona. *Puercosuchus traverorum* n. gen. n. sp. is a carnivorous malerisaurine that is closely related to *Malerisaurus robinsonae* from the Maleri Formation of India and to *Malerisaurus langstoni* from the Dockum Group of western Texas. Dentigerous elements from *Puercosuchus traverorum* n. gen. n. sp. confirm that some Late Triassic tooth morphotypes thought to represent early dinosaurs cannot be differentiated from, and likely pertain to, *Puercosuchus*-like malerisaurine taxa. These bonebeds from northern Arizona support the hypothesis that non-archosauriform archosauromorphs were locally diverse near the middle Norian and experienced an extinction event prior to the end-Triassic mass extinction coincidental with the Adamanian-Revueltian boundary recognized at Petrified Forest National Park. The relatively late age of this early-diverging taxon (Norian) suggests that the diversity of azendohsaurids is underrepresented in Middle and Late Triassic fossil records around the world.

UUID: http://zoobank.org/e6eeefd2-a0ae-47fc-8604-9f45af8c1147.

Introduction

Azendohsaurids are a clade of Middle–Late Triassic allokotosaurian non-archosaur archosauromorphs (Nesbitt et al., 2015) that until recently only included the herbivorous *Azendohsaurus laaroussii* Dutuit, 1972, *Azendohsaurus madagaskarensis* Flynn et al., 2010, and *Shringasaurus indicus* Sengupta, Ezcurra, and Bandyopadhyay, 2017. Earlier-diverging azendohsaurids now are recognized from previously known taxa (Nesbitt et al., 2021) such as *Pamelaria dolichotrachela* Sen, 2003, and the Malerisaurinae (e.g., *Malerisaurus robinsonae* Chatterjee, 1980, and *Malerisaurus langstoni* Chatterjee, 1986) that exhibit the tall-crowned, pointed marginal teeth found in most archosauromorphs. Unfortunately, the record of malerisaurine azendohsaurids currently is represented by fragmentary, ambiguously associated, and generally poorly preserved taxa (Nesbitt et al., 2021), which makes understanding the acquisition of azendohsaurid skeletal traits difficult to determine and difficult to compare with the morphologies of other allokotosaurs and closely related archosauromorphs such as rhynchosaurs, tanystropheids, and archosauriforms (Ezcurra, 2016; Pritchard and Sues, 2019; Pritchard et al., 2021; Spiekman et al., 2021).

Here we describe a new taxon of malerisaurine azendohsaurid from a monodominant bonebed at Petrified Forest National Park (PEFO; Fig. 1.1, 1.2; Marsh et al., 2017) that preserves nearly the entire skeleton represented by at least eight individuals of varying size (and presumably, varying skeletal maturity). This bonebed and a similar bonebed of the same taxon from near St. Johns, Arizona (Spielmann et al., 2013b), represent a unique opportunity to understand the skeletal anatomy of early-diverging, but relatively late-surviving allokotosaurs from one

*Corresponding author.

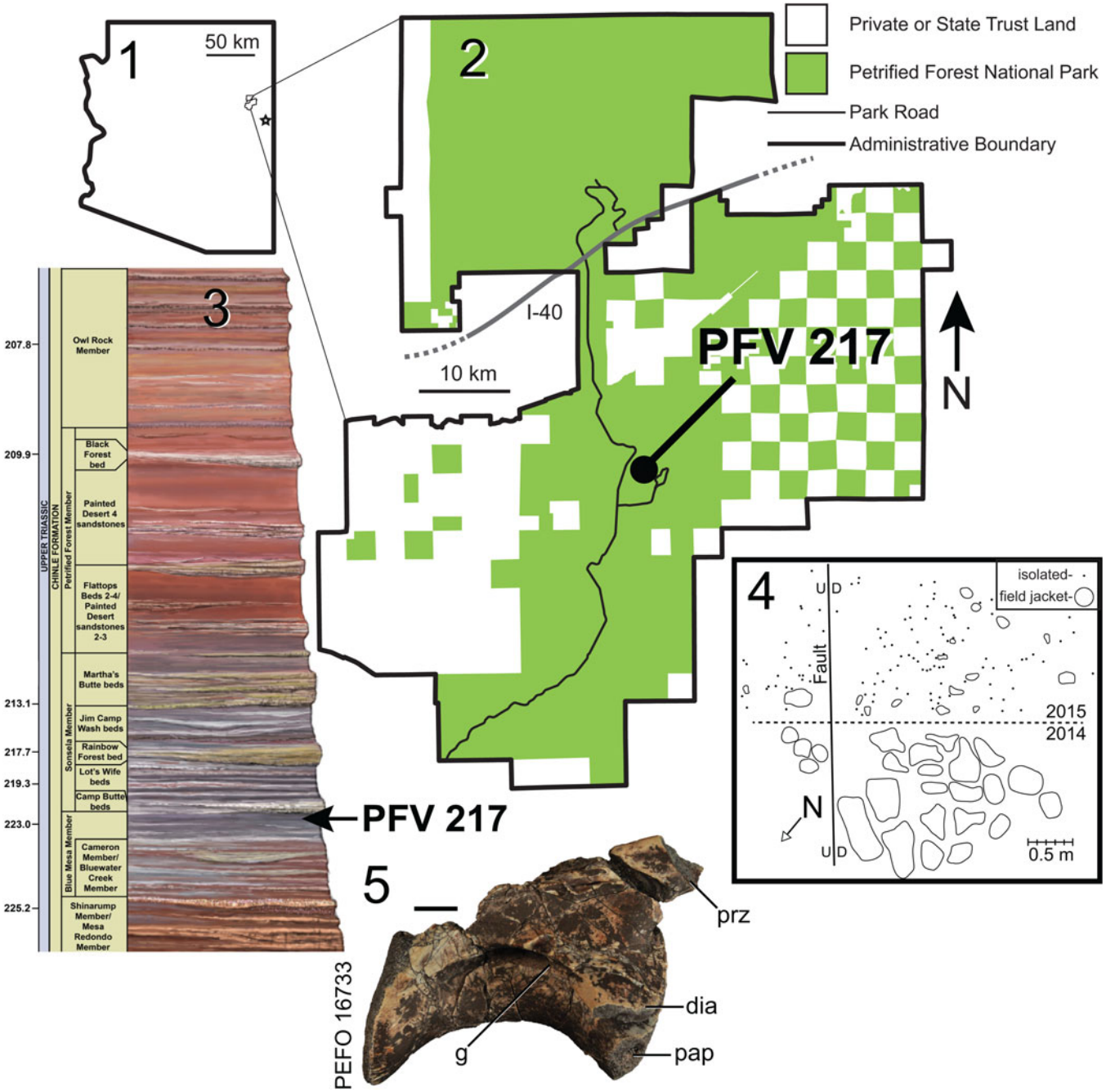

Figure 1. (**1**) Location of Petrified Forest National Park in Arizona; (**2**) location of PFV 217 within PEFO; (**3**) stratigraphic position of PFV 217 within the Chinle Formation at PEFO; (**4**) quarry map of PFV 217; and (**5**) initial 'plateosaurid' vertebra PEFO 16733 found at PFV 217. The star in (**1**) indicates the location of NMMNH L-3764 near St. Johns, Arizona. Composite stratigraphic section in (**3**) is ~400 m thick; U-Pb ages from Ramezani et al. (2011) and Atchley et al. (2013). d = downthrown side of fault; dia = diapophysis; g = groove; I-40 = US Interstate Highway 40; pap = parapophysis; prz = prezygapophysis; u = upthrown side of fault. Scale bar in (**5**) = 1 cm.

of the best-known continental Late Triassic records in the world prior to the decline of non-archosaur archosauromorphs coincidental with the Adamanian-Revueltian boundary at PEFO (Parker and Martz, 2010; Kligman et al., 2020).

Methods

Collection, preparation, and photography.—The bonebed at locality PFV 217 was found during an outreach event in 2014 and was excavated during the summers of 2014 and 2015 using hand tools (e.g., sharpened awls and small blades). The fossils were consolidated in the field using Paraloid B-72. Fossils were either removed directly from the rock in the field and wrapped in tissue and aluminum foil (dots in Fig. 1.4) or were removed in plaster bandage jackets (round shapes in Fig. 1.4). In 2014, material was collected in larger blocks with the general relationships of the blocks roughly depicted on a quarry map (Fig. 1.4). Isolated elements between the main

https://doi.org/10.1017/jpa.2022.49 Published online by Cambridge University Press

blocks were removed and wrapped in foil; the exact location of these elements was not always noted. In 2015, isolated bones and small plaster jackets were mapped directly in the quarry before removal.

The fossils were prepared under Leica Wild microscopes using carbide steel needles in pin vices connected to foot-operated compressed air (Pin Vice Puffer), and they were consolidated and repaired using Paraloid B-72 and/or Butvar B-76. Locations and associations of bones within larger jackets were documented during preparation via photographs and preparation records that are now part of PEFO archives.

When possible, direct linear measurements were taken using digital calipers. Specimen photographs were taken using a Nikon D-90 camera. A stratigraphic section was measured and described near PFV 217 from the Newspaper Rock Bed (sensu Parker, 2006; Martz and Parker, 2010) to the lowest unit of the Sonsela Member using a Precision Jacob's staff (ASC Scientific), Brunton pocket transit, and Munsell Rock Color Book.

Repositories and institutional abbreviations.—FMNH, Field Museum of Natural History, Chicago, Illinois, USA; GR, The Ruth Hall Museum of Paleontology at Ghost Ranch, Abiquiu, New Mexico, USA; ISIR, Indian Statistical Institute, Reptiles, Kolkata, India; MNA, Museum of Northern Arizona, Flagstaff, Arizona, USA; NMMNH, New Mexico Museum of Natural History and Science, Albuquerque, New Mexico, USA; PEFO, Petrified Forest National Park, Arizona, USA; TMM, Vertebrate Paleontology Collections, University of Texas at Austin, Austin, Texas, USA; TTU/MOTT, Museum of Texas Tech University, Lubbock, Texas, USA; UWBM, Burke Museum of Natural History and Culture, Seattle, Washington, USA.

Systematic paleontology

Archosauromorpha Huene, 1946, sensu Dilkes, 1998
Allokotosauria Nesbitt et al., 2015
Azendohsauridae Nesbitt et al., 2015
Malerisaurinae Nesbitt et al., 2021

Revised phylogenetic definition.—The most-inclusive clade containing *Malerisaurus robinsonae* Chatterjee, 1986; but not containing *Azendohsaurus madagaskarensis* Flynn et al., 2010; *Trilophosaurus buettneri* Case, 1928; *Tanystropheus longobardicus* Bassani, 1886; *Proterosuchus fergusi* Broom, 1903; *Protorosaurus speneri* von Meyer, 1832; *Rhynchosaurus articeps* Owen, 1842; or *Passer domesticus* Linnaeus, 1758.

Remarks.—A mistake in our original definition of Malerisaurinae (Nesbitt et al., 2021) was recently recognized, so we revised the definition from 'least-inclusive' to 'most inclusive' to incorporate our original intent for the definition of the clade.

Puercosuchus new genus

Type species.—*Puercosuchus traverorum* n. gen. n. sp. (by monotypy).

Diagnosis.—As for type species by monotypy.

Etymology.—'Puerco' refers to the Puerco River that runs through Petrified Forest National Park, Arizona, just north of the holotype locality, and is Spanish vernacular for 'mucky' or 'foul' referring to the muddy water of the river. Here, 'suchus' invokes the sprawling crocodylian-like body plan of allokotosaurs.

Remarks.—Despite *Puercosuchus* n. gen. being phylogenetically closely aligned to the genus *Malerisaurus* and other *Malerisaurus*-like azendohsaurids, in a recent study (Nesbitt et al., 2021) we proposed a new genus to avoid inferring phylogenetic relationships through taxonomy. In that study (Nesbitt et al., 2021, p. 5, fig. 5a, c), the hypodigm of *Puercosuchus traverorum* n. gen. n. sp. was coded as "*Malerisaurus*-like taxon PEFO" and was recovered in a polytomy with *Malerisaurus langstoni* and larger malerisaurines from Texas (e.g., the holotype specimen of '*Otischalkia elderae*' Hunt and Lucas, 1991). Future analyses may provide increased resolution for this clade (or recover alternate relationships), and we do not think nomenclatural acts (i.e., sharing a genus name) should describe or infer phylogenetic relationships (Parker, 2018). The hypodigms of both species of *Malerisaurus* are incomplete and problematic in their own ways (Nesbitt et al., 2021, figs. 1, 2), and referring a more complete and anatomically different taxon to that genus is not preferred (Parker, 2018, p. 36). The genus traditionally has been treated as a relatively subjective Linnean rank compared to the species (Vences et al., 2013), and our treatment of the genus (i.e., "a genus should be monophyletic, reasonably compact, and ecologically, morphologically, or biogeographically distinct"; Gill et al., 2005, p. 140) has changed since the genus *Malerisaurus* and its two valid species were erected (Chatterjee, 1980, 1986) to infer close evolutionary relationships in the pre-cladistic era.

Puercosuchus traverorum new species
Figures 2–17, 18.1–18.14

Holotype specimen.—PEFO 43914; associated right premaxilla and maxilla.

Diagnosis.—Azendohsaurid with the following unambiguous autapomorphies: procumbent mesial premaxillary tooth (unknown in the holotypes of *Malerisaurus langstoni* and *Malerisaurus robinsonae*); heterodont maxillary dentition (apicobasally long, curved anterior teeth with small serrations grading into apicobasally short, straight posterior teeth with large serrations) (unknown in *Malerisaurus langstoni*). Because *Puercosuchus traverorum* n. gen. n. sp. is hypothesized to be the only allokotosaur at PFV 217 (see below), we also provide additional autapomorphies present in the hypodigm (made of 491 specimens) that can be used to diagnose the species: midline keel on frontal (unknown in the holotypes of *Malerisaurus langstoni* and *Malerisaurus robinsonae*); hooked and pointed quadrate head with foramen penetrating the body of the quadrate (unknown in the holotypes of *Malerisaurus langstoni* and *Malerisaurus robinsonae*); tooth on cultriform process of parabasisphenoid (unknown in the holotypes of *Malerisaurus langstoni* and *Malerisaurus robinsonae*); foramen

https://doi.org/10.1017/jpa.2022.49 Published online by Cambridge University Press

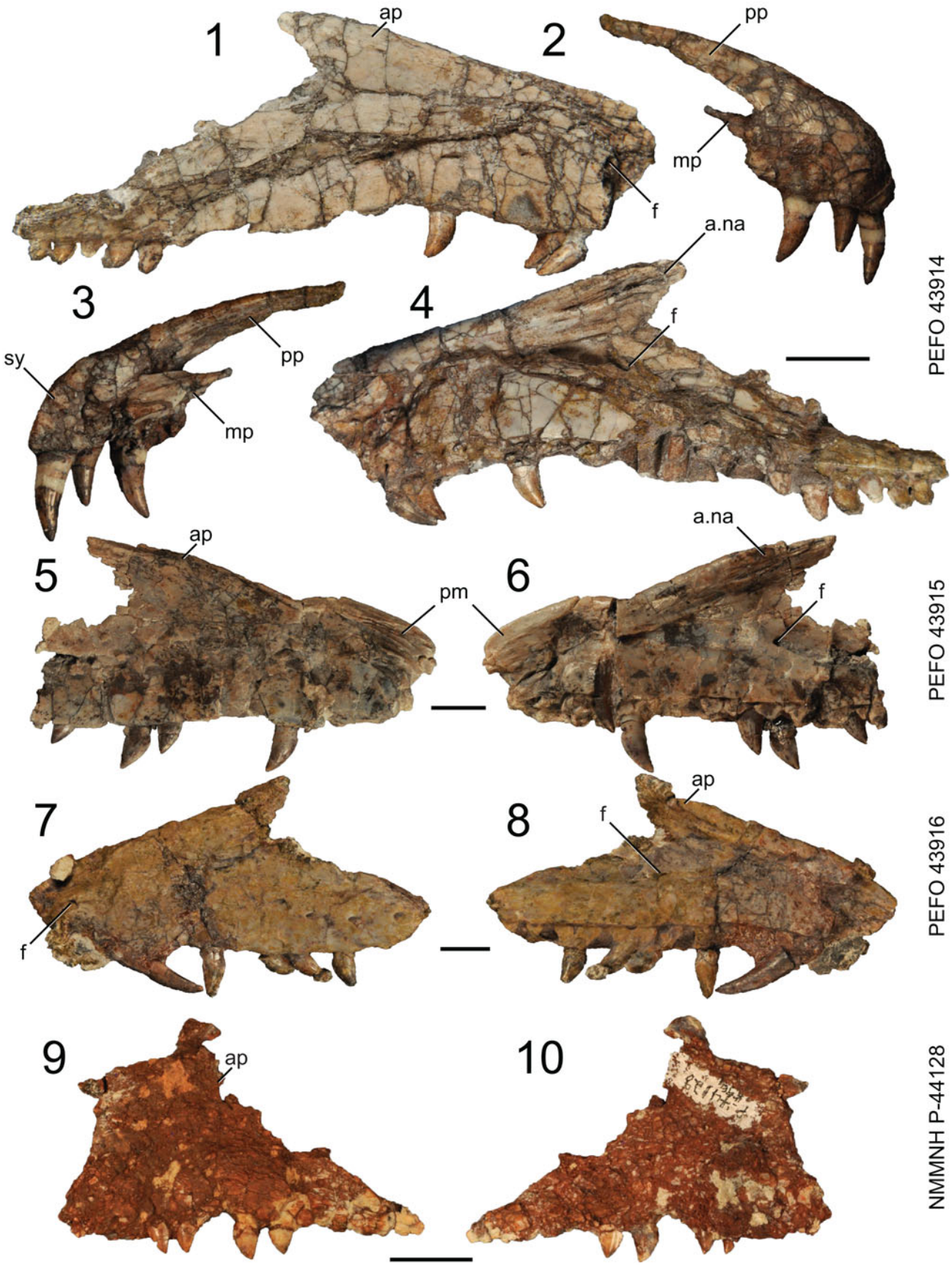

Figure 2. *Puercosuchus traverorum* n. gen. n. sp. in lateral (**1, 2, 5, 7, 9**) and medial (**3, 4, 6, 8, 10**) views. (**1–4**) Holotype right premaxilla and maxilla PEFO 43914; (**5, 6**) right maxilla PEFO 43915; (**7, 8**) left maxilla PEFO 43916; and (**9, 10**) left maxilla NMMNH P-44128. a.na = articular surface for nasal; ap = ascending process; f = foramen; mp = medial process; pm = premaxilla; pp = posterior process; sy = symphysis. Scale bars = 1 cm.

https://doi.org/10.1017/jpa.2022.49 Published online by Cambridge University Press

present through ventral ramus of the opisthotic (uncertain in the holotype of *Malerisaurus langstoni*); anterior process present and taller than posterior process (neural spine) on posterior caudal vertebrae; hooked anteromedial process of ulna in proximal view; ridge on medial side of distal end of fibula; tubercle on dorsal surface of metatarsal V.

Occurrence.—PFV 217 (Fig. 1; holotype locality, Dinosaur Wash, field numbers WGP 14/24 and ADM 15/17, ADM 15/18, ADM 15/24–ADM 15/32, ADM 15/34, ADM 15/35; locality information archived at PEFO), within the upper part of the Blue Mesa Member (Chinle Formation, ca. 218–220 Ma; Fig. 1.3; Ramezani et al., 2011; Atchley et al., 2013; Rasmussen et al., 2020). The bone layer is 8.9 m below the lowest tongue of the Camp Butte beds of the Sonsela Member, which interfingers with the upper part of the Blue Mesa Member in this region of PEFO, thus not representing an unconformable surface thought to indicate the 'Tr-4 regional unconformity' of Lucas (1993) (Parker, 2006; Woody, 2006; Martz and Parker, 2010; Rasmussen et al., 2020). This locality number describes a general area along the slope in the upper bone layer of PFV 122 (Dying Grounds; Long and Murry, 1995). The bonebed occurs in a discrete interval circumscribing ~10 m^2 (Fig. 1.4). In addition to *Puercosuchus traverorum* n. gen. n. sp., this bonebed includes a coelacanth opercle (PEFO 44409), hybodont shark spine (PEFO 44410), dipnoan tooth plate (PEFO 44407), actinopterygian dentigerous elements (PEFO 44408, PEFO 48105), large skull bones (PEFO 44404) and small pectoral elements (PEFO 44390) of metoposaurid temnospondyls, a non-desmatosuchin aetosaurian paramedian osteoderm (PEFO 44381), metatarsal I of a dinosauromorph (PEFO 44217), a paracrocodylomorph tooth (PEFO 44383), tanystropheid (PEFO 44386) and *Vancleavea campi* Long and Murry, 1995, vertebrae (PEFO 44221), phytosaur teeth (PEFO 44222), and an osteoderm of *Acaenasuchus geoffreyi* Long and Murry, 1995 (PEFO 44219). Despite extensive excavation and screen-washing of matrix removed from numerous field jackets, there is no evidence of a second allokotosaur (e.g., teeth of *Trilophosaurus* Case, 1928) at the site. Where they are present, there appears to be only one taxon of malerisaurine azendohsaurid in any given assemblage, and most of the variation across elements relates to ontogenetic changes (Nesbitt et al., 2021), especially regarding a significantly larger cervical vertebra that was surface collected from PFV 217 decades earlier (PEFO 16733; Fig. 1.5).

NMMNH L-3764 (Krzyzanowski bonebed; Heckert, 2004; Heckert et al., 2004, 2005) also includes fragments of large metoposaurids (e.g., NMMNH P-34086) and skull bones, teeth, and osteoderms of phytosaurs (e.g., NMMNH P-63322). Further discussion of previously identified taxa from this bonebed is provided in the Discussion. This site is located in the Blue Mesa Member, Chinle Formation (Heckert et al., 2001a, 2004, 2005; Heckert, 2004; Spielmann et al., 2013b), near St. Johns, AZ (Fig. 1.1).

Description.—We describe the cranial and postcranial anatomy of *Puercosuchus traverorum* n. gen. n. sp. focusing on the PEFO specimens, supplemented with those from the Krzyzanowski bonebed. Most anatomical comparisons are made with respect to other azendohsaurid allokotosaurs, but additional comparisons of malerisaurine azendohsaurids to other archosauromorphs are provided by Nesbitt et al. (2021). All vertebrae were found disarticulated; their positions in the presacral column are estimated based on information from other archosauromorphs. The metapodials were preserved in isolation, and their identifications were made using comparisons to taxa such as *Azendohsaurus madagaskarensis* (FMNH PR 3820 and FMNH PR 2776) and *Trilophosaurus buettneri* Case, 1928 (TMM 31025-140). Owing to the lack of association of the preserved elements, relative lengths of long bones and metapodials were impossible to determine.

Skull: premaxilla.—Representative specimens: Holotype PEFO 43914, right (associated with maxilla); PEFO 38605, left; PEFO 43917, left).

The main body of the premaxilla is sub-elliptical in lateral view and has a straight ventral margin (Fig. 2.2, 2.3). Similar to the condition in *Azendohsaurus madagaskarensis* (FMNH PR 2751), there is no anterior process, so the naris opens anterodorsally and the premaxilla forms the anterior and ventral borders of the external naris. The anterodorsal margin of the posterior process is convex in lateral view, similar to that of *Shringasaurus indicus* (Sengupta and Bandyopadhyay, 2022, fig. 3a), whereas it is concave in lateral view in *Shringasaurus indicus* and *Azendohsaurus madagaskarensis* (Flynn et al., 2010, text-fig. 3a). The posterior process is half the length of the entire element and projects straight posteriorly as it tapers. It is more gracile than the robust posterior process of *Shringasaurus indicus* (Sengupta and Bandyopadhyay, 2022, fig. 3a). The lateral surface of the premaxilla lacks the transverse groove and longitudinal striations found in *Azendohsaurus madagaskarensis* (FMNH PR 2751) and *Shringasaurus indicus* (Sengupta and Bandyopadhyay, 2022, fig. 3a), and there are no foramina on the lateral surface. There is a slot for articulation with the maxilla between the posterior process and medial process, which is absent in *Azendohsaurus madagaskarensis* (FMNH PR 2751). The medial process of *Puercosuchus traverorum* n. gen. n. sp. projects posteriorly and is visible in medial and lateral views (Fig. 2.2, 2.3). It articulates with the vomer medially and the maxilla laterally (Fig. 2.2, 2.3). The articular surface (= midline symphysis) for the other premaxilla is a flat, triangular facet on the front of the medial surface, whereas this articulation in *Azendohsaurus madagaskarensis* (FMNH PR 2751) is rectangular and strongly interdigitating. The ventral surface medial to the tooth row forms a broad shelf.

The premaxilla contains four alveoli. The anterior teeth are the largest and are slightly procumbent (Fig. 3.3, 3.4), similar to those of *Azendohsaurus madagaskarensis* (FMNH PR 2751) and other malerisaurines (e.g., TTU-P 11212; Nesbitt et al., 2021). The premaxillary teeth are sub-elliptical to sub-circular in cross section at the base but taper labiolingually apically. Mesial and distal carinae are present and finely serrated (worn in larger teeth, e.g., holotype PEFO 43914), but serrations are not present on the first premaxillary tooth. The teeth are ankylothecodont when fully erupted like those of other azendohsaurids and early diverging archosauromorphs (Nesbitt et al., 2015); interdental plates/foramina are present and co-ossified to the teeth when they are erupted.

https://doi.org/10.1017/jpa.2022.49 Published online by Cambridge University Press

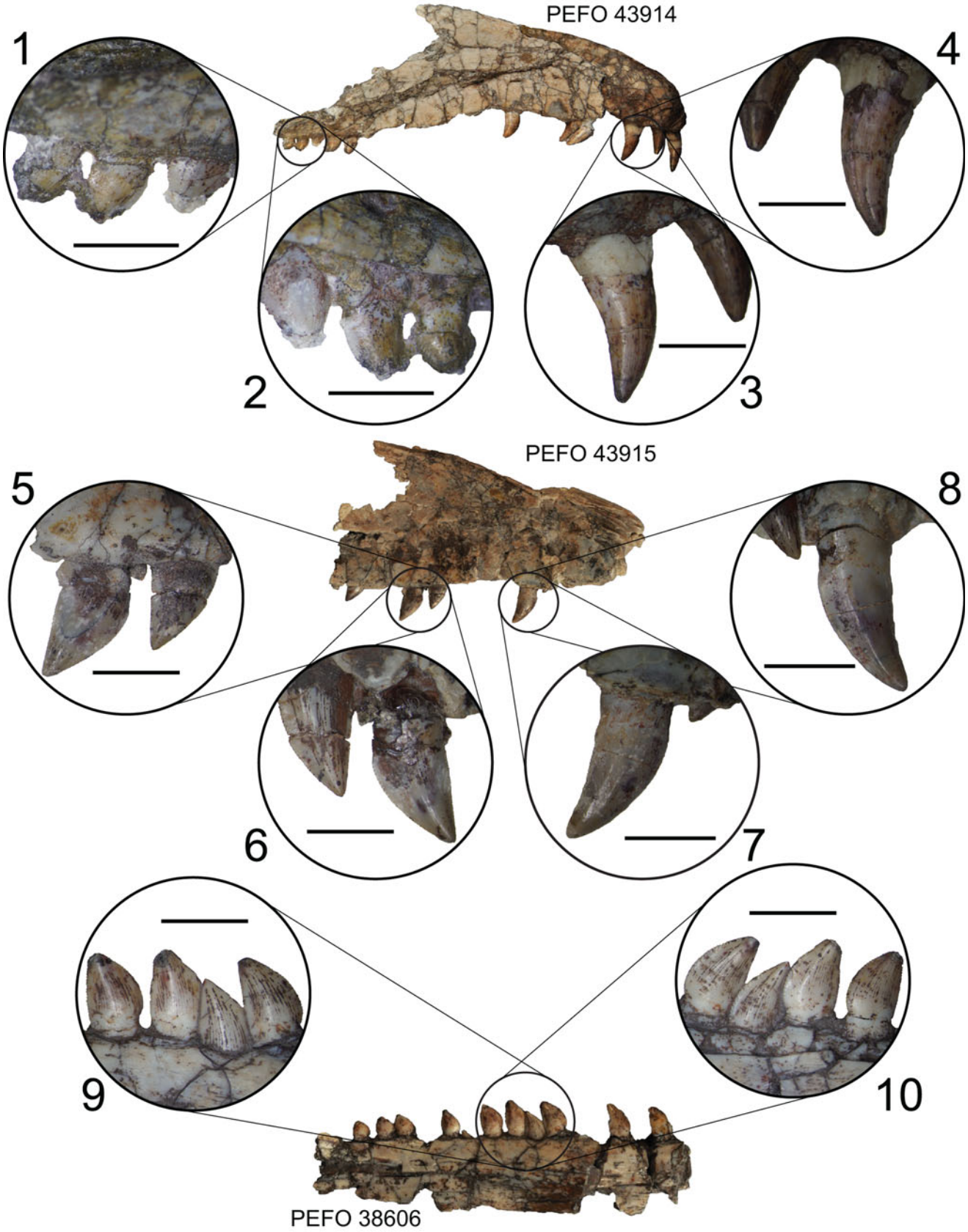

Figure 3. Representative teeth of *Puercosuchus traverorum* n. gen. n. sp. in labial (**1, 3, 5, 7, 9**) and lingual (**2, 4, 6, 8, 10**) views. (**1, 2**) Right posterior maxillary teeth of holotype PEFO 43914; (**3, 4**) right premaxillary teeth of holotype PEFO 43914; (**5, 6**) right middle maxillary teeth of PEFO 43915; (**7, 8**) right anterior maxillary teeth of PEFO 43915; and (**9, 10**) right middle dentary teeth of PEFO 38606. Scale bars = 5 mm.

https://doi.org/10.1017/jpa.2022.49 Published online by Cambridge University Press

Skull: maxilla.—Representative specimens: Holotype PEFO 43914, right (associated with premaxilla); PEFO 43915, right; PEFO 43916, left; NMMNH P-44128, left.

The maxilla is dorsoventrally narrow and triangular in lateral outline with a short tapered ascending process (Fig. 2) like that of early diverging archosauromorphs, but unlike *Azendohsaurus madagaskarensis* (FMNH PR 2751), which has a much taller ascending process. The ascending process and anterodorsal margin dorsal to the articulation with the premaxilla form a narrow flat surface lateral to the external naris. Articulation with the nasal occurs on the medial side of the ascending process along a striated suture; this articular surface is smooth in *Azendohsaurus madagaskarensis* (FMNH PR 2751). The anterolateral margin of the anterior process is a triangular, striated surface that articulates between the posterior process and medial process of the premaxilla. Only the anterior half of the anterodorsal surface of the maxilla articulates with the premaxilla, unlike that of *Azendohsaurus madagaskarensis* (FMNH PR 2751), in which the premaxilla articulates with the entire anterodorsal surface of the maxilla. The ventral margin of the maxilla is straight in lateral view and confluent with the ventral margin of the premaxilla when they are in articulation (note that holotype PEFO 43914 is slightly crushed in this region; Fig. 2.1). A large lateral foramen is present just posterior to the articulation with the premaxilla (Fig. 2.1, 2.7), and smaller, regularly spaced foramina that open posteroventrally occur along the length of the element parallel to and just dorsal to the tooth row. The posterior process of the maxilla gradually tapers posteriorly, whereas the posteriormost point of the maxilla of *Azendohsaurus madagaskarensis* (FMNH PR 2751) projects posteroventrally. The medial surface of the maxilla is flat dorsal to the tooth row and lacks the ridge present in *Azendohsaurus laaroussii* (Gauffre, 1993, fig. 5) and *Azendohsaurus madagaskarensis* (FMNH PR 2751), but it has a triangular, anteriorly tapering fossa between the ascending process and the posterior process. The maxilla of *Puercosuchus traverorum* n. gen. n. sp. lacks the defined medial fossa for articulation with the palatine that is found in *Azendohsaurus madagaskarensis* (FMNH PR 2751). A large medial foramen that opens posteriorly occurs below the base of the ascending process (Fig. 2.4, 2.8). The dorsal edge of the posterior process of the maxilla lacks the longitudinal groove for the articulation with the prefrontal, lacrimal, and jugal that is found in *Azendohsaurus madagaskarensis* (FMNH PR 2751).

The more complete specimens preserve ~19 alveoli; 12–14 maxillary teeth are found in *Azendohsaurus madagaskarensis* (FMNH PR 2751). This is the only malerisaurine currently known with a nearly complete maxilla. Heterodonty is present between the anterior and posterior maxillary teeth. The more-anterior teeth are labiolingually compressed, curve distally at their tips (the mesial margin is convex and the distal margin is concave), and are blade-shaped (Fig. 3.5). The more-posterior teeth become apicobasally shorter, labiolingually wider, and mesiodistally broader, and are leaf-shaped (= convex mesial and distal edges) and less curved distally at their tips (Fig. 3.1). All maxillary teeth have serrated mesial and distal carinae; the anterior teeth have many fine denticles (9–10/mm) and the posterior teeth have fewer broad denticles (6–7/mm). Denticles in the serrated premaxillary, maxillary, and dentary teeth form sharp-tipped triangles. In each serrated tooth, denticle size decreases apically. The maxillary teeth are ankylothecodont when fully erupted and are co-ossified to triangular interdental plates/foramina, as in other azendohsaurids.

Skull: nasal.—Representative specimen: PEFO 43947, right.

The nasal is a mediolaterally narrow element; it tapers anteriorly and the lateral suture with the maxilla is straight and flat (Fig. 4.1, 4.2). The articulated nasals form a confluent external narial opening that opens anterodorsally, as in *Azendohsaurus madagaskarensis* (FMNH PR 2785; Nesbitt et al., 2015, fig. 75d), *Mesosuchus browni* Watson, 1912 (Dilkes, 1998, fig. 5a), *Tanystropheus hydroides* Spiekman et al., 2020a, and *Tanystropheus longobardicus* Bassani, 1886 (Spiekman et al., 2020b, fig. 3b, e), and *Shringasaurus indicus* (Sengupta and Bandyopadhyay, 2022, fig. 2b); but, unlike in *Shringasaurus indicus*, the nasal of *Puercosuchus traverorum* n. gen. n. sp. lacks a midline contribution to an internarial bar.

Skull: frontal.—Representative specimens: PEFO 43927, right; PEFO 43928, right.

In dorsal view the frontal is subrectangular; it does not taper anteriorly or posteriorly (Fig. 4.3, 4.4). The anterior end is dorsoventrally thin where it abuts the nasal, but the posterior edge is thicker at the interdigitating suture with the parietal. The dorsal surface of the frontal is flat and lacks any boss or the strong horn protuberance found in *Shringasaurus indicus* (ISIR 781; Sengupta et al., 2017, fig. 2; Sengupta and Bandyopadhyay, 2022, fig. 4c, d). The orbital margin between the articulations with the prefrontal and postfrontal is smooth, not rugose like that of *Azendohsaurus madagaskarensis* (FMNH PR 2751). The medial articular surface on the midline for the other frontal is flat, and it is lipped dorsally, forming a midline dorsal keel (Fig. 4.5) that is unique among azendohsaurids with preserved frontals, but similar to that found in *Tanystropheus hydroides* (Spiekman et al., 2020b, fig. 9C). The ventral slotted articulations for the prefrontal and postfrontal occur lateral to the curving margin of the olfactory tract; these articular surfaces are less defined in *Azendohsaurus madagaskarensis* (FMNH PR 2751).

Skull: prefontal.—Representative specimen: PEFO 43931, right.

The prefrontal curves to form the anterodorsal portion of the orbit (Fig. 4.6, 4.7) and is a triradiate element with ventral, posterodorsal, and medial processes. The lateral side that forms the orbital ridge is robust and rugose and is thickest dorsally, like that of *Azendohsaurus madagaskarensis* (FMNH PR 2751). The medial side of the element forms a triangular fossa. A small fossa occurs on the anterodorsal margin of the prefrontal, and it is visible in lateral view. The articular surfaces are missing and impossible to determine from the only preserved element.

Skull: postfontal.—Representative specimen: PEFO 44249, left.

The postfrontal is a dorsoventrally tall element (Fig. 4.8, 4.9) that would have been oriented anteromedially/ventrolaterally to form the posterodorsal margin of the orbit. This differs from the broader triangular shape found in *Macrocnemus bassanii* Nopsca, 1930 (Miedema et al., 2020, fig. 3a) and *Tanystropheus longobardicus* (Spiekman et al., 2020b, fig. 3e) and the

https://doi.org/10.1017/jpa.2022.49 Published online by Cambridge University Press

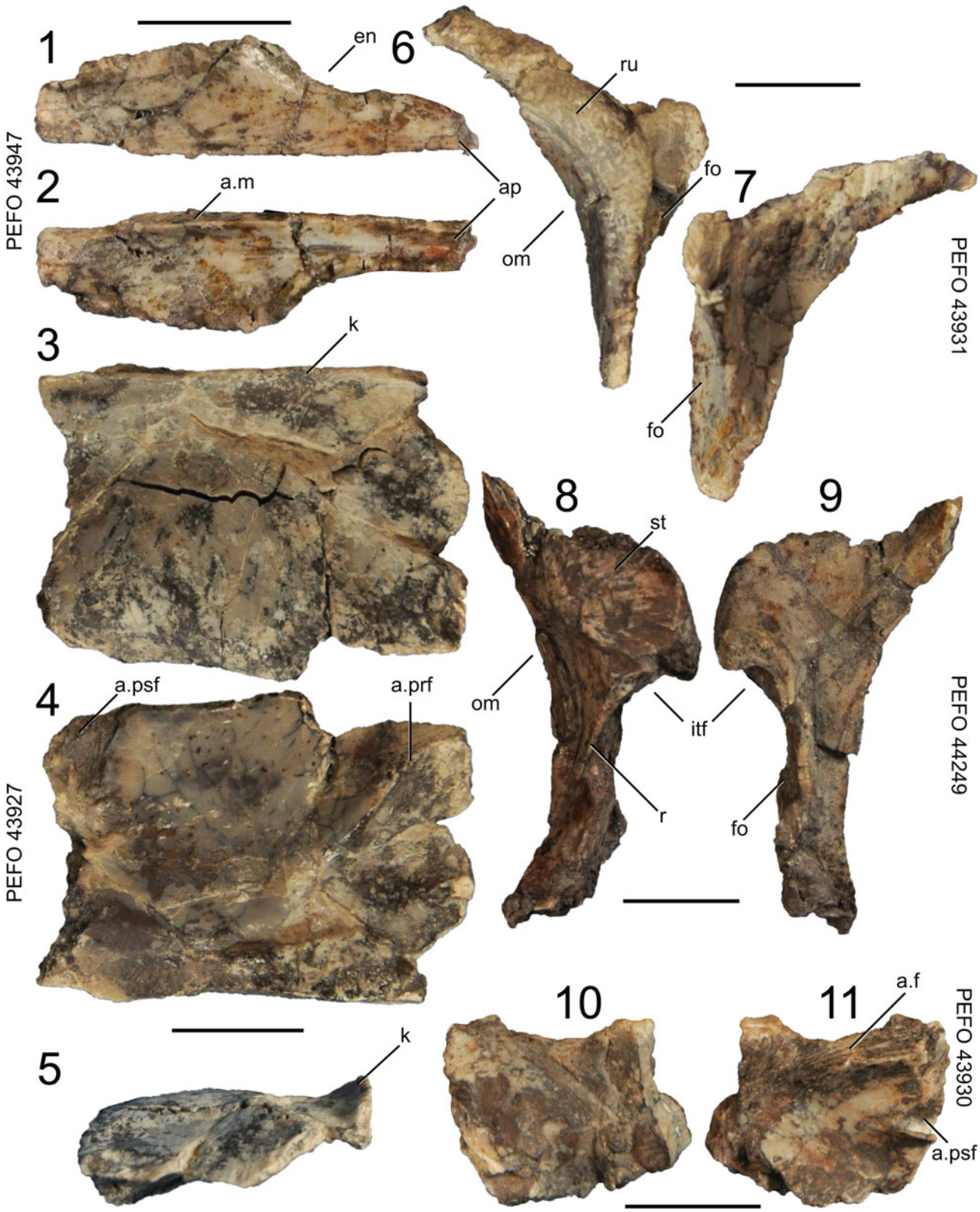

Figure 4. *Puercosuchus traverorum* n. gen. n. sp. in dorsal (**1, 3, 10**), ventral (**2, 4, 11**), lateral (**6, 8**), medial (**7, 9**), and anterior (**5**) views. (**1, 2**) Right nasal PEFO 43947; (**3–5**) right frontal PEFO 43927; (**6, 7**) right prefrontal PEFO 43931; (**8, 9**) left postfrontal PEFO 44249; and (**10, 11**) partial left parietal PEFO 43930. a.f = articular surface for frontal; a.m = articular surface for maxilla; a.prf = articular surface for prefrontal; a.psf = articular surface for postfrontal; ap = anterior process; en = external naris; fo = fossa; itf = infratemporal fenestra; k = keel; om = orbital margin; r = ridge; ru = rugosity; st = striations. Scale bars = 1 cm.

https://doi.org/10.1017/jpa.2022.49 Published online by Cambridge University Press

small element of *Tanystropheus hydroides* (Spiekman et al., 2020b, fig. 3b). The ventral process has a lateral ridge that extends dorsally and posteriorly to form the anterodorsal margin of the infratemporal fenestra. A subcircular fossa is present between the ventral and posterior processes that opens posteroventrally into the infratemporal fenestra. The dorsal half of the lateral surface of the postfrontal is flat (similar to the flat subtriangular surface of *Azendohsaurus madagaskarensis*; Flynn et al., 2010, text-fig. 1) with short striations extending posterodorsally. The edges and processes of the postfrontal are too broken to determine articular surfaces with neighboring elements.

Skull: parietal.—Representative specimen: PEFO 43930, left.

The only recovered parietal is highly fragmentary and preserves a thickened interdigitating suture with the frontal, a slotted articular surface ventrally for the postfrontal, and a flat midline articulation with the other parietal (Fig. 4.10, 4.11). The element is too fragmentary to determine the presence or position of the pineal foramen, present in other reptiles.

Skull: quadrate.—Representative specimens: PEFO 43941, left; PEFO 43938, right.

The dorsal articular head of the quadrate has a pointed hook that is posteriorly situated and directed (Fig. 5.1–5.3), as in other allokotosaurs (Nesbitt et al., 2015) and *Tanystropheus hydroides* (Spiekman et al., 2020b, fig. 14a, b). However, the dorsal articular head of *Puercosuchus traverorum* n. gen. n. sp. is not rounded like the quadrate head in *Azendohsaurus madagaskarensis* (FMNH PR 2751) or *Shringasaurus indicus* (Sengupta and Bandyopadhyay, 2022, fig. 4h). A small foramen penetrates the element ventral to the hook on the posterior surface, which is absent in *Azendohsaurus madagaskarensis* (FMNH PR 2751) and *Shringasaurus indicus* (ISIR 797). The dorsal articular surface is subtriangular in dorsal view. The concave otic notch is present just below the hooked dorsal head. The dorsal margin of the quadratojugal ramus is confluent with the dorsal articulation surface, but that of the pterygoid ramus is offset ventrally. The quadratojugal ramus is a broad sheet of bone and has a convex anterior margin; the anterior margin is concave in *Azendohsaurus madagaskarensis* (FMNH PR 2751) and *Shringasaurus indicus* (ISIR 797). It is not clear where the quadrate foramen passes through the quadratojugal ramus. The pterygoid ramus is incomplete in most specimens, but it widens considerably near the ventral articular surface and forms a subtriangular platform in ventral view (Fig. 5.4), similar to that of *Azendohsaurus madagaskarensis* (FMNH PR 2751) and *Trilophosaurus buettneri* (TMM 31025-140). The ventral articular surface is convex ventrally; in ventral view the articular surface has a straight anterior edge and a rounded posterior edge.

Skull: palatine.—Representative specimen: PEFO 43937, right.

The medial edge of the palatine that articulates with the pterygoid is longer than the lateral edge that articulates with the maxilla (Fig. 5.5, 5.6). The posterior margin of the element is straight and angled anterolaterally. A short process projects anterolaterally from the base of the maxillary process lateral to the posterior half of the internal choana that articulates with the vomer. The maxillary process has a circular foramen positioned laterally. Overall, the palatine of *Puercosuchus traverorum* n. gen. n. sp. is more similar to the plesiomorphic archosauromorph condition (e.g., that of *Macrocnemus bassanii*; Miedema et al., 2020, fig. 3b) rather than the more mediolaterally restricted element of *Azendohsaurus madagaskarensis* (Flynn et al., 2010, text-fig. 8b).

The socketed palatine teeth (~15) occur on a single, roughly anteroposteriorly directed ridge on the lateromedial center of the ventral surface of the element (Fig. 5.6). The teeth are larger anteriorly and are similar in shape to those on the pterygoid. The simple peg teeth differ from the mediolaterally compressed and serrated palatine teeth of *Azendohsaurus madagaskarensis* (Flynn et al., 2010, text-fig. 8c).

Skull: pterygoid.—Representative specimen: PEFO 43934, left.

The pterygoid is a flat element and is dorsoventrally shorter than that of *Azendohsaurus madagaskarensis* (FMNH PR 2751). The subtriangular palatal/anterior process tapers anteriorly and is separated from the shorter lateral ramus by a concavity (Fig. 5.7, 5.8). The posterior process has an elongate ventral fossa. The articular surface for the parabasisphenoid is a paddle-shaped medial flange between the anterior, lateral, and posterior processes. The lateral process has a flat articular surface for the ectopterygoid.

Pterygoid teeth are present ventrally in fields T1, T2, and T3 (Welman, 1998; Ezcurra, 2016), and are inset in sockets on longitudinal ridges that are offset ventrally from the rest of the anterior and lateral processes (Fig. 5.8, 5.9). A single row of ~five teeth occur in T1. The teeth in the T2 field (~22 teeth) are split into T2a and T2b ridges that bifurcate from a single ridge (same as in *Malerisaurus langstoni* TMM 31099-11). More teeth are present on the T2a ridge in *Puercosuchus traverorum* n. gen. n. sp. than in *Azendohsaurus madagaskarensis* (FMNH PR 2751). The T3 field (~30 teeth) is also split into T3a and T3b ridges that bifurcate closer to the articular surface with the parabasisphenoid. There are approximately four teeth in the T4 field medial to the T3 ridges. The pterygoid teeth are socketed, conical, and curve slightly posteriorly.

Braincase: parabasisphenoid.—Representative specimen: PEFO 38604 (adhered to unidentified skull bones).

The parabasisphenoid is an anteroposteriorly long element in which the cultriform process forms half the length of element (Fig. 6.1–6.3). The cultriform process is deflected such that the posterior half projects anterodorsally and the anterior half projects anteriorly. A longitudinal groove is present on the dorsal margin of the cultriform process that widens posteriorly into the hypophyseal fossa (Fig. 6.3), similar to the condition in *Pamelaria dolichotrachela* (Sen, 2003, p. 667). *Puercosuchus traverorum* n. gen. n. sp. lacks the knob on the dorsal surface of the cultriform process found in *Azendohsaurus madagaskarensis* (FMNH PR 2755). A single conical, pointed tooth occurs on the ventral margin of the cultriform process between the basipterygoid processes (Fig. 6.4), differing from the process in *Pamelaria dolichotrachela*, which was described by Sen (2003) as edentulous. Dentition on the ventral surface of the parasphenoid component of the parabasisphenoid is present in the early-diverging diapsids *Petrolacosaurus kansensis* Lane, 1945 (Peabody, 1952, fig. 1b), *Orovenator mayorum* Reisz, Modesto, and Scott, 2011 (Pritchard et al., 2021, supplemental information), *Claudiosaurus germaini* Carroll, 1981 (Pritchard

https://doi.org/10.1017/jpa.2022.49 Published online by Cambridge University Press

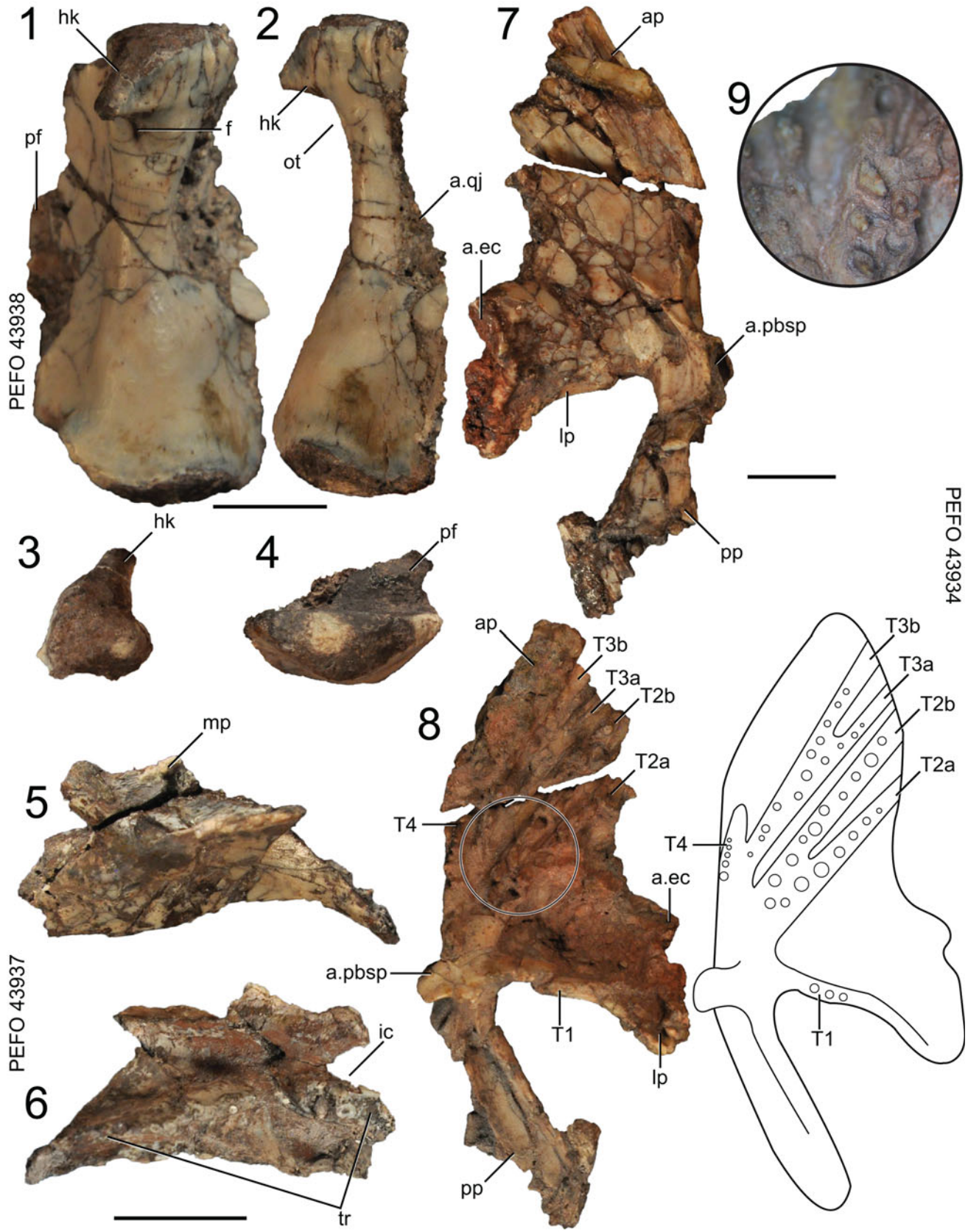

Figure 5. *Puercosuchus traverorum* n. gen. n. sp. in posterior (**1**), lateral (**2**), dorsal (**3, 5, 7**), and ventral (**4, 6, 8, 9**) views. (**1–4**) Right quadrate PEFO 43938; (**5, 6**) right palatine PEFO 43937; and (**7–9**) left pterygoid PEFO 43934. a.ec = articular surface for ectopterygoid; a.pbsp = articular surface for parabasisphenoid; a.qj = articular surface for quadratojugal; ap = anterior/palatal process; f = foramen; hk = hook; ic = internal choana; lp = lateral process; mp = maxillary process; ot = otic notch; pf = pterygoid flange; pp = posterior process; T = pterygoid tooth field (sensu Ezcurra, 2016); tr = tooth row. Scale bars = 1 cm.

https://doi.org/10.1017/jpa.2022.49 Published online by Cambridge University Press

et al., 2021, supplemental information), and some kuehneosaurids (Robinson, 1962; Colbert, 1970; Evans, 2009), which in some phylogenetic hypotheses are recovered as allokotosaurs (Pritchard and Nesbitt, 2017; Pritchard et al., 2018; Nesbitt et al., 2021) or are closely related to them (Ezcurra, 2016). We do note that teeth could be present in other allokotosaurs in the same region, but identification and retention of this dentition requires exceptional preservation and careful fossil preparation.

The basipterygoid processes and basal tubera of *Puercosuchus traverorum* n. gen. n. sp. are prominent ventrolateral processes similar to those figured by Chatterjee (1980, fig. 5b) for *Malerisaurus robinsonae* and as seen in *Malerisaurus langstoni* (TMM 31099-11). The space between the basipterygoid processes is slightly mediolaterally wider than that between the two basal tubera of the parabasisphenoid. The posterior margins of the basipterygoid processes have a ridge that extends dorsally up the side of the parabasisphenoid. The basipterygoid processes project ventrolaterally directly from the base of element and do not share a basal stalk like those of *Azendohsaurus madagaskarensis* (FMNH PR 2755). The parabasisphenoid portion of the basal tubera are thick subrectangular processes in posterior view that project posterolaterally. A deep anteroposteriorly long fossa occurs on the ventral surface of the parabasisphenoid, similar to that of *Azendohsaurus madagaskarensis* (FMNH PR 2755). The hypophyseal fossa is not walled off laterally. The floor of the endocranial cavity is divided into two bilateral, anteroposteriorly elongate fossae by a low midline ridge (Fig. 6.3). The articular surface for the prootic is triangular.

Braincase: opisthotic + supraoccipital + prootic.—Representative specimen: PEFO 49442, both opisthotics co-ossified to the supraoccipital and prootics.

The supraoccipital is broad and gently convex dorsally (Fig. 6.5). The exoccipitals are missing and unknown; the posteroventral surface of the supraoccipital is smooth. Without preservation of any exoccipitals, it is not clear if the supraoccipital contributed to the foramen magnum. The anterolateral surface of the supraoccipital has a pair of bilateral short processes that articulate with the parietal (Fig. 6.6).

The prootic has a tapered lateral process that projects posterolaterally along the anterior margin of the paroccipital process of the opisthotic and a short posterior ramus that contributes to the fenestra ovalis. The ventral process articulates with the parabasisphenoid ventral to the anterior notch for the exit of the trigeminal nerve (CN V). The lateral exit for the facial nerve (CN VII) is a foramen housed in an elongate, narrow groove near the edge of the lateral process posterior to the trigeminal notch (Fig. 6.9). The dorsal margin of the prootic is inflected dorsomedially and contributes to the roof of the endocranial cavity. The medial side of the prootic is concave and includes a deep auricular fossa dorsally (Fig. 6.5). The notch posterior to the floccular fossa is the medial exit for CN VII.

The opisthotic includes a relatively narrow paroccipital process with a dorsoventrally expanded lateral end (Fig. 6.6). The foramen ovale is a posterodorsally inclined opening ventral to the paroccipital process in lateral view (Fig. 6.8, 6.9). The ventral ramus of the opisthotic forms the anterior margin of the metotic fissure, which is incomplete owing to the missing (and not co-ossified) exoccipital (Fig. 6.7, 6.9). The ventral rami of both opisthotics are each pierced by a single foramen (which occurs posterior to the foramen ovale and anterior to the metotic fissure and lateral exits of CN XII that would occur on the exoccipital); the function and homology of this foramen are unknown and we consider it an autapomorphy of *Puercosuchus traverorum* n. gen. n. sp. among allokotosaurs. There are two articular surfaces for the exoccipital on the posterior surface of the opisthotic (Fig. 6.7, 6.8). The dorsal articular surface is present just above the dorsolateral midpoint of the opisthotic and the ventral articular surface is present on the posteroventral margin of the bone.

Braincase: basioccipital.—Representative specimens: PEFO 38603; PEFO 43926.

The occipital condyle forms half of the anteroposterior length of the bone. The condyle itself has a midline dorsal ridge that separates the articular surfaces for the left and right exoccipitals (Fig. 6.10). The condyle has a shallow central fossa on its posteriormost extent. In ventral view the condyle has a transverse lip at its mediolaterally widest point; the basioccipital narrows anterior to the lip before widening anteriorly. The basal tubera are formed by discrete anterolaterally oriented short ventral processes (Fig. 6.12), similar to those of *Malerisaurus langstoni* (TMM 31099-11) but unlike the broad shelf-like basal tubera found in *Azendohsaurus madagaskarensis* (Flynn et al., 2010, fig. 2b). A triangular fossa occurs on the midline of the basioccipital anterior to the basal tubera, and a pair of deep fossae excavate the dorsolateral surfaces of the anterior half of the element (Fig. 6.12). Articulations with the opisthotics, exoccipitals, and parabasisphenoid are simple abutting surfaces.

Mandible: dentary.—Representative specimens: PEFO 43920, right; PEFO 43919, right; PEFO 44246, right; PEFO 38606, right; NMMNH P-60127, left.

The dentary is long anteroposteriorly, narrow dorsoventrally, and expands slightly dorsoventrally towards its posterior extent (Fig. 7.1–7.6), much like that of *Pamelaria dolichotrachela* (ISIR 316/1). The anterior end is rounded and asymmetrical in lateral view such that the anteroventral margin is longer than the anterodorsal margin; this configuration is found in other azendohsaurids (Nesbitt et al., 2021). The dorsal and ventral margins of the dentary are straight and parallel like those of other malerisaurines. The anteriormost end of the dentary has several circular foramina on the lateral surface and regularly spaced foramina below the tooth row down the length of the element. Long transverse striations extend away from the anterior end along the lateral surface. The anteroventral margin is slightly expanded ventrally, but the anterior end of the dentary is not deflected ventrally as in *Azendohsaurus madagaskarensis* (FMNH PR 2751), *Azendohsaurus laaroussii* (Nesbitt et al., 2015, fig. 7h), and early sauropodomorphs (Sereno, 1999). The Meckelian canal is open medially (it is open ventromedially in *Azendohsaurus madagaskarensis*, FMNH PR 2751) and widens dorsoventrally at the posterior end (Fig. 7.4). Several long posteriorly opening foramina occur within the Meckelian canal posterior to the mandibular symphysis. The Meckelian canal continues anteriorly through the symphysis of *Puercosuchus traverorum* n. gen. n. sp., but terminates posterior to the symphysis *Azendohsaurus madagaskarensis* (FMNH PR 2751). The symphysis itself is made up of two smooth medial

https://doi.org/10.1017/jpa.2022.49 Published online by Cambridge University Press

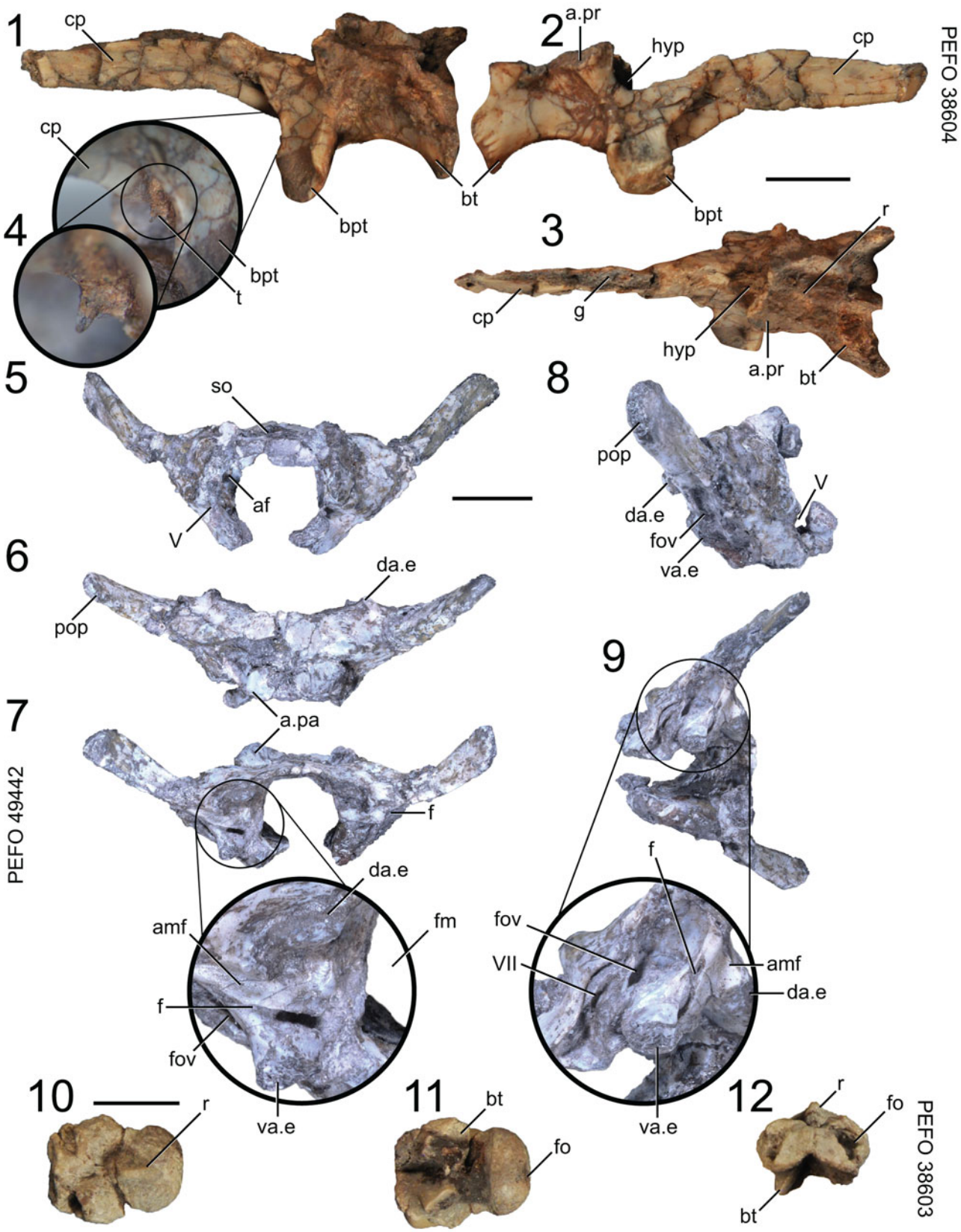

Figure 6. *Puercosuchus traverorum* n. gen. n. sp. in left lateral (**1**), right lateral (**2, 8**), dorsal (**3, 6, 10**), anterior (**5, 12**), posterior (**7**), ventral (**11**), ventrolateral (**9**), and anteroventral (**4**) views. (**1–4**) Parabasisphenoid PEFO 38604; (**5–9**) co-ossified supraoccipital, prootics, and opisthotics PEFO 49442; and (**10–12**) basioccipital PEFO 38603. a.pa = articular surface for parietal; a.pr = articular surface for prootic; af = auricular fossa; amf = anterior margin of metotic fissure; bpt = basipterygoid process; bt = basal tuber; cp = cultriform process; da.e = dorsal articulation with exoccipital; f = foramen; fm = foramen magnum; fo = fossa; fov = foramen ovale; g = groove; hyp; hypophyseal fossa; pop = parapophysis; r = ridge; so = supraoccipital; t = tooth; V = notch for trigeminal nerve (CN V); VII = foramen for facial nerve (CN VII); va.e = ventral articulation with exoccipital. Scale bars = 1 cm.

https://doi.org/10.1017/jpa.2022.49 Published online by Cambridge University Press

surfaces (Class I, sensu Holliday and Nesbitt, 2013); the dorsal surface is subrectangular and oriented anteroposteriorly, and the ventral surface is subelliptical and oriented more dorsoventrally. This is unlike the single irregular surface found in *Azendohsaurus madagaskarensis* (FMNH PR 2751). Overall, the dentary is similar in shape to those previously attributed to 'saurischian dinosaurs' (TTU-P10514, TTU-P10515) and an unidentified archosauromorph (TTU-P10517) from the Dockum Group of Texas (Sarigül, 2017), but those specimens likely represent malerisaurine azendohsaurid allokotosaurs based on their apomorphies (Lessner et al., 2018; Nesbitt et al., 2021).

Nineteen alveoli are in the most complete dentary of *Puercosuchus traverorum* n. gen. n. sp. (PEFO 38606; Fig. 7.1, 7.2). *Pamelaria dolichotrachela* (ISIR 316/1) also has 19 dentary teeth (Sen, 2003), similar to the number (17) estimated for *Malerisaurus robinsonae* (Chatterjee, 1980) and *Azendohsaurus madagaskarensis* (Flynn et al., 2010). The dentary teeth closely resemble those of the maxilla in shape and heterodonty (Fig. 3.9, 3.10), where the more-anterior teeth are clearly different from the posteriormost teeth. Some dentary teeth bear small wear facets obliquely truncating the tooth apices, forming an apicolabially facing planar surface at the tooth apex (Fig. 3.9). The dentary teeth are ankylothecodont when fully erupted, wherein triangular interdental plates are present and co-ossified to the teeth. The first alveolus occurs nearly at the anterior end of the dentary.

Mandible: angular.—Representative specimens: PEFO 44251, right; PEFO 44250, left.

The angular is anteroposteriorly elongate and dorsoventrally tallest anteriorly (Fig. 7.7, 7.8). There is no evidence of an external mandibular fenestra. The ventral margin of the element is straight and the dorsal margin slightly concave. The lateral surface is smooth, but the medial surface has longitudinal striations. The dorsal margin is mediolaterally thin. The ventral margin curves dorsomedially to form a shallow shelf along the length of the medial surface of the element that articulates with the prearticular.

Mandible: prearticular.—Representative specimens: PEFO 43948, left; PEFO 42253, left.

The prearticular is concave dorsally and convex ventrally (Fig. 7.9, 7.10). It tapers posteriorly where it has a slight dorsoventral expansion and dorsolateral depression that articulates with the articular. The element is widest anteriorly, has a mediolaterally thin dorsal margin, and a mediolaterally thickened ventral margin that forms a lateral shelf that may have articulated with the angular or surangular.

Mandible: surangular.—Representative specimens: PEFO 43945, left; PEFO 44256, left; PEFO 43944, right.

A lateral foramen is present on the surangular anteroventral to the coronoid eminence (Fig. 7.11). An additional posterior lateral foramen occurs adjacent to the articular. The dorsoventrally widest portion of the surangular occurs at the coronoid eminence, and the surangular tapers posteriorly towards the articular. The dorsal margin is mediolaterally thickened and forms a rounded ridge medially. The coronoid eminence is subtriangular (Fig. 7.11–7.15), and an articular fossa for the coronoid bone is present anterior to the coronoid eminence on the dorsomedial surface. The bone is concave medially beneath the dorsal ridge. Longitudinal striations are present on the lateral surface next to the articular as well as on the medial surface of the coronoid eminence.

Mandible: articular.—Representative specimens: PEFO 43945, left; PEFO 44256, left; PEFO 43944, right. All articulars are co-ossified to the surangular.

The articular has a short mediolaterally compressed retroarticular process (Fig. 7.13, 7.16). The glenoid is dorsoventrally deep, mediolaterally wide, and bordered posteromedially by a transverse ridge. That ridge forms the anteromedial margin of a subtriangular dorsomedial fossa behind the glenoid, which is continuous with the dorsal surface of a medioventral process that expands distally (Fig. 7.12, 7.13, 7.15, 7.16). The retroarticular process is upturned (sensu Ezcurra, 2016) and forms a dorsal tubercle. The articular lacks a medial foramen.

Vertebral column and ribs: atlas.—Representative specimens: PEFO 44259 (atlantal intercentrum); PEFO 44006, right (atlantal neurapophysis).

The atlantal intercentrum is wedge-shaped, concave dorsally, convex ventrally, and tapers anteriorly (Fig. 8.1–8.3). The posterior articular surface for the axial intercentrum is slightly concave. The lateral articular surface for the neurapophysis is a subelliptical fossa that has a short groove extending anteroventrally; this groove, which is visible in anterior view (Fig. 8.1), also is present in *Pamelaria dolichotrachela* (ISIR 316/3; Sen, 2003, fig. 7a). The dorsal surface of the intercentrum is smooth where it articulates with the atlantal pleurocentrum (odontoid/dens). The atlantal neurapophysis (Fig. 8.4, 8.5) has an oval postzygapophysis and distinct articular facets for the atlantal intercentrum and proatlas. The epipophysis is confluent with a strong ridge on the lateral surface that extends from between the articular surfaces for the proatlas and atlantal intercentrum.

Vertebral column and ribs: axis.—Representative specimens: PEFO 44257; PEFO 44008; PEFO 44007 (axial pleurocentra only; the axial intercentra/atlantal pleurocentrum are not ossified to the axial pleurocentrum as seen in some specimens of *Azendohsaurus madagaskarensis* [Nesbitt et al., 2015, fig. 12] and in *Shringasaurus indicus* [Sengupta et al., 2017, fig. 3]).

The axial pleurocentrum (Fig. 8.6–8.11) is opisthocoelous; the anterior surface is a broad, flat area that abuts the rest of the atlas-axis complex. In lateral view the centrum is inclined anteriorly so that the dorsal margins of the centrum faces are anterior to the ventral margins. A strong ventral keel is present, as is a deep fossa on the ventrolateral side of the centrum (Fig. 8.8, 8.9). The neural arch is co-ossifed to the centrum in all specimens of *Puercosuchus traverorum* n. gen. n. sp. The parapophysis occurs on the upper half of the centrum just ventral to the prezygapophysis. A longitudinal fossa is present ventral and posterior to the parapophysis. The parapophysis projects farther laterally than the prezygapophysis. The prezygapophysis is a short, curving dorsolateral surface, and it does not project anterior to the anterior face of the centrum. The postzygapophysis extends slightly farther posteriorly than the centrum face, but it is extended considerably farther laterally than the centrum. The pointed epipophysis projects past the posterior margin of postzygapophysis (Fig. 8.11), and it is confluent with the bifurcated posterior margin of the neural spine, as in *Azendohsaurus madagaskarensis* (FMNH PR 3823). A small gap occurs

https://doi.org/10.1017/jpa.2022.49 Published online by Cambridge University Press

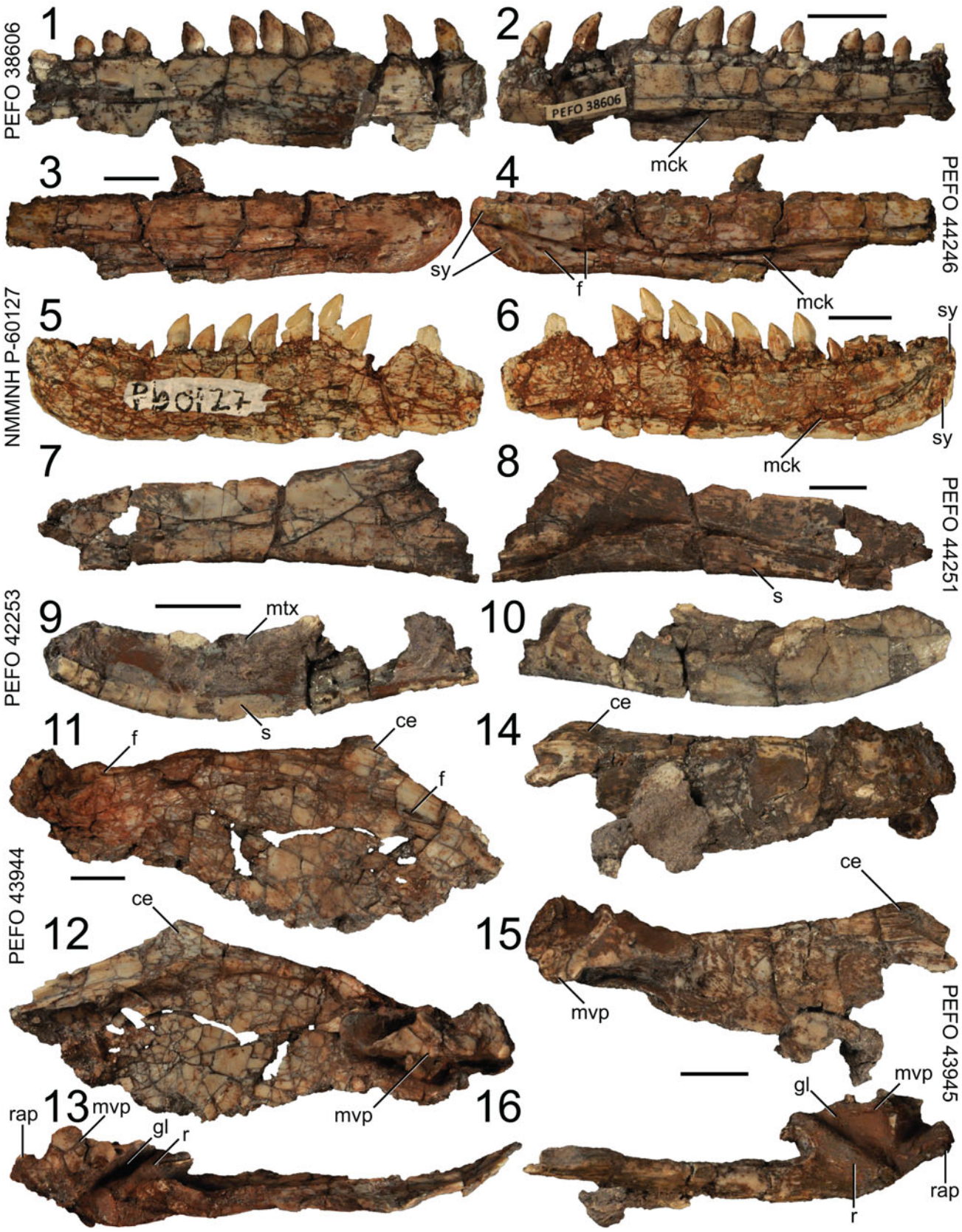

Figure 7. *Puercosuchus traverorum* n. gen. n. sp. in lateral (**1, 3, 5, 7, 9, 11, 14**), medial (**2, 4, 6, 8, 10, 12, 15**), and dorsal (**13, 16**) views. (**1, 2**) Right dentary PEFO 38606; (**3, 4**) right dentary PEFO 44246; (**5, 6**) left dentary NMMNH P-60127; (**7, 8**) right angular PEFO 44251; (**9, 10**) left prearticular PEFO 42253; (**11–13**) right articular and surangular PEFO 43944; and (**14–16**) left articular and surangular PEFO 43945. ce = coronoid eminence; f = foramen; gl = glenoid; mck = Meckelian canal; mtx = matrix; mvp = medioventral process; r = ridge; rap = retroarticular process; s = shelf; sy = symphysis. Scale bars = 1 cm.

https://doi.org/10.1017/jpa.2022.49 Published online by Cambridge University Press

between the articular surfaces of the postzygapophyses in dorsal view. A deep spinopostzygapophyseal fossa (sensu Wilson et al., 2011) is present between the postzygapophyses and neural spine. Anteriorly, the neural spine overhangs and extends beyond the centrum (Fig. 8.8), as in *Azendohsaurus madagaskarensis* (FMNH PR 3823). The dorsal margin of the neural spine is gently convex and does not expand laterally and dorsally, as in *Azendohsaurus madagaskarensis* (FMNH PR 3823). In dorsal view, the posterior portion of the neural spine does not expand laterally into a block-like structure like that of *Azendohsaurus madagaskarensis* (FMNH PR 3823).

Vertebral column and ribs: post-axial anterior cervical vertebrae.—Representative specimens: PEFO 43981; PEFO 43992; PEFO 43983; NMMNH P-60208. All centra are co-ossified to their respective neural arches throughout the entire size range. Intercentra are absent, as in other azendohsaurids (Nesbitt et al., 2015).

The centrum is weakly procoelous, elongate, and inclined anteriorly in lateral view such that a plane parallel with the anterior or posterior face of the centrum is 20° offset from vertical (Fig. 9.2, 9.9). A ventral keel is variably present; in some specimens it extends the entire length of the centrum, and in others it is present on only the posterior half of the centrum. PEFO 43983 has a pair of short ridges dorsolateral to the ventral keel at the posterior end of the centrum. The anterior and posterior centrum faces are subcircular in outline. The anterior centrum face has a sharp rim, but the rim is more rounded on the shallower posterior face, making this condition weakly procoelous like in *Trilophosaurus buettneri* (TMM 31025-140) but unlike the

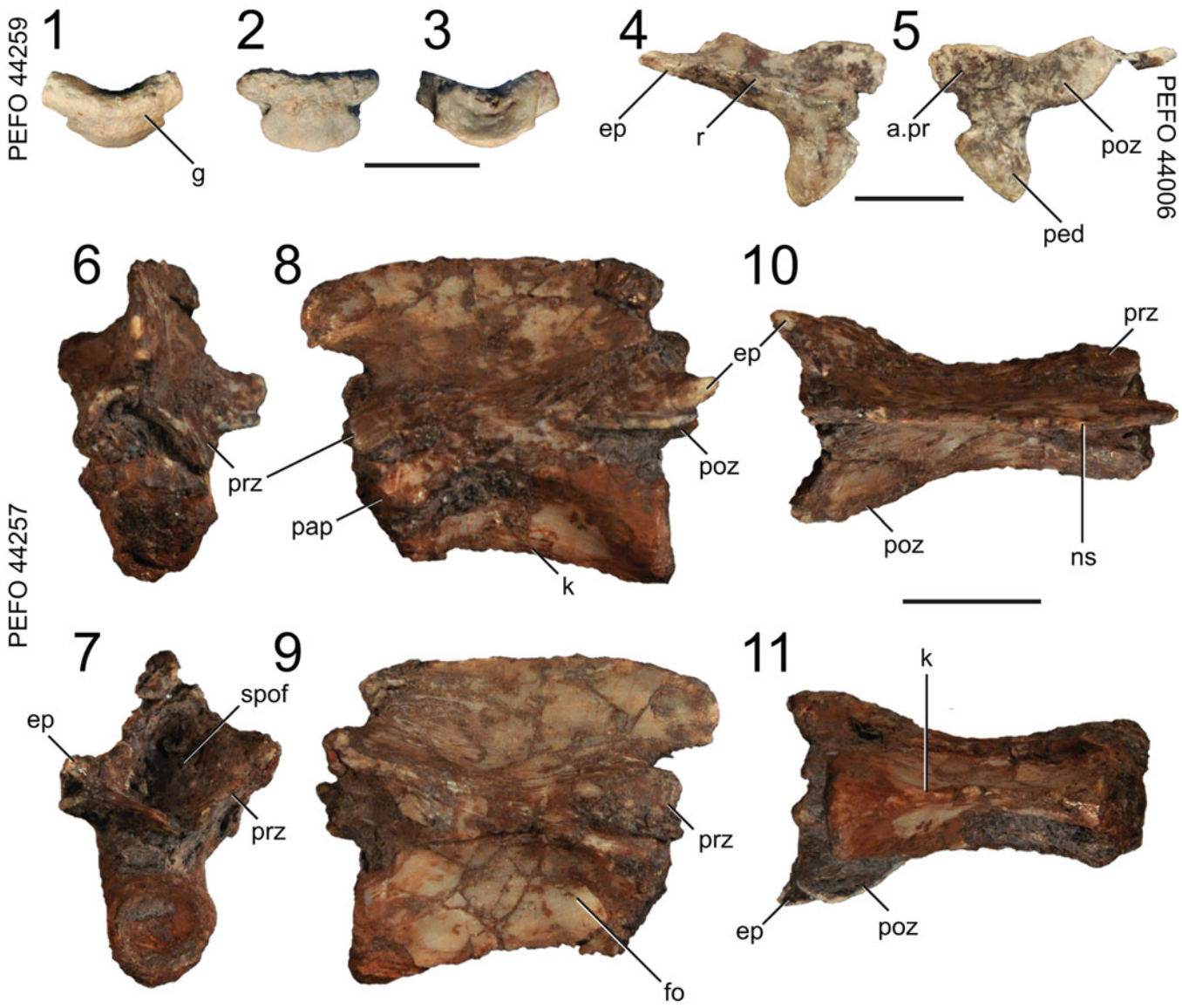

Figure 8. *Puercosuchus traverorum* n. gen. n. sp. in anterior (**1, 6**), posterior (**3, 7**), right lateral (**4, 9**), left lateral (**8**), medial (**5**), dorsal (**10**), and ventral (**2, 11**) views. (**1–3**) Atlantal intercentrum PEFO 44259; (**4, 5**) right atlantal neurapophysis PEFO 44006; and (**6–11**) axis PEFO 44257. a.pr = articular surface for proatlas; ep = epipophysis; fo = fossa; g = groove; k = keel; ns = neural spine; pap = parapophysis; ped = pedicle; poz = postzygapophysis; prz = prezygapophysis; r = ridge; spof = spinopostgyapophyseal fossa. Scale bars = 1 cm.

https://doi.org/10.1017/jpa.2022.49 Published online by Cambridge University Press

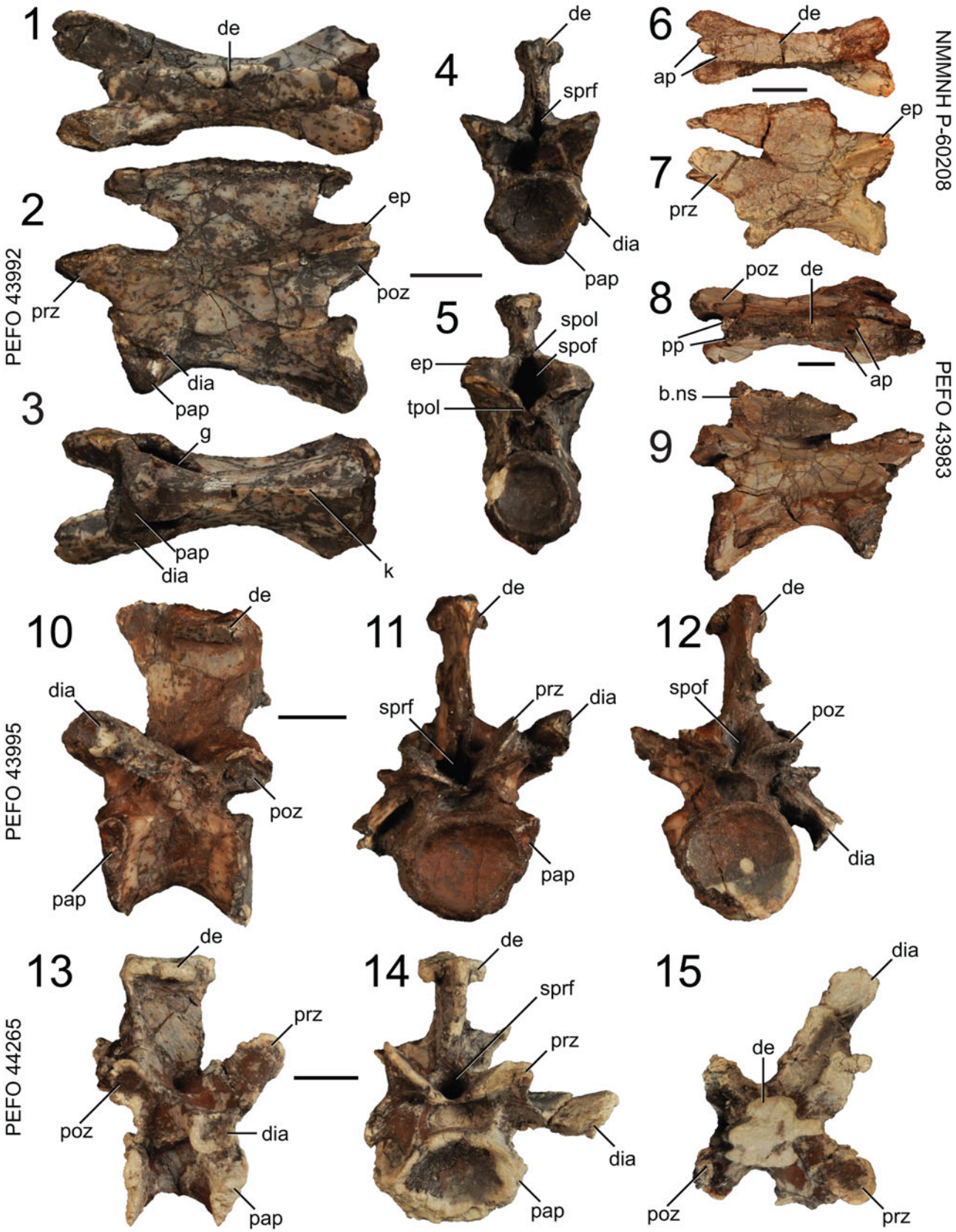

Figure 9. *Puercosuchus traverorum* n. gen. n. sp. in dorsal (**1, 6, 8, 15**), lateral (**2, 7, 9, 10, 13**), ventral (**3**), anterior (**4, 11, 14**), and posterior (**5, 12**) views. (**1–5**) Anterior cervical vertebra PEFO 43992; (**6, 7**) anterior cervical vertebra NMMNH P-60208; (**8, 9**) anterior cervical vertebra PEFO 43983; (**10–12**) posterior cervical vertebra PEFO 43995; and (**13–15**) posterior cervical vertebra PEFO 44265. ap = anterior process; b.ns = broken neural spine; de = dorsal expansion; dia = diapophysis; ep = epipophysis; g = groove; k = keel; pap = parapophysis; poz = postzygapophysis; pp = posterior process; prz = prezygapophysis; spof = spinopostzygapophyseal fossa; spol = spinopostzygapophyseal lamina; sprf = spinoprezygapophyseal fossa; tpol = intrapostzygapophyseal lamina. Scale bars = 1 cm.

https://doi.org/10.1017/jpa.2022.49 Published online by Cambridge University Press

amphicoelous condition in *Azendohsaurus madagaskarensis* (FMNH PR 2791). The diapophysis occurs on the ventral half of the centrum near the parapophysis, and the two structures are separated by a groove (Fig. 9.3) roofed by the posterior centrodiapophyseal lamina (Wilson, 1999). This groove extends posteriorly along the centrum and forms the dorsal margin of a long fossa that is deepest anteriorly, as in other long-necked archosauromorphs. In lateral outline the parapophysis is subtriangular and the diapophysis is subtrapezoidal. The prezygapophysis and postzygapophysis extend anterodorsally and posterodorsally, respectively, beyond the centrum; in dorsal view, the postzygapophysis projects more laterally than the prezygapophysis (Fig. 9.1). The epipophysis on the dorsal surface of the postzygapophysis is tall and mediolaterally wide, and it terminates anterior to the distal end of the postzygapophysis. This form of epipophysis is common to other malerisaurines, *Azendohsaurus madagaskarensis*, and trilophosaurids. The postzygapophysis has an accessory fossa and ridge ventral to the articular surface, which is also found in *Azendohsaurus madagaskarensis* (FMNH PR 2791). The intrapostzygapophyseal lamina connects the ventral rims of the postzygapophyses medially and forms the floor of a deep triangular spinopostzygapophyseal fossa beneath the neural spine. The spinopostzygapophyseal lamina is prominent, and a spinoprezygapophyseal fossa is present. In lateral view, the neural spine expands anteroposteriorly towards its dorsal edge; the anterior margin of the neural spine is more inclined than the posterior margin. The top of the neural spine is flat dorsally but expanded laterally along its length (Fig. 9.4, 9.5), as in *Malerisaurus robinsonae* (ISIR 150); this feature is a character state that unites malerisaurines (Nesbitt et al., 2021), but it is also found in some tanystropheids, such as *Macrocnemus fuyuanensis* Li et al., 2007 (Spiekman et al., 2021, fig. 22a), *Macrocnemus bassanii* (Spiekman et al., 2021, supplemental information), and GR 269 (Pritchard et al., 2015, fig. 2a, d). This dorsal expansion in *Puercosuchus traverorum* n. gen. n. sp. has short anterior and posterior processes that are bifurcated anteriorly/posteriorly (Fig. 9.6, 9.8). In dorsal view, the expanded top of the of neural spine is widest anteriorly.

Vertebral column and ribs: post-axial posterior cervical vertebrae.—Representative specimens: PEFO 44265; PEFO 43995. We identify these as posterior cervical vertebrae because the parapophysis remains on the centrum in these vertebrae, but they share transitional anatomy with the most-anterior trunk vertebrae documented in other archosauromorphs such as *Prolacerta broomi* Parrington, 1935 (Gow, 1975, fig. 21), *Tanystropheus longobardicus* (Nosotti, 2007, fig. 4), and *Protorosaurus speneri* von Meyer, 1832 (Gottmann-Quesada and Sander, 2009, text-figs. 12, 13). All centra are co-ossified to their respective neural arches throughout the entire size range, even in the smallest preserved specimen (PEFO 44260, 19.7 mm anteroposterior centrum length). Intercentra are absent.

The centrum is less elongate than the anterior cervicals and it is weakly procoelous (Fig. 9.10). The anterior and posterior centrum faces are subcircular; the anterior face is slightly mediolaterally wider than the posterior face. A ventral keel is absent. The diapophysis is positioned more dorsally in the posterior cervicals, and its articular facet is sub-elliptical in lateral view. The diapophysis occurs on robust transverse processes that shift in their projection from ventrolaterally to laterally to dorsolaterally progressing posteriorly along the neck. Lateral fossae are present on the centrum below the transverse process, and the four main centrodiapophyseal laminae (prezygodiapophyeal lamina, postzygodiapophyseal lamina, anterior centrodiapophyseal lamina, posterior centrodiapophyseal lamina) are present (Fig. 9.11–9.14) along with their associated fossae (centrodiapophyseal fossa, prezygapophyseal centrodiapophyseal fossa, postzygapophyseal centrodiapophyseal fossa, spinodiapophyseal fossa). The zygapophyses project slightly past the centrum anteriorly and posteriorly. In dorsal view, the prezygapophysis projects slightly more laterally than the postzygapophysis. The epipophysis is either a small bump or is absent. The spinopostzygapophyseal lamina is less developed in the posterior cervical vertebrae. The dorsal extent of the neural spine is barely expanded anteroposteriorly. The top of the neural spine is laterally expanded only at its anteroposterior midpoint (Fig. 9.10, 9.15; = mammillary processes; Ezcurra and Butler, 2015; Ezcurra, 2016; Spiekman et al., 2021), like that of other malerisaurines (Nesbitt et al., 2021) and the archosauromorphs *Prolacerta broomi* (Gottmann-Quesada and Sander, 2009, fig. 21), *Boreopricea funerea* Tatarinov, 1978 (Benton and Allen, 1997, fig. 7d), *Protorosaurus speneri* (Gottmann-Quesada and Sander, 2009, text-fig. 12), and *Proterosuchus alexanderi* Hoffman, 1965 (Ezcurra and Butler, 2015, fig. 4E). The anterior and posterior ends of the expanded neural spine of *Puercosuchus traverorum* n. gen. n. sp. are not bifurcated, but there are shallow anterior and posterior depressions between the main body of the neural spine and the lateral expansion, which are best seen in dorsal view. The spinoprezygapophyseal and spinopostzygapophyseal fossae are present.

Vertebral column and ribs: trunk vertebrae.—Representative specimens: PEFO 44274 (anterior); PEFO 43974 (anterior); PEFO 43977 (middle); PEFO 43963 (posterior); PEFO 44276 (posterior). No trunk vertebra is preserved in which the parapophysis and diapophysis are found on the same lateral process, except in the most posterior trunk vertebra. All centra are co-ossified to their respective neural arches throughout the entire size range. Intercentra are absent.

The centrum is relatively elongate anteroposteriorly (compared to *Azendohsaurus madagaskarensis*, FMNH PR 2779) and is just slightly longer than the anteroposterior length of the neural spine (Fig. 10.1). The anterior and posterior centrum faces are slightly concave. The centrum lacks a ventral keel (unlike in *Malerisaurus langstoni*, TMM 31099-11) and a lateral fossa. The parapophysis is present on the anteroventral corner of the neural arch pedicle, where it projects laterally as a short oval stalk (Fig. 10.2). The diapophysis is a longer dorsolateral process and occurs just anterior to the anteroposterior midpoint of the neural arch above the pedicle (Fig. 10.3). The anterior centrodiapophyseal and posterior centrodiapophyseal laminae are absent, but the postzygodiapophyseal and paradiapophyseal laminae are present. The spinoprezygapophyseal fossa and spinopostzygapophyseal fossa are much smaller and shallower than in the cervical vertebrae. The prezygapophysis is laterally wider than the postzygapophysis in dorsal view (Fig. 10.4). The posterior margin of the neural spine is flush with the posterior

https://doi.org/10.1017/jpa.2022.49 Published online by Cambridge University Press

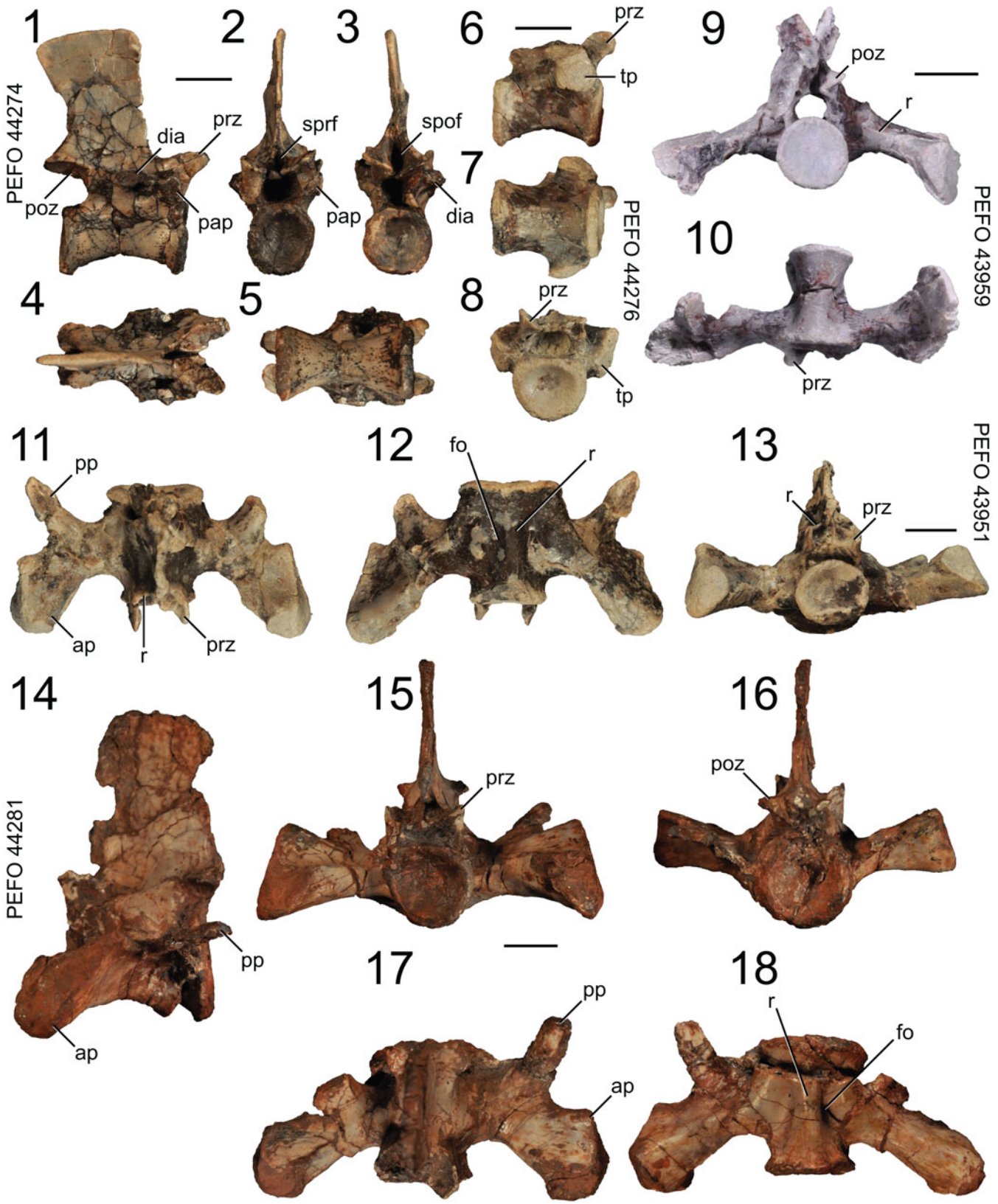

Figure 10. *Puercosuchus traverorum* n. gen. n. sp. in lateral (**1, 6, 14**), anterior (**2, 8, 13, 15**), posterior (**3, 9, 16**), dorsal (**4, 11, 17**), and ventral (**5, 7, 10, 12, 18**) views. (**1–5**) Anterior trunk vertebra PEFO 44274; (**6–8**) posterior trunk vertebra PEFO 44276; (**9, 10**) first sacral vertebra PEFO 43959; (**11–13**) second sacral vertebra PEFO 43951; and (**14–18**) second sacral vertebra PEFO 44281. ap = anterior process; dia = diapophysis; fo = fossa; pap = parapophysis; poz = postzygapophysis; pp = posterior process; prz = prezygapophysis; r = ridge; spof = spinopostzygapophyseal fossa; sprf = spinoprezygapophyseal fossa; tp = transverse process. Scale bars = 1 cm.

https://doi.org/10.1017/jpa.2022.49 Published online by Cambridge University Press

margin of the centrum, and the anterior margin of the neural spine occurs just anterior to the anteroposterior position of the diapophysis. The dorsal extent of the neural spine expands slightly anteroposteriorly. The dorsal edge of the neural spine is flat (Fig. 10.2), and is either smooth (PEFO 44274), rugose laterally (PEFO 44273), or slightly expanded laterally (PEFO 43974). The postzygapophysis barely projects past the centrum, but the prezygapophysis projects farther past the centrum (Fig. 10.5). Hyposphene-hypantrum articulations are absent in the anterior trunk vertebrae.

The centrum length of the posterior trunk vertebra (Fig. 10.6–10.8) is similar to that of the rest of the trunk vertebrae; it is not foreshortened like that of the last trunk vertebra in *Azendohsaurus madagaskarensis* (FMNH PR 2780). Vertebral laminae are absent on the posterior trunk vertebra. The anterolateral transverse process is relatively short but robust, occupying much of the anterior half of the neural arch. The articular surface of the transverse process is double-lobed and waisted in the middle dorsoventrally. Hyposphene-hypantrum articulations on the posterior trunk vertebra are absent, but it does preserve the spinoprezygapophyseal and spinopostzygapophyseal fossae.

Vertebral column and ribs: first sacral vertebra.—Representative specimen: PEFO 43959.

The centrum faces are weakly concave and have strong rounded rims (Fig. 10.9). Two-thirds of the first sacral rib occurs on the centrum and one-third of it occurs on the neural arch (Fig. 10.9). The sacral rib is positioned on the anterior half of the vertebra (Fig. 10.10) and takes up more of the centrum than in *Azendohsaurus madagaskarensis* (FMNH PR 2780). It is so far forward that it is nearly confluent with the anterior margin of the centrum. The first sacral rib projects ventrolaterally, but more laterally than ventrally, unlike in *Azendohsaurus madagaskarensis* (FMNH PR 2780). A small fossa is present on the anterior surface of the base of the rib, and a second, deeper fossa is present on the posterior side. A spinoprezygapophyseal fossa is present, but a spinopostzygapophyseal fossa is absent. Laterally, the first sacral rib expands anteroposteriorly; in lateral view the articular surface is dorsoventrally tall and anteroposteriorly wide and it tapers anteriorly where it connects to a thin anterior process. A prominent horizontal ridge is present on the posterior edge of the sacral rib (Fig. 10.9). In dorsal view, the anterior margin of the sacral rib is broadly concave and the posterior margin is convex. The zygapophyses are short; the prezygapophysis projects past the centrum but the postzygapophysis does not. The neural spine of the only first sacral vertebra specimen is too fragmentary to determine its size and shape. Unlike in *Azendohsaurus madagaskarensis* (FMNH PR 2780), hyposphene-hypantrum articulation is absent in the first sacral vertebra.

Vertebral column and ribs: second sacral vertebra.—Representative specimens: PEFO 44281; PEFO 43951.

The centrum faces are weakly concave and have strongly rounded rims (Fig. 10.13, 10.15, 10.16). The posterior centrum face is larger than the anterior face. The second sacral rib is located exclusively on the posterior two-thirds of the centrum (Fig. 10.12, 10.15), not on any part of the neural arch. The ventral surface of the rib is confluent with the ventral surface of the centrum. A fossa is present at the anterior end of the base of the rib that opens anterolaterally, forming a rounded keel in ventral view (Fig. 10.12, 10.18). A foramen occurs inside of this fossa, which is absent in *Azendohsaurus madagaskarensis* (FMNH PR 2777). The second sacral rib projects straight laterally and expands anteroposteriorly towards its lateral extent into two processes (Fig. 10.12). The anterior process is the largest, and its long axis is oriented posterodorsally in lateral view. The anterior process has two distinct articular surfaces: the first is a rounded dorsolateral surface that articulates with the first sacral rib, and the second is an oblong lateral surface that articulates with the ilium. The posterior process tapers distally and projects posterolaterally; *Azendohsaurus madagaskarensis* (FMNH PR 2777) lacks this posterior process. A concavity is present between the anterior and posterior processes of the rib in dorsal view (Fig. 10.11, 10.17). This bifurcation of the second sacral rib and the same distal articulations (ilium, first sacral rib) also occurs in *Pamelaria dolichotrachela* (Sen, 2003) and other archosauromorphs (Pritchard et al., 2015; Ezcurra, 2016; Spiekman et al., 2021). Like those of the first sacral rib, the zygapophyses of the second rib are short and both barely extend past the centrum. The prezygapophysis is roofed dorsally by a ridge of bone that overlies the postzygapophysis of the first sacral vertebra when articulated; this ridge is absent in *Azendohsaurus madagaskarensis* (FMNH PR 2777). These are different from hyposphene-hypantrum articulations, which are also absent in the second sacral vertebra. In lateral view, the neural spine is tall, subrectangular in outline (Fig. 10.14), and the dorsal margin is slightly convex.

Vertebral column and ribs: anterior caudal vertebrae.—Representative specimens: PEFO 44009; PEFO 44285. All centra are co-ossified to their respective neural arches.

These centra are the shortest anteroposteriorly in the vertebral column relative to the height of the centrum faces. The centrum faces are slightly concave, and in lateral view they are vertical and subparallel (Fig. 11.1). The chevron facet is prominent posteriorly, and a ventral groove on the centrum is absent. The prominent dorsoventrally thin transverse process projects laterally from the base of the neural arch and is positioned on the anterior half of the vertebra. In anterior view, the transverse process curves ventrolaterally. A shallow fossa occurs posteroventrally at the base of the transverse process (Fig. 11.1). The prezygapophysis is rounded, and the postzygapophysis is positioned relatively high on the neural arch (Fig. 11.2). In lateral view, the neural spine is subrectangular, projects dorsally, and is dorsoventrally tall. No vertebral laminae are present.

Vertebral column and ribs: middle caudal vertebrae.—Representative specimens: PEFO 44017; PEFO 44028; PEFO 44029. All centra are co-ossified to their respective neural arches.

The centrum in these vertebrae is relatively more elongate than in the anterior caudal vertebrae. Chevron facets are prominent on the anterior and posterior rims of the centrum (Fig. 11.3). The transverse planes of the anterior and posterior centrum faces are inclined towards one another ventrally in lateral view. A shallow anteroposteriorly oriented ventral groove is present on the centrum, and it is deepest posteriorly (Fig. 11.4). The transverse process is dorsoventrally thin and projects laterally from just behind the anteroposterior midpoint of the base of the neural

https://doi.org/10.1017/jpa.2022.49 Published online by Cambridge University Press

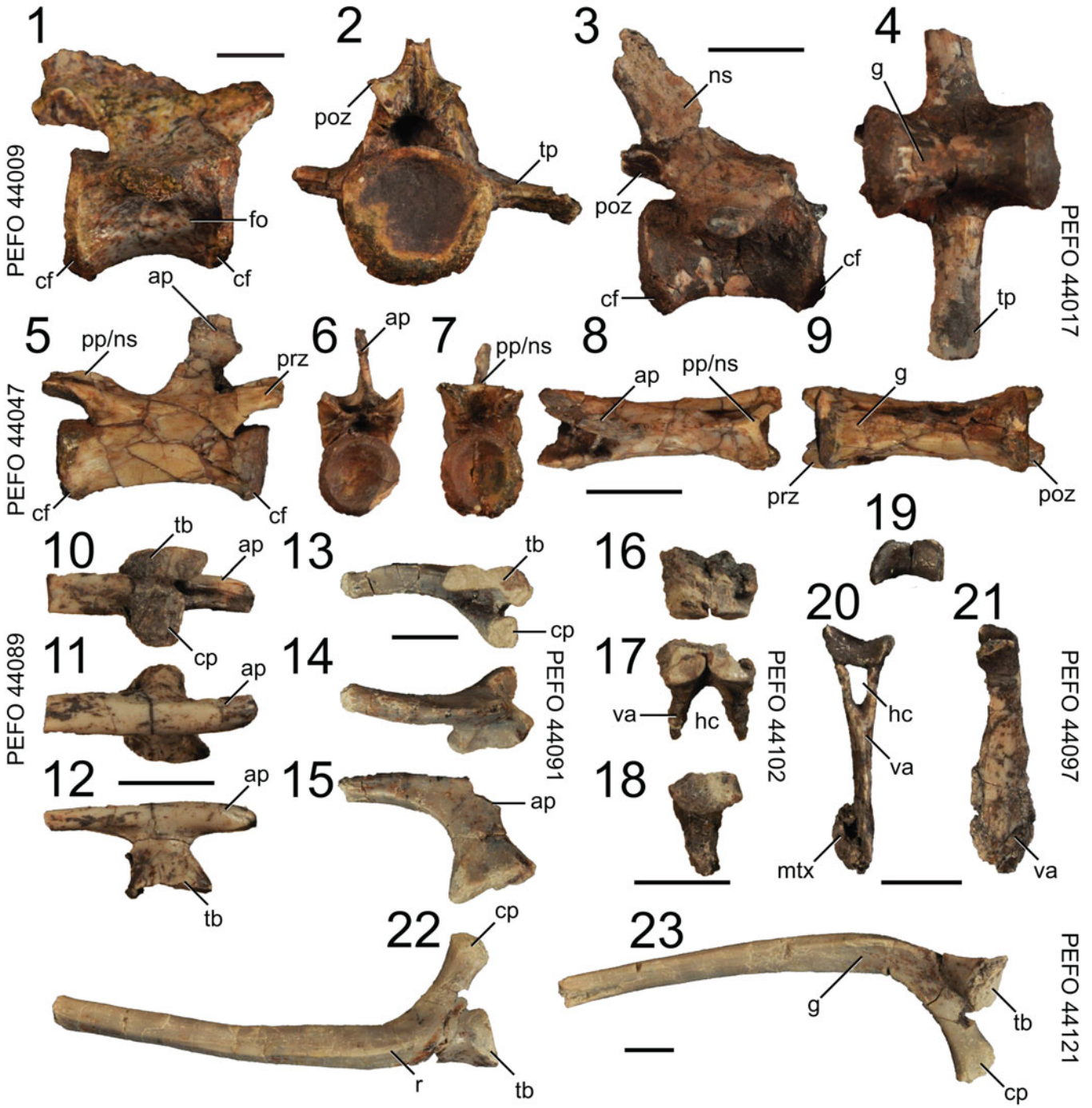

Figure 11. *Puercosuchus traverorum* n. gen. n. sp. in lateral (**1, 3, 5, 11, 14, 18, 21, 22**), medial (**10, 13, 23**), anterior (**6**), posterior (**2, 7, 17, 20**), dorsal (**8, 12, 15, 16, 19**), and ventral (**4, 9**) views. (**1, 2**) Anterior caudal vertebra PEFO 44009; (**3, 4**) middle caudal vertebra PEFO 44017; (**5–9**) posterior caudal vertebra PEFO 44047; (**10–12**) anterior cervical rib PEFO 44089; (**13–15**) posterior cervical rib PEFO 44091; (**16–18**) anterior chevron PEFO 44102; (**19–21**) posterior chevron PEFO 44097; and **(22, 23)** trunk rib PEFO 44121. ap = anterior process; cf = chevron facet; cp = capitulum; fo = fossa; g = groove; hc = hemal canal; mtx = matrix; ns = neural spine; pp = posterior process; poz = postzygapophysis; prz = prezygapophysis; r = ridge; tb = tuberculum; tp = transverse process; va = ventral arm. Scale bars = 1 cm.

arch. The prezygapophysis is more elongate than in the anterior caudal vertebrae, and it projects past the centrum. Posteriorly, the postzygapophysis terminates just posterior of the centrum. The neural spine is positioned on the posterior half of the neural arch (Fig. 11.3). It projects posterodorsally; in lateral view the anterior margin is convex and the posterior margin is concave. The distal end of the neural spine is rounded and slightly expanded anteroposteriorly.

Vertebral column and ribs: posterior caudal vertebrae.—Representative specimens: PEFO 44011; PEFO 44044; PEFO 44047. All centra are co-ossified to their respective neural arches.

https://doi.org/10.1017/jpa.2022.49 Published online by Cambridge University Press

The centrum is elongate and has a shallow ventral anteroposteriorly oriented groove. The elongated centra of *Puercosuchus traverorum* n. gen. n. sp. and other malerisaurines are in contrast to the stockier distal caudals of *Azendohsaurus madagaskarensis* (Nesbitt et al., 2015). The articular faces are subcircular and have small chevron facets anteriorly and posteriorly. These vertebrae lack transverse processes (Fig. 11.5–11.9). The zygapophyses project farther anteriorly and posteriorly than the centrum faces. Two dorsal processes are present on the neural arch; the posterior process (homologous to the neural spine of more-anterior vertebrae) is a low ridge found on the raised surface between the postzygapophyses, and the anterior process is taller and mediolaterally thin, originating posterior to the prezygapophysis and projecting anterodorsally (Fig. 11.5, 11.8). This anterior process is slightly rounded and anteroposteriorly expanded distally. In the posteriormost caudal vertebrae, the posterior process is not present.

Vertebral column and ribs: cervical ribs.—Representative specimens: PEFO 44087; PRFO 44089; PEFO 44091.

The cervical ribs are dichocephalous and possess anterior processes. More-anterior cervical ribs (Fig. 11.10–11.12) are anteroposteriorly longer and dorsoventrally narrow; more-posterior cervical ribs are shorter and rounded (Fig. 11.13–11.15). Unfortunately, all of these specimens are broken distally and their lengths relative to individual cervical vertebrae cannot be determined. In general, the capitulum is round in cross section, and the tuberculum is anteromedially wide, corresponding to those shapes on the parapophysis and diapophysis of the anterior cervical vertebrae, respectively.

Vertebral column and ribs: trunk ribs.—Representative specimens: PEFO 44125; PEFO 44121; PEFO 44117.

The preserved trunk ribs are dichocephalous (Fig. 11.22, 11.23), but because the diapophysis and parapophysis are combined on the posterior trunk vertebrae (Fig. 10.6), the posterior trunk ribs were likely holocephalous. The capitulum and tuberculum of more-anterior trunk ribs are separated by a broad concave margin, but these are much closer together in more-posterior trunk ribs. The articular surfaces are flat and subcircular to suboval in cross section. A short ridge extends from the tuberculum on the posterior edge of the rib. A proximal ridge is present laterally, and a longitudinal groove extends down the medial surface of element. The rib shaft is triangular in cross section proximally and flattens transversely distally.

Vertebral column and ribs: gastral ribs.—Representative specimen: PEFO 44105.

Preserved gastralia are common enough to suggest that an ossified gastral basket was present, but these elements are not associated. The gastral ribs are thin, often overlapping cylindrical elements, with a very gradual taper on both ends.

Vertebral column and ribs: chevrons.—Representative specimens: PEFO 44101 (anterior); PEFO 44102 (anterior); PEFO 44098 (middle); PEFO 44099 (middle); PEFO 44097 (posterior).

The anterior chevrons (Fig. 11.16–11.18) have a large, rounded proximal articular surface. The ventral arms are short and do not meet at the midline, instead they taper ventrally to a point. The middle and posterior chevrons are typical of archosauromorphs (Fig. 11.19–11.21); the ventral arm is anteroposteriorly flat and anteroposteriorly wider in lateral view in the middle chevrons than in the posterior chevrons, which are more tapered and pointed ventrally.

Pectoral girdle: clavicle.—Representative specimen: PEFO 44342, left (distal end).

Of the clavicle, only the distal portion that articulates with the scapula is known (Fig. 12.1–12.3); it is widest distally and tapers proximally. A groove is present on the lateral surface. The articular facet for the scapula is flat.

Pectoral girdle: interclavicle.—Representative specimens: PEFO 44067; PEFO 44068. Both elements are missing the posterior end of the midline process.

The anterior portion of the interclavicle is T-shaped, and the lateral processes taper to rounded points laterally (Fig. 12.4–12.6). In ventral view, the lateral processes are subtriangular. These processes project posterolaterally, and each has an anterior groove for articulation with the clavicles; the interclavicle of *Azendohsaurus madagaskarensis* (FMNH PR 2781) lacks these anterior grooves, but they are present in other archosauromorphs such as *Macrocnemus fuyuanensis* (Jaquier et al., 2017, fig. 6) and *Prolacerta broomi* (Gow, 1975, fig. 23e). The anterior articular grooves of *Puercosuchus traverorum* n. gen. n. sp. do not meet at the midline (Fig. 12.4), similar to those of *Malerisaurus langstoni* (TMM 31099-11). A pair of short bilateral anterior processes is present just lateral to the midline on the anterior edge of the interclavicle (Fig. 12.5, 12.6), differing from the single anterior process found in *Azendohsaurus madagaskarensis* (FMNH PR 2781) and *Shringasaurus indicus* (ISIR 950). The interclavicle of *Malerisaurus langstoni* was reconstructed as lacking any anterior process (Chatterjee, 1986, fig. 6a). Two anterior processes on the interclavicle are also present in *Prolacerta broomi* (Gow, 1975, fig. 233), *Macrocnemus fuyuanensis* (Jaquier et al., 2017, fig. 6), and *Proterosuchus fergusi* Broom, 1903 (Ezcurra, 2016, fig. 38c). A dorsal concavity is present at the junction of the posterior and lateral processes of *Puercosuchus traverorum* n. gen. n. sp.

Pectoral girdle: scapula.—Representative specimens: PEFO 44075 L, PEFO 44076 R (associated with coracoid).

The scapula is an anteroposteriorly broad element that is not co-ossified to the coracoid in any of the specimens (independent of overall size); the two elements in PEFO 44076 are associated, but are disarticulated and not co-ossified (Fig. 12.7–12.12). The scapula is a dorsoventrally tall element like that of other allokotosaurs (TMM 31025-140; Nesbitt et al., 2015, fig. 35; Nesbitt et al., 2021, fig. 1k) and unlike the relatively squat and anteroposteriorly expanded scapula of tanystropheids such *as Macrocnemus fuyuanensis* (Jaquier et al., 2017, fig. 6) and *Tanystropheus longobardicus* (Nosotti, 2007, fig. 7). The glenoid is subtriangular in shape and is roofed dorsally by a rounded ridge (Fig. 12.7). The overall shape is very similar to that of other malerisaurines, including *Malerisaurus robinsonae* (Chatterjee, 1980) and *Malerisaurus langstoni* (Chatterjee, 1986), as well as *Pamelaria dolichotrachela* (ISIR 316/47), *Shringasaurus indicus* (Sengupta and Bandyopadhyay, 2022, fig. 13d), and *Azendohsaurus madagaskarensis* (FMNH PR 2798), although the scapulae of *A. madagaskarensis*, *M. langstoni*, and *S. indicus* are less anteroposteriorly broad and instead, are constricted in lateral view. The glenoid opens posterolaterally (Fig. 12.9). An elliptical

https://doi.org/10.1017/jpa.2022.49 Published online by Cambridge University Press

Figure 12. *Puercosuchus traverorum* n. gen. n. sp. in distal (**1**), lateral (**2, 7, 10**), medial (**3, 8, 11**), anterior (**4**), posterior (**9, 12**), dorsal (**5**), and ventral (**6**) views. (**1–3**) Distal end of left clavicle PEFO 44342; (**4–6**) anterior portion of interclavicle PEFO 44068; (**7–9**) left scapula PEFO 44075; and (**10–12**) right scapula and coracoid PEFO 44076. a.sc = articular surface for scapula; acp = acromion process; ap = anterior process; cof = coracoid foramen; g = groove; gl = glenoid; lp = lateral process; pgp = postglenoid process; tc = tubercle; vt = vertebra. Scale bars = 1 cm.

https://doi.org/10.1017/jpa.2022.49 Published online by Cambridge University Press

tubercle is present on all well-preserved specimens just dorsal to the glenoid, as in *Azendohsaurus madagaskarensis* (Fig. 12.10, 12.12; Nesbitt et al., 2015, fig. 36). The scapular blade and acromion process are mediolaterally thin but anteroposteriorly wide (Fig. 12.7–12.12). The anteroposteriorly expanded dorsal margin of the scapular blade is gently convex. The posterior margin of the element is asymmetrically concave such that the deepest point is just dorsal to the glenoid and ventral to the expansion of the blade. Only one specimen preserves the anterior margin (PEFO 44075), but it is not markedly concave as in *Azendohsaurus madagaskarensis* (FMNH PR 2798).

Pectoral girdle: coracoid.—Representative specimens: PEFO 44339, right (associated with scapula).

The coracoid contribution to the glenoid is suboval and bordered ventrally by a horizontal rounded ridge. The coracoid foramen is suboval and located near the articular margin with the scapula anteroventral to the glenoid. A rounded postglenoid process (Fig. 12.10, 12.11) projects posteriorly just beyond the glenoid, similar to that of *Azendohsaurus madagaskarensis* (FMNH PR 2771) and *Shringasaurus indicus* (Sengupta and Bandyopadhyay, 2022, fig. 13f), but it is not long and rectangular like that of *Trilophosaurus buettneri* (TMM 31025-140).

Forelimb: humerus.—Representative specimens: PEFO 38627, left; PEFO 44129, left; PEFO 47788, right.

The humeri from PFV 217 are badly crushed, making the description and direct comparisons challenging. The proximal surface of the humerus comprises the mediolaterally broad head, a small medial tuberosity, and a prominent lateral tuberosity that projects proximally to the same extent as the head (Fig. 13.1–13.3); this is most similar to *Malerisaurus langstoni* (TMM 31099-11), *Malerisaurus robinsonae* (ISIR 150), and the malerisaurine '*Otischalkia elderae*' (TMM 31025-263), but it is not present in *Azendohsaurus madagaskarensis* (FMNH PR 3816). The deltopectoral crest (Fig. 13.4, 13.5) is robust and expanded mediolaterally much more prominently than that of *Trilophosaurus buettneri* (TMM 31025-140). The dorsal surface of the humerus has a longitudinal ridge similar to that of *Azendohsaurus madagaskarensis* (FMNH PR 3816), but lacks the muscle scar. The midshaft is subcircular in cross section and is more gracile than that of *Azendohsaurus madagaskarensis* (FMNH PR 3816) and *Shringasaurus indicus* (Sengupta and Bandyopadhyay, 2022, fig. 14a–d). The distal half of the humerus is mediolaterally expanded and is slightly wider than the proximal end. A distinct roller surface is present distally for articulation with the radius and ulna; this surface is concave distally, forms two rounded surfaces ventrally, and forms one semilunate surface dorsally. A cuboid fossa is present on the ventral surface of the distal end (Fig. 13.1). In dorsal view, the lateral side of the distal end projects farther distally than the medial side. The ectepicondylar groove is prominent and visible in dorsal view, as it is in many non-archosauriform archosauromorphs (Ezcurra, 2016; Spiekman et al., 2021). A prominent pyramidal process is present on the dorsal surface between the ectepicondylar groove and antebrachial articular surface (Fig. 13.3, 13.6). This process is present in *Azendohsaurus madagaskarensis* (FMNH PR 3816), *Azendohsaurus laaroussii* (Cubo and Jalil, 2019, fig. 1a), *Malerisaurus langstoni* (TMM 31099-11), *Malerisaurus robinsonae* (ISIR 150), and *Shringasaurus indicus* (Sengupta et al., 2017, fig. 3p), but not in *Trilophosaurus buettneri* (TMM 31025-140). Short longitudinal grooves occur on the dorsal surface of the epicondyles of *Puercosuchus traverorum* n. gen. n. sp. The entepicondyle is subsquare in dorsal view, not angled like that of *Trilophosaurus buettneri* (TMM 31025-140). The degree of torsion between the proximal and distal ends is not preserved in any specimen.

Forelimb: radius.—Representative specimens: PEFO 44344, left; NMMNH P-60208, left.

The radius is anteroposteriorly wider proximally than distally (Fig. 13.7, 13.8). In lateral view, the proximal end is subtriangular in outline and has a curved posterior process that extends farther proximally than the rest of the articular surface; *Malerisaurus langstoni* (TMM 31099-11) and *Malerisaurus robinsonae* (ISIR 150) have a pointed posterior process, but it does not extend proximally to the same extent as in *Puercosuchus traverorum* n. gen. n. sp. The presence of such a prominent process across these taxa is a feature that unites them in the Malerisaurinae (Nesbitt et al., 2021). In proximal view, the articular surface is subtriangular in shape; it has a flat medial surface, an anterolateral process, and a tapered posterior process (Fig. 13.9). The proximal surface is concave, not flat like *Azendohsaurus madagaskarensis* (FMNH PR 3816). The distal end is flat and suboval in outline (Fig. 13.10).

Forelimb: ulna.—Representative specimens: PEFO 44131, left; PEFO 47803, right; NMMNH P-63289, left.

The ulna is more expanded proximally than distally (Fig. 13.11, 13.12). The posterior surface is nearly flat, and the anterior surface is rounded. In lateral view, the olecranon process is rounded proximally, not pointed as in *Azendohsaurus madagaskarensis* (FMNH PR 3816). In proximal view (Fig. 13.13), the anteromedial process is pointed and hooked, not round as it is in *Azendohsaurus madagaskarensis* (FMNH PR 3816). In proximal view, a distinct concavity is present between the anteromedial process and olecranon process; this is flat in *Azendohsaurus madagaskarensis* (FMNH PR 3816). In anterior view, the lateral margin is straight and the medial margin is concave. Four longitudinal ridges are present and visible in anterior view (Fig. 13.12, 13.17); these occur on the lateral edge and medial edge, and two ridges extend down the anterior surface. The medial tubercle found below the anteromedial process of *Azendohsaurus madagaskarensis* (FMNH PR 3816) is not present. The distal end of the ulna is suboval in cross section, but is more anteroposteriorly compressed than that of the radius (Fig. 13.14). Two referred ulnae of *Puercosuchus traverorum* n. gen. n. sp. from the Krzyzanowski bonebed (NMMNH P-60209, NMMNH P-63289) include a tall accessory olecranon ossification co-ossified to the proximal end of the element; on both specimens, a suture is visible between the ulna and the ossification in lateral view (Fig. 13.15–13.17). This does not occur in any of the hypodigm, but it is similar to the proximal end of a previously published ulna from the Dockum Group of Texas (TTU-P 11386; Lessner et al., 2018, fig. 5g). Among reptiles, hypertrophic olecranon ossifications like these are also known in some archosauromorphs (e.g., *Protorosaurus speneri*; Gottmann-Quesada and Sander, 2009, text-fig. 22) and the sauropodomorph dinosaur *Saturnalia tupiniquim* Langer et al., 1999 (Langer et al., 2007, fig. 8).

https://doi.org/10.1017/jpa.2022.49 Published online by Cambridge University Press

Figure 13. *Puercosuchus traverorum* n. gen. n. sp. in ventral (**1**), lateral (**2, 16**), dorsal (**3**), medial (**4**), proximal (**5, 9, 13**), distal (**6, 10, 14**), anterior (**7, 12, 17**), and posterior (**8, 11, 15**) views. (**1–6**) Left humerus PEFO 38627; (**7–10**) left radius PEFO 44344; (**11–14**) left ulna PEFO 44131; and (**15–17**) left ulna NMMNH P-63289. Arrows point in anterior direction. amp = anteromedial process; cbf = cuboid fossa; dpc = deltopectoral crest; g = groove; h = head; ltb = lateral tuberosity; mtb = medial tuberosity; oo = olecranon ossification; op = olecranon process; pmp = pyramidal process; pp = posterior process; r = ridge; s = suture; st = striations. Scale bars = 1 cm.

https://doi.org/10.1017/jpa.2022.49 Published online by Cambridge University Press

Forelimb: metacarpals.—Representative specimens (Fig. 14.1–14.6): PEFO 44366 I, left; PEFO 44365 II, right; PEFO 44181 III, left; PEFO 44364 IV, left; PEFO 44178 V, right.

The proximal end of metacarpal I is not known from any specimens. The distal end is triangular in outline and is dorsoventrally tallest laterally. On the distal end, a fossa is present

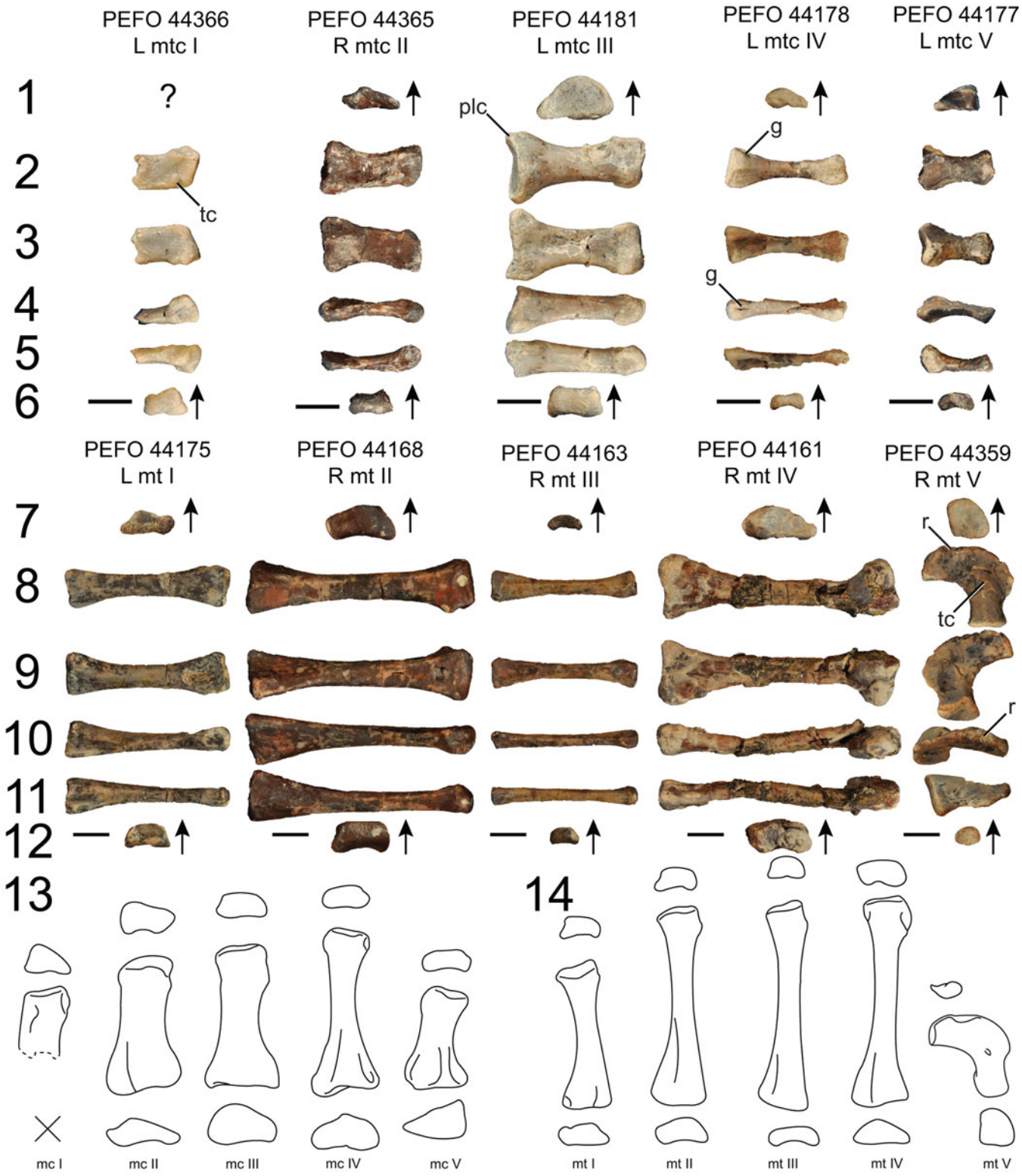

Figure 14. *Puercosuchus traverorum* n. gen. n. sp. in proximal (**1, 7**), dorsal (**2, 8**), ventral (**3, 9**), lateral (**4, 10**), medial (**5, 11**), and distal (**6, 12**) views. (**1–6**) Metacarpals; (**7–12**) metatarsals; reconstructions of right metacarpals (**13**) and right metatarsals (**14**) are shown in proximal, dorsal, and distal views. Arrows point in dorsal direction. g = groove; mtc = metacarpal; mt = metatarsal; plc = posterolateral corner; r = ridge; tc = tubercle. Scale bars = 1 cm.

https://doi.org/10.1017/jpa.2022.49 Published online by Cambridge University Press

on the lateral side and a tubercle is present on the dorsal surface near the medial edge (Fig. 14.2).

The proximal end of metacarpal II is slightly concave in dorsal view. The proximal outline is subtriangular with an apex closer to the medial side (Fig. 14.1). In proximal view, the ventral margin is concave. In dorsal view, the lateral concavity is deeper than the medial concavity. The distal end bears a lateral ligament fossa.

The proximal outline of metacarpal III is dorsoventrally tall, more so medially than laterally. In dorsal view, the proximolateral corner projects proximally (Fig. 14.2). In dorsal view, the lateral concavity is deeper than the medial concavity. The distal end has a lateral ligament fossa.

The lateral half of the proximal end of metacarpal IV is concave, and the articular surface is visible in dorsal view. The medial side of the articular surface is offset proximally. In proximal view, there is a concavity on the ventral margin. A groove is present proximally on the dorsal surface near the lateral edge (Fig. 14.2, 14.4). The distal end lacks ligament fossae, but the lateral side has a rounded tubercle.

Metacarpal V is proximodistally short. The proximal outline is strongly triangular (Fig. 14.1), and the dorsoventral tallest point is on the lateral side. In dorsal view, the proximal surface is concave. The proximodorsal surface is gently concave and the distal end lacks ligament fossae.

Pelvic girdle: ilium.—Representative specimens: PEFO 44069, right; PEFO 44336, left.

The preacetabular process (Fig. 15.1, 15.2) is rounded, but is much shorter than that of *Azendohsaurus madagaskarensis* (FMNH PR 2794) and *Shringasaurus indicus* (Sengupta and Bandyopadhyay, 2022, fig. 16a), and is more similar to that of *Trilophosaurus buettneri* (TMM 31025-140), *Malerisaurus robinsonae* (Chatterjee, 1980, fig. 10a), *Macrocnemus fuyuanensis* (Jaquier et al., 2017, fig. 8f), *Tanystropheus longobardicus* (Nosotti, 2007, fig. 25), and *Prolacerta broomi* (Spiekman, 2018, fig. 11a). The postacetabular process is elongate, extending well beyond the posterior margin of the ischial peduncle. It tapers posteriorly and has longitudinal striations extending from the dorsal edge of the blade anteroventrally on the lateral and medial sides (Fig. 15.1, 15.2). The supraacetabular crest is prominent; it extends from the anteroposterior midpoint above the acetabulum to the anterior tip of the pubic peduncle. In lateral view, the ischiac peduncle is kinked such that anterior half faces posteroventrally and the posterior half faces ventrally (Fig. 15.1). The ischiac peduncle has a prominent lateral spur (best seen in ventral view; Fig. 15.3), which is absent in *Trilophosaurus buettneri* (TMM 31025-77) and *Azendohsaurus madagaskarensis* (FMNH PR 2794). This prominent lateral spur could be a unique character of *Puercosuchus traverorum* n. gen. n. sp. or a synapomorphy of Malerisaurinae. Two tubercles are present on the lateral surface of the ilium (robust in PEFO 44336, small in PEFO 44069); one is positioned at the tallest point of the supraacetabular crest, the other occurs near the anteriormost portion of the preacetabular process (Fig. 15.1, 15.3), and neither is present in *Azendohsaurus madagaskarensis* (FMNH PR 2794) or *Shringasaurus indicus* (Sengupta and Bandyopadhyay, 2022, fig. 16a). The tubercle on the preacetabular process, which is present in some specimens of *Trilophosaurus buettneri* (e.g., TMM 31025-77), may be homologous to a similar feature found in some tanystropheids such as *Tanystropheus longobardicus* (Spiekman et al., 2021, fig. 32b) and *Macrocnemus bassanii* (Rieppel, 1989, fig. 4b). The dorsal margin of the postacetabular process is straight, unlike the gently concave dorsal margin in *Azendohsaurus madagaskarensis* (FMNH PR 2794) and *Shringasaurus indicus* (Sengupta et al., 2017, fig. 3k). In medial view, the depressed articular surface for the first sacral rib occurs just behind the preacetabular process and is subcircular (Fig. 15.2). The articular surface for the second sacral rib is a flat, suboval surface on the anteroventral surface of the postacetabular process. The articular surfaces for the two sacral ribs are separated from one another and do not touch near the center of the element, unlike those of *Azendohsaurus madagaskarensis* (FMNH PR 2794).

Pelvic girdle: ischium.—Representative specimen: PEFO 44458, left.

The ischium (Fig. 15.4–15.6), which is very similar in shape to that of *Azendohsaurus madagaskarensis* (FMNH PR 2794), projects farther posteriorly than in *Trilophosaurus buettneri* (TMM 31025-140). In lateral view, the posterodorsal edge posterior to the acetabulum is concave, and the ventral margin is straight. The medial surface lacks the broad ventral articular facet for the other ischium that is found in *Azendohsaurus madagaskarensis* (FMNH PR 2794). The anterior margin is gently concave, similar to that of *Trilophosaurus buettneri* (TMM 31025-78), *Azendohsaurus madagaskarensis* (FMNH PR 2794), and *Prolacerta broomi* (Spiekman, 2018, fig. 11a), but it is not deeply excavated like in some tanystropheids (Nosotti, 2007, fig. 25; Jaquier et al., 2017, fig. 8h).

Pelvic girdle: pubis.—Representative specimen: PEFO 44080, left.

The anterior margin of the pubis is thickened and forms the anterodorsal rim of the pubic apron. The ambiens process (Fig. 15.7, 15.8) is a short flange that is continuous with the acetabulum, which is similar to that of *Azendohsaurus madagaskarensis* (FMNH PR 2794) and other malerisaurines, but not a tall crest like in *Trilophosaurus buettneri* (TMM 31025-140). The single pubic (obturator) foramen penetrates the pubic apron proximally near the contact with the ischium. The proximal portion of the pubis is concave laterally, and the ventral part of the pubic apron is anteroposteriorly broad and concave laterally.

Hindlimb: femur.—Representative specimens: PEFO 44191, right; PEFO 44190, left; PEFO 44189, left and right; PEFO 44194, right; NMMNH P-60208, right.

The femur (Fig. 16.1–16.12) is sigmoid in dorsal outline and more gracile (= smaller diameter at midshaft relative to length) than that of *Azendohsaurus madagaskarensis* (FMNH PR 2749) and *Shringasaurus indicus* (Sengupta and Bandyopadhyay, 2022, fig. 17a–d). The proximal third includes a prominent internal trochanter that is squared-off at its proximal margin in ventral view (Fig. 16.8). The internal trochanter is blade-like (most similar to *Malerisaurus langstoni* [TMM 31099-11] and *Malerisaurus robinsonae* [ISIR 150]) as opposed to the rounded knob found in *Azendohsaurus madagaskarensis* (FMNH PR 2749), *Azendohsaurus laaroussii* (Cubo and Jalil, 2019, fig. 1c), and *Shringasaurus indicus* (Sengupta and Bandyopadhyay, 2022, fig. 17c); these differences in the feature are likely correlated with differences in absolute size (Nesbitt et al., 2021). The proximal height of the internal

https://doi.org/10.1017/jpa.2022.49 Published online by Cambridge University Press

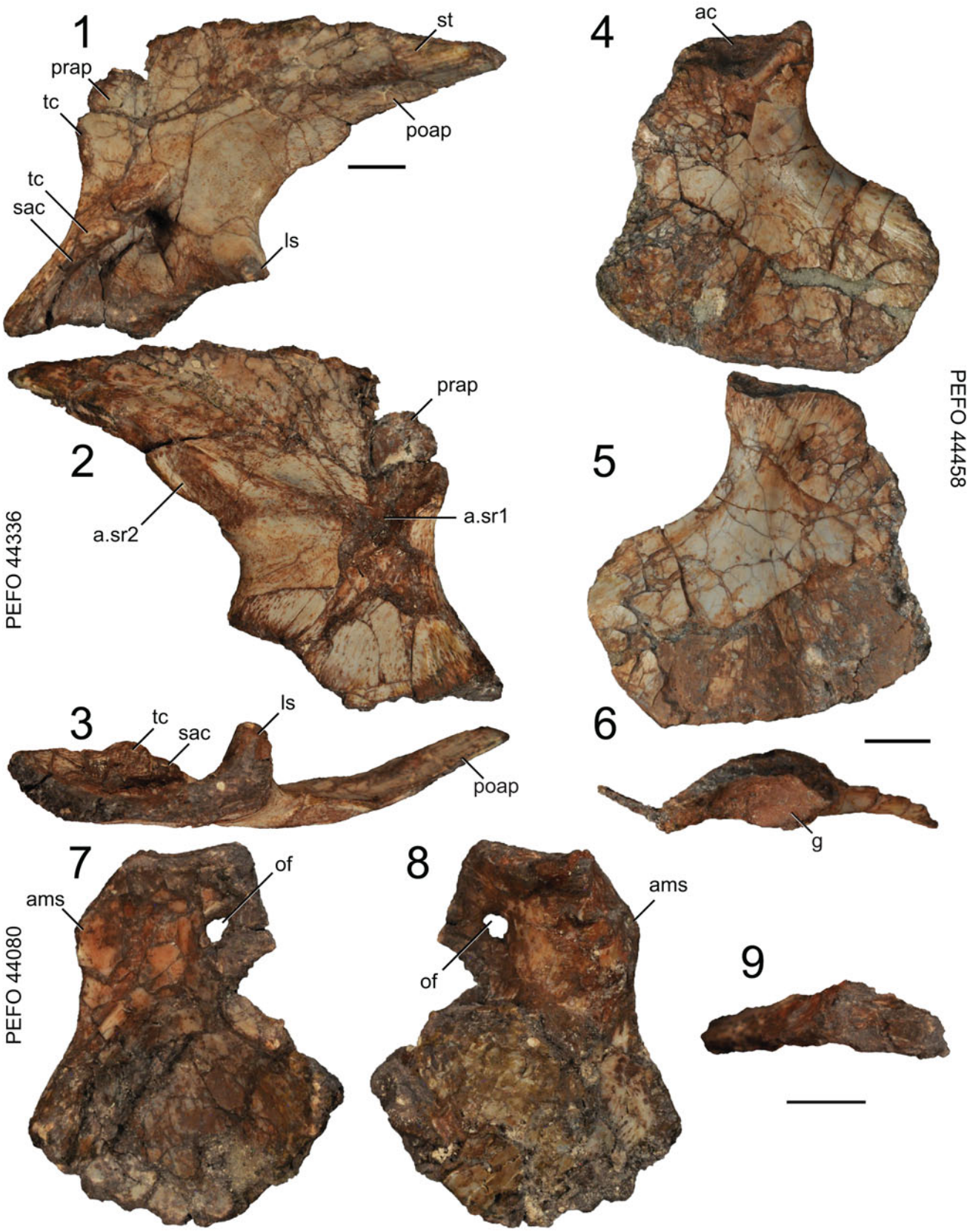

Figure 15. *Puercosuchus traverorum* n. gen. n. sp. in lateral (**1, 4, 7**), medial (**2, 5, 8**), ventral (**3**), and dorsal (**6, 9**) views. (**1–3**) Left ilium PEFO 44336; (**4–6**) left ischium PEFO 44458; and (**7–9**) left pubis PEFO 44080. a.sr1 = articular surface for first sacral rib; a.sr2 = articular surface for second sacral rib; ac = acetabulum; ams = ambiens process; g = groove; ls = lateral spur; of = obturator foramen; poap = postacetabular process; prap = preacetabular process; sac = supraacetabular crest; st = striations; tc = tubercle. Scale bars equal 1 cm.

https://doi.org/10.1017/jpa.2022.49 Published online by Cambridge University Press

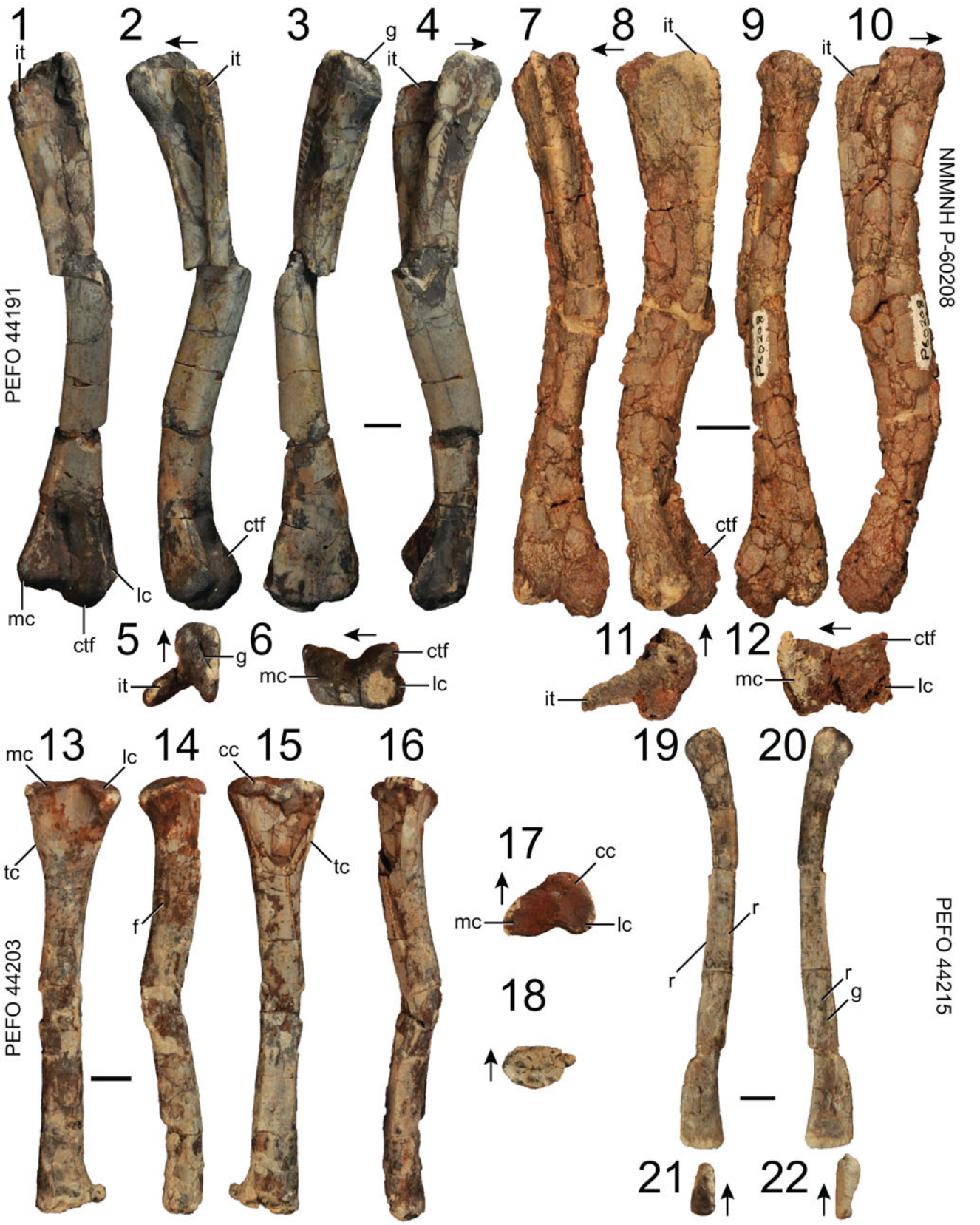

Figure 16. *Puercosuchus traverorum* n. gen. n. sp. in posteroventral (**1, 7**), ventral (**2, 8**), anterodorsal (**3, 9**), dorsal (**4, 10**), posterior (**13**), anterior (**15**), lateral (**14, 19**), medial (**16, 20**), proximal (**5, 11, 17, 21**), and distal (**6, 12, 18, 22**) views. (**1–6**) Right femur PEFO 44191; (**7–12**) right femur NMMNH P-60208; (**13–18**) right tibia PEFO 44203; and (**19–22**) left fibula PEFO 44215. Arrows point in anterior direction. cc = cnemial crest; ctf = crista tibiofibularis; f = foramen; g = groove; it = internal trochanter; lc = lateral condyle; mc = medial condyle; r = ridge; tc = tubercle. Scale bars = 1 cm.

https://doi.org/10.1017/jpa.2022.49 Published online by Cambridge University Press

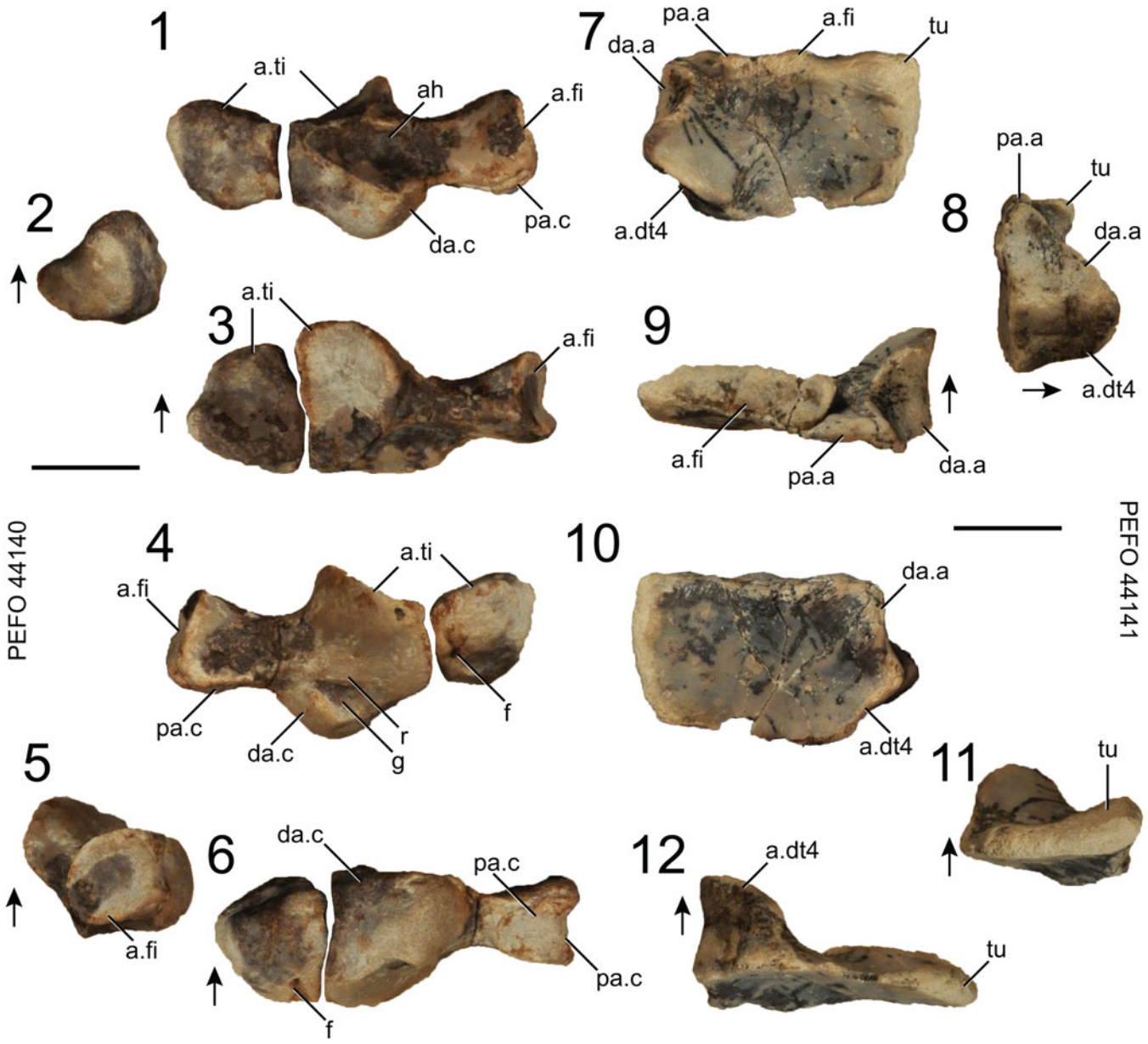

Figure 17. *Puercosuchus traverorum* n. gen. n. sp. in dorsal (**1, 7**), medial (**2, 8**), proximal (**3, 9**), ventral (**4, 10**), lateral (**5, 11**), and distal (**6, 12**) views. (**1–6**) Left astragalus and pedal centrale PEFO 44140; and (**7–12**) left calcaneum PEFO 44141. Arrows point in dorsal direction. a.dt4 = articular surface for distal tarsal 4; a.fi = articular surface for fibula; a.ti = articular surface for tibia; ah = anterior hollow; da.a = distal articular surface for astragalus; da.c = distal articular surface for calcaneum; f = foramen; g = groove; pa.a = proximal articular surface for astragalus; pa.c = proximal articular surface for calcaneum; r = ridge; tu = calcaneal tuber. Scale bars = 1 cm.

trochanter is variable in *Puercosuchus traverorum* n. gen. n. sp.—sometimes it is even with the proximal end (Fig. 16.8), and sometimes it is set down-shaft from the proximal end by a short flat area (Fig. 16.4), similar to the sample of *Trilophosaurus buettneri* from Otis Chalk Quarry 1 (TMM 31025). The internal trochanter is perpendicular to the long axis of the proximal end. The proximal outline is triangular, thickens anteriorly, and has a transverse groove (Fig. 16.5). This is unlike the condition of *Azendohsaurus madagaskarensis* (FMNH PR 2749) and *Shringasaurus indicus* (Sengupta et al., 2017, fig. 3j), in which the proximal end is more rounded and lacks the transverse groove. The midshaft is hollow and suboval in cross section. The distal end is transversely expanded into prominent lateral and medial condyles. The crista tibiofibularis is large and extends distally past the lateral condyle in ventral view. A deep groove is present laterally between the crista tibiofibularis and the lateral condyle (Fig. 16.6, 16.12). A shallower groove is present distally between the lateral and medial condyles. The medial condyle tapers to a point medioventrally in distal view. A sharp ridge extends down the posteroventral surface of the crista tibiofibularis. The anterodorsal surface of the distal end is rugose in some specimens (e.g., PEFO 44367). A large nutrient foramen is present at the proximodistal midpoint of the femur on the dorsal surface.

Hindlimb: tibia.—Representative specimens: PEFO 44202, right; PEFO 44203, right; PEFO 44197, left.

https://doi.org/10.1017/jpa.2022.49 Published online by Cambridge University Press

The tibia has a subtle anterior convexity along its length. The posterior cleft between the proximal medial condyle and lateral condyle (Fig. 16.17) is more prominent than in *Azendohsaurus madagaskarensis* (FMNH PR 3814). The cnemial crest is not as prominent as that of *Azendohsaurus madagaskarensis* (FMNH PR 3814) anteriorly. The anteromedial depression found in *Azendohsaurus madagaskarensis* (FMNH PR 3814) is present, but is usually distorted as a result of taphonomy. In posterior view, the medial surface of the proximal medial condyle has a low tubercle (Fig. 16.13, 16.15), which is also present in *Malerisaurus langstoni* (TMM 31099-11) and *Malerisaurus robinsonae* (ISIR 150), but is absent in *Azendohsaurus madagaskarensis* (FMNH PR 3814). A large nutrient foramen is positioned on the lateral surface below the lateral condyle on the proximal half of the element (Fig. 16.14). The shaft of the tibia lacks the medial ridge found in *Azendohsaurus madagaskarensis* (FMNH PR 3814). The proximal half of the shaft is subtriangular in cross section and it transitions to a subcircular cross section distally. The distal end is subtriangular but rounded in outline (Fig. 16.18).

Hindlimb: fibula.—Representative specimens: PEFO 44372, left; PEFO 44212, right; PEFO 44215, left.

The fibula is sigmoid in medial and lateral view (Fig. 16.19, 16.20); the proximal half is convex anteriorly, and the distal half is convex posteriorly. The element is mediolaterally compressed down its length. The distal end is anteroposteriorly longer than the proximal end, as it is in *Azendohsaurus madagaskarensis* (FMNH PR 3813). Two ridges are present on the anterior and posterior edges (Fig. 16.19), as in *Azendohsaurus madagaskarensis* (FMNH PR 3813). A rounded ridge and corresponding groove on the medial surface of the distal end is present (Fig. 16.20). The proximal outline is mediolaterally compressed, but the posterior end is slightly wider than the anterior end. The distal outline is widest anteriorly. The largest specimen (PEFO 44212) is very robust and has a number of prominent muscle scars not found on smaller specimens, including a tubercle on the medial side of the proximal end and tubercles on the anterior and posterior edge on the distal half. The rounded ridge on the medial surface of the distal end is rugose and striated.

Hindlimb: astragalus + centrale.—Representative specimen: PEFO 44140, left.

These two elements were found tightly articulated, but not co-ossified (Fig. 17.1–17.6), similar to the condition in *Trilophosaurus buettneri* (Gregory, 1945; TMM 31025-140). The centrale is a rounded element with flat articular surfaces for the tibia and astragalus. The ventral side of the centrale has a foramen near the articular surface for the astragalus (Fig. 17.4). In proximal view, the centrale has a subtle medial point. Overall, the astragalus is more similar in shape to that of *Trilophosaurus buettneri* (TMM 31025-140) than *Azendohsaurus madagaskarensis* (FMNH PR 2776). The astragalus is relatively mediolaterally wider than that of *Azendohsaurus madagaskarensis* (FMNH PR 2776), especially along the process extending from the main body of the element that includes the articular surface for the fibula. That process has a concave, saddle-shaped articular surface for the fibula laterally and a grooved proximal articular surface for the calcaneum visible in distal view (Fig. 17.6). The distal articular surface for the calcaneum is broad and has a ventral lip. A short mediolateral ridge is found on the ventral surface proximal to the distal articular surface for the calcaneum (Fig. 17.4). This ridge is not present in any other allokotosaur, but the groove formed between it and the distal articular surface for the calcaneum (Fig. 17.4) is equivalent to the 'posterior groove' (Gower, 1996, p. 353) found in *Azendohsaurus madagaskarensis* (FMNH PR 2776) and several other archosauromorphs (Nesbitt, 2011, p. 166). The anterior hollow is prominent on the dorsal surface of the astragalus (Fig. 17.1). The articular surface for the tibia is concave proximally and has a proximoventral lip (Fig. 17.3).

Hindlimb: calcaneum.—Representative specimen: PEFO 44141 L.

The calcaneum (Fig. 17.7–17.12) is subrectangular in dorsal outline. It lacks a distal concavity; the distal and proximal edges are straight. The lateral margin is slightly rounded, as it is in *Azendohsaurus madagaskarensis* (FMNH PR 2776), but not as rounded as that of *Trilophosaurus buettneri* (TMM 31025-140). Much of the proximal surface forms the long articular surface for the fibula (Fig. 17.9). A gap between the fibular facet and proximal articular surface for the astragalus forms a canal when articulated with the astragalus. The medial foramen found in *Azendohsaurus madagaskarensis* (FMNH PR 2776) is not present. The medial end of the calcaneum forms a concave distal articular surface for the astragalus and a flat articular surface that faces mediodistally for distal tarsal 4. The calcaneal tuber is dorsoventrally thickened along its laterodistal corner (Fig. 17.11). The dorsal and ventral surfaces are mostly flat, and the element lacks a ventral concavity found in *Azendohsaurus madagaskarensis* (FMNH PR 2776).

Hindlimb: metatarsals.—Representative specimens (see Fig. 14.7–14.13): PEFO 44175 I, left; PEFO 44168 II, right; PEFO 44163 III, right; PEFO 44161 IV, right; PEFO 44359 V, right.

The proximal end of metatarsal I is rotated 45° medially relative to the distal end. In proximal view, the proximal end has a tall central process and secondary medial process (Fig. 14.7), with a depression between these in dorsal view. The proximal surface is flat and mediolaterally expanded. The distal end has a lateral ligament fossa. In dorsal view, the medial concavity is deeper than the lateral concavity.

The dorsal margin of the proximal outline of metatarsal II is convex and the ventral margin is concave (Fig. 14.7). The proximal end is rotated 60° medially relative to the distal end. The proximal surface is flat, and the proximal outline is asymmetrical such that the dorsoventral height is greatest closer to the lateral side. The distal end has a lateral ligament fossa.

Overall, metatarsal III is very similar in shape to metatarsal II, but it is relatively shorter dorsoventrally. The degree of proximodistal torsion is not evident due to poor preservation.

The proximal outline of metatarsal IV is subtriangular; the triangle is dorsoventrally tallest closer to the medial side (Fig. 14.7). The proximal surface is slightly concave and has a proximomedial projection. Lateral and medial distal ligament fossae are present, but the medial fossa is very faint. There is very little proximodistal torsion.

The proximal articular surface of metatarsal V is subtrapezoidal in outline. In dorsal view, the proximal process is intermediate in length between the short process of *Azendohsaurus*

https://doi.org/10.1017/jpa.2022.49 Published online by Cambridge University Press

madagaskarensis (FMNH PR 2776) and the long process of *Trilophosaurus buettneri* (TMM 31025-140). The distal end is dorsoventrally thickened, and the lateral edge has a rounded ridge (Fig. 14.8) dorsally, which is also present in *Azendohsaurus madagaskarensis* (FMNH PR 2776). A tubercle is present on the dorsal surface between the articular surface and the distal process (Fig. 14.8), which is not present in *Azendohsaurus madagaskarensis* (FMNH PR 2776) or *Trilophosaurus buettneri* (TMM 31025-140).

Etymology.—'traverorum' honors Brad and Denise Traver, the former Superintendent at Petrified Forest National Park and his wife who strongly supported the paleontology program at the park.

Materials.—491 specimens from PFV 217 are considered referred specimens (see Supplemental Data 1 for complete list), comprising the premaxilla, maxilla, nasal, frontal, prefrontal, parietal, quadrate, dentary, surangular, articular, palatine, pterygoid, basioccipital, parabasisphenoid, opisthotics + supraoccipital, prootic, cervical, trunk, sacral, and caudal vertebrae, clavicle, interclavicle, scapula, coracoid, humerus, radius, ulna, metacarpals and some manual phalanges, ilium, ischium, pubis, femur, tibia, fibula, astragalus, pedal centrale, calcaneum, metatarsals, and some pedal phalanges. Unopened field jackets are still being prepared, so more specimens may be added as referred specimens. Additional referred materials include associated and isolated cranial and postcranial elements from NMMNH L-3764 that previously were identified as *Trilophosaurus* cf. *T. jacobsi* Murry, 1987 (Spielmann et al., 2013b) or other taxa (see Supplemental Data 1 for complete list). Linear measurements of select long bones from PEFO and NMMNH are found in Supplemental Data 2.

Remarks.—*Puercosuchus traverorum* n. gen. n. sp. is diagnosed based on an associated maxilla and premaxilla, given that these elements are clearly unique among all other archosauromorphs. However, differentiating *Puercosuchus traverorum* n. gen. n. sp. from its close relatives, *Malerisaurus robinsonae* and *Malerisaurus langstoni*, solely based on the premaxilla and maxilla is difficult given that these elements in the holotypes and referred specimens of both *M. robinsonae* and *M. langstoni* are absent or poorly preserved, which will always be the case for comparisons across these taxa. The differences between *Puercosuchus traverorum* n. gen. n. sp. and *Malerisaurus* spp. largely lie in the postcrania, and although these elements of *Puercosuchus traverorum* n. gen. n. sp. will always be considered referred specimens, they are almost certainly from the same species, or possibly even the same individual as the holotype.

Discussion

Taphonomy of PFV 217.—As of September 23, 2021, 492 individual elements were catalogued from PFV 217 that belong to the hypodigm of *Puercosuchus traverorum* n. gen. n. sp. (Supplemental Data 1), and there are hundreds more elements in unprepared field jackets. The vast majority of the collected elements were disarticulated and unassociated, and no preferred direction was observed in the field (although directional measurements were not taken). The front half of the quarry (~3 m) was more fossiliferous than the back half of the quarry, resulting in more field jackets being collected from the former; elements were more often collected in isolation from the latter (Fig. 1.3).

The bones were most concentrated on the lower surface of a sheet-like clay-supported sandstone unit that overlies a fine-grained paleosol. The upper fossiliferous unit is 0.68 m thick at the quarry and is interpreted to represent a thin crevasse channel or crevasse splay that quickly concentrated skeletal remains from overbank surfaces and swept them into a localized topographic low (e.g., Miall, 1996, 2010), similar to what has been interpreted for NMMNH L-3764 (Heckert, 2004) and the *Shringasaurus indicus* bonebed (Sengupta and Sengupta, 2021). The bone layer at PFV 217 is a poorly sorted, yellowish gray (5Y 8/1), very fine-grained, clay-supported sandstone that includes chert pebbles, granule-sized quartz grains, and vertebrate bones and teeth. It overlies a grayish blue (5PB 5/2) siltstone that includes yellowish gray (5Y 8/1) reduction halos and mottles and dark reddish brown (10R 3/4) iron oxide stains along pervasive slickensides. The slickensides are present to a lesser degree in the bone layer itself, and they often result in microfaulting of the skeletal elements themselves (Fig. 18.2). The surface between the upper bone layer and the lower siltstone is hummocky, and vertical dikes comprising the lithology of the upper layer extend down into the lower unit, indicating that this sequence represents a vertisol paleosol (Tabor et al., 2017). A prominent normal fault with an estimated displacement of ~30 cm is present on the east side of the quarry. Because the fault was not excavated laterally, its dip direction could not be accurately measured.

Of the bones collected and prepared from PFV 217, the vast majority (>90%) are referred to the malerisaurine azendohsaurid *Puercosuchus traverorum* n. gen. n. sp., with isolated bones and teeth of at least 12 other vertebrate taxa (see Occurrence above). Thus, this death assemblage is considered a relatively high diversity, multitaxic but monodominant, mixed microfossil- and macrofossil-dominated bonebed (Eberth et al., 2007). The bones are disarticulated, and association is rare, even within collected field jackets. In fact, the only obviously associated remains of *Puercosuchus traverorum* n. gen. n. sp. at PFV 217 are the holotype right premaxilla and maxilla (PEFO 43914), a right scapula and coracoid (PEFO 44076), and left femur and right tibia (PEFO 44190). There is a minimum of 6–8 individuals of *Puercosuchus traverorum* n. gen. n. sp. based on six right quadrates, seven left fibulae, and eight right fibulae. Many of the long bones are missing one or both ends or the midshaft (Fig. 13.1–13.4), and the pedogenic slickensides through the quarry often results in warping or short displacements (Figs. 16.1–16.4, 18.2, 18.5, 18.6). Unlike the rare associations found at PFV 217, more of the elements preserved at the Krzyzanowski bonebed (NMMNH L-3764) were found in association (Heckert, 2004), including NMMMNH P-44128 (dentigerous and post-dentary bones), NMMNH P-62816 (hindlimb and pes), NMMNH P-60208 (vertebrae, humerus, radius, and femora), NMMNH P-44174 (ilium and ischium), and NMMNH P-40939 (vertebrae and ilium).

https://doi.org/10.1017/jpa.2022.49 Published online by Cambridge University Press

Figure 18. *Puercosuchus traverorum* n. gen. n. sp. in anterior (**1–4**), lateral (**5**), medial (**6**), proximal (**7, 13**), distal (**8, 14**), posteroventral (**9**), ventral (**10, 15**), anterodorsal (**11**), and dorsal (**12, 16**) views. (**1**) Right tibia PEFO 44190; (**2**) right tibia PEFO 44200; (**3**) right tibia PEFO 44203; (**4**) left tibia PEFO 44197; (**5–8**) robust right fibula PEFO 44212; (**9–14**) pathological right femur PEFO 44194; and (**15–16**) large left humerus PEFO 38268, similar to the hypodigm of '*Otischalkia elderae*'. Arrows point in anterior direction. ctf = crista tibiofibularis; dpc = deltopectoral crest; g = groove; h = head; it = internal trochanter; lc = lateral condyle; ltb = lateral tuberosity; mc = medial condyle; mf = microfault; mtb = medial tuberosity; pmp = pyramidal process; pth = pathology; r = ridge; tc = tubercle. Scale bars = 1 cm.

https://doi.org/10.1017/jpa.2022.49 Published online by Cambridge University Press

Intraspecific variation in Puercosuchus traverorum *n. gen. n. sp.*—The number of individuals in PFV 217 provides some opportunities to assess different sources of intraspecific variation in this new malerisaurine azendohsaurid. The most obvious evidence of intraspecific variation in *Puercosuchus traverorum* n. gen. n. sp. is the relative size of its skeletal elements, especially the long bones (Fig. 18.1–18.4). For example, the length of the proximodistally shortest complete tibia (PEFO 44205) is 64 mm and the longest complete tibia (PEFO 44190) is 150 mm, with 11 other complete tibiae of intermediate lengths (Supplemental Data 2). When plotted against the minimum midshaft diameters, the proximodistal lengths of all tibiae (n = 13) fit a linear regression line with a $R^2 = 0.86$ (Fig. 19). Indeed, most other non-metapodial long bones fit lines with a similar slope (0.093–0.14) except for the humeri (0.28; Fig. 19), although n = 4 for those elements. This suggests that if relative size is a proxy for ontogenetic status (see below), most of the limb bones grew isometrically with respect to an individual element (i.e., all femora) as well as other types of elements (i.e., all femora, tibiae, and fibulae).

Of course, it has been demonstrated that relative size (as approximated from long-bone lengths) is not necessarily a good indicator of ontogenetic status in saurians (Griffin et al., 2020, p. 496) "for taxa that have poorly constrained life histories" in the absence of a robust estimate of the size range for that taxon unless "used in conjunction with other methods of assessing maturity to bolster a diagnosis." We argue that at least the extreme ends of the size range found at PFV 217 (i.e., the shortest and longest limb bones) represent less mature and more mature individuals, respectively, because certain long-bone elements differ in the number and/or robusticity of muscle scars (Griffin and Nesbitt, 2016; Griffin, 2018; Müller et al., 2019; Griffin et al., 2020). For example, one of the shortest fibulae (PEFO 44215, 110 mm) has a ridge on both the anterior and posterior edges (Fig. 16.19), while one of the longest fibulae (PEFO 44212, 134 mm) has prominent tubercles in the place of those ridges and an additional tubercle on the medial surface of the proximal end (Fig. 18.6). Further, histological analyses of larger (PEFO 38627) and smaller (TMM 31099-84 and TMM 31099-1488) humeri from malerisaurine azendohsaurids, including *Puercosuchus traverorum* n. gen. n. sp. (PEFO

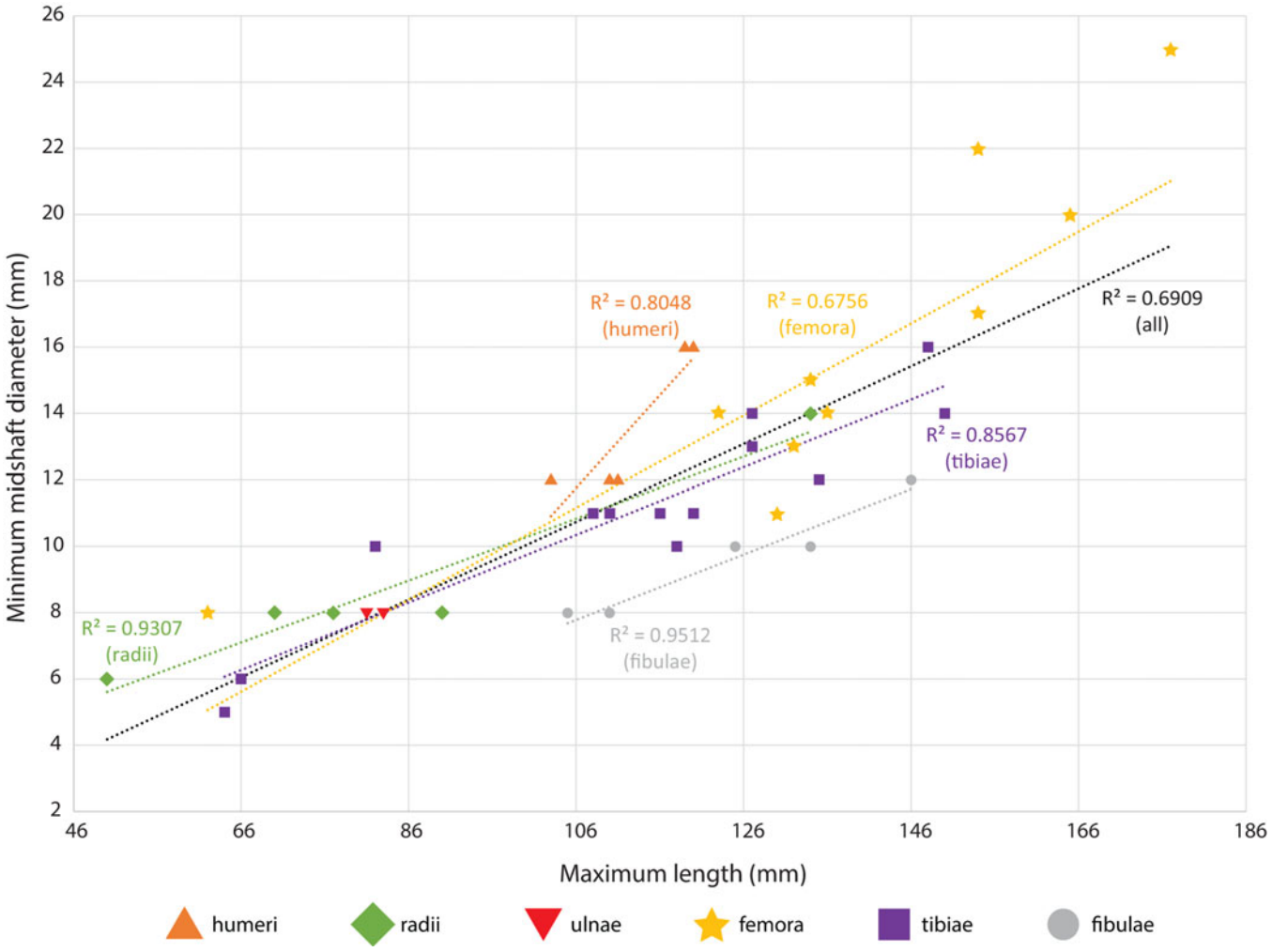

Figure 19. Maximum proximodistal length and minimum midshaft diameter of non-metapodial long bones from *Puercosuchus traverorum* n. gen. n. sp. at PFV 217, with linear regression lines and R^2 values. Note that only two ulnae preserve both of these measurements, so a linear regression was not provided. Measurements are provided in Supplemental Data 2.

https://doi.org/10.1017/jpa.2022.49 Published online by Cambridge University Press

38627), suggest that larger humeri are associated with osteohistological characteristics of more skeletally mature individuals, including a relatively open medullary cavity, more lines of arrested growth, and the presence of an external fundamental system (Nesbitt et al., 2021, figs. 9, 10). In the absence of more histological analyses of elements from *Puercosuchus traverorum* n. gen. n. sp. (see Nesbitt et al., 2021, p. 19) similar to those performed on other members of the Allokotosauria and closely related groups (e.g., Werning and Irmis, 2010; Mukherjee, 2015; Werning and Nesbitt, 2016; Jaquier and Scheyer, 2017; Cubo and Jalil, 2019), we refrain from hypothesizing on metabolic rate, growth, and other paleobiological traits (e.g., herding behavior; Sengupta and Sengupta, 2021).

The shortest complete femur of *Puercosuchus traverorum* n. gen. n. sp. (PEFO 44194) is artificially short as a result of a pathology that occurred on the distal third of the element (Fig. 18.9–18.12). The shaft is dramatically warped and constricted dorsoventrally and the bone surface is scarred and hyperossified. Whether this pathology is a healed fracture, a cancerous growth, infection (e.g., osteomyelitis), or some kind of metabolic (e.g., osteomalacia) or developmental (e.g., osteogenesis imperfecta) bone disease requires further investigation.

Referral of the Krzyzanowski bonebed material.—NMMNH L-3764 is a bonebed from relatively low in the Blue Mesa Member (Chinle Formation) near St. Johns, Arizona, USA, ~64 km from PFV 217 (Fig. 1.1). According to Heckert (2004), Spielmann et al. (2013b), and unpublished identifications on specimen labels at the NMMNH, the bonebed includes actinopterygians, theropod, sauropodomorph, and ornithischian dinosaurs, parasuchid phytosaurs, sphenosuchian crocodylomorphs, fragmentary skeletons of *Trilophosaurus* cf. *T. jacobsi*, and indeterminate reptilian and archosauromorph elements (in addition to some named tooth taxa, see below). However, with the discovery of *Azendohsaurus madagaskarensis* (Flynn et al., 2010; Nesbitt et al., 2015) and *Shringasaurus indicus* (Sengupta et al., 2017; Sengupta and Bandyopadhyay, 2022), recognition of malerisaurine azendohsaurids (Nesbitt et al., 2021), the identification and redistribution of important character states (Ezcurra, 2016; Pritchard and Sues, 2019; Nesbitt et al., 2021), and the use of apomorphy-based identifications of Triassic reptiles (e.g., Nesbitt and Stocker, 2008; Martz et al., 2013; Lessner et al., 2018; Pritchard and Sues, 2019; Hégron et al., 2020; Marsh and Parker, 2020), we can now refer all of the specimens representing those taxa from NMMNH L-3764 to *Puercosuchus traverorum* n. gen. n. sp. (see explicit assignment below).

Not only is there not a single tooth assignable to *Trilophosaurus* present in NMMNH L-3764, the isolated and associated skeletal remains from that quarry share apomorphies tying them to the Azendohsauridae (e.g., concave anterior face of anterior cervical vertebrae; pinched ventral surface of second sacral vertebra; pyramidal process on distal end of the humerus; lateral spur of ischiac peduncle present on ilium; relatively long fibular process of astragalus; lateral ridge on metatarsal V), Malerisaurinae (distally recurved maxillary teeth; interdental plates on maxilla; lateral expansions of the dorsal end of cervical neural spines; cervical epipophyses; radius with posteroproximal expansion), and *Puercosuchus traverorum* n. gen. n. sp. (anterior process present and taller than neural spine on posterior caudal vertebrae; hooked proximal anteromedial process of ulna; tubercle on dorsal surface of metatarsal V). For example, 'osteichthyan' (NMMNH P-44157, NMMNH P-44150) and 'Pisces' (NMMNH P-63271) jaws are malerisaurine pterygoids, the 'parasuchid' phytosaur ilium (NMMNH P-34098) is that of an azendohsaurid, a femur of a 'sphenosuchian' (NMMNH P-40938) belongs to an azendohsaurid, and the proximal metapodials associated with that latter specimen are identical to those of *Puercosuchus traverorum* n. gen. n. sp. Similarly, another 'sphenosuchian' specimen (NMMNH P-40939), comprising a partial ilium and vertebrae, belongs to a malerisaurine azendohsaurid. Some elements identified as *Trilophosaurus* cf. *T. jacobsi* such as the 'coracoid' (NMMNH P-44168) and indeterminate reptilian elements such as an isolated posterior caudal vertebra (NMMNH P-34613) and a posterior caudal vertebra associated with a dentary, partial quadrate, radius, ulna, ilia, and femur (NMMNH P-60209) preserve autapomorphies unique to *Puercosuchus traverorum* n. gen. n. sp. (see above). Thus, with the absence of any material possessing the apomorphies uniting Trilophosauridae or *Trilophosaurus*, we refer most of the material at NMMNH L-3764 to a single malerisaurine azendohsaurid taxon, *Puercosuchus traverorum* n. gen. n. sp.

In addition to the specimens from the Krzyzanowski bonebed mentioned above, we also refer all of the putative dinosaur material from that site to *Puercosuchus traverorum* n. gen. n. sp. with the same justification. An isolated 'dinosaur astragalus' (NMMNH P-34567) is the ventral half of a malerisaurine quadrate. Two isolated 'saurischian' proximal metapodials, NMMNH P-34628 and NMMNH P-34640, are identical to the proximal ends of metacarpal III and metatarsal II, respectively, of *Puercosuchus traverorum* n. gen. n. sp. The 'theropod' femur NMMNH P-37829 belongs to an azendohsaurid allokotsaur. An isolated part of a 'prosauropod' mandible, including a tooth (NMMNH P-34224), an isolated 'ornithischian' tooth identified as *Pekinosaurus olseni* Hunt and Lucas, 1994 (NMMNH P-34095), and an isolated 'ornithischian' tooth identified as *Protecovasaurus lucasi* Heckert, 2004 (NMMNH P-34095) are all well within the morphological range of marginal teeth found in complete maxillae and dentaries of *Puercosuchus traverorum* n. gen. n. sp., including the dentary NMMNH P-60127. This further supports the hypothesis that many isolated tooth morphotypes from the Upper Triassic Chinle Formation and Dockum Group of the western United States, as well as those from the Pekin Formation of North Carolina, actually belong to pseudosuchians (Parker et al., 2005) or non-archosaur archosauromorphs and not sauropodomorph and/or ornithischian dinosaurs (Irmis et al., 2007; Nesbitt et al., 2007; Marsh and Parker, 2020), and in some cases may belong to a single taxon that exhibits different tooth shapes within the same dentigerous element, such as *Puercosuchus traverorum* n. gen. n. sp.

Biostratigraphic significance.—Recognition of and use of apomorphies to diagnose and identify allokotosaur clades (Flynn et al., 2010; Martz et al., 2013; Nesbitt et al., 2015; Ezcurra, 2016; Sengupta et al., 2017; Lessner et al., 2018; Pritchard and Sues, 2019; Hégron et al., 2020; Nesbitt et al., 2021) has allowed for the recognition of numerous additional

https://doi.org/10.1017/jpa.2022.49 Published online by Cambridge University Press

Table 1. List of allokotosaur specimens from the Chinle Formation at Petrified Forest National Park.

Specimen	Locality	Element	Identification (previous identification)	Unit
PEFO 16721	PFV 217 Dinosaur Wash	Partial vertebrae	Allokotosauria (N/A)	Blue Mesa Member (upper part)
PEFO 16733	PFV 217 Dinosaur Wash	Cervical vertebra	Azendohsauridae (Plateosauridae)	Blue Mesa Member (upper part)
PEFO 38268	PFV 150 Paulsell 4	Humerus	Azendohsauridae (N/A)	Blue Mesa Member (upper part)
PEFO 47767	PFV 150 Paulsell 4	Pubes	Azendohsauridae (N/A)	
PEFO 50111	PFV 150 Paulsell 4	Humerus	Azendohsauridae (N/A)	Blue Mesa Member (upper part)
PEFO 34614	PFV 142 Blue Mesa E	Femur, distal end	Allokotosauria (N/A)	Blue Mesa Member (upper part)
Various (e.g., PEFO 3893, PEFO 3894)	PFV 122/PFV 188 Camp Butte N1/Dying Grounds	Teeth	*Trilophosaurus buettneri*	Blue Mesa Member (upper part)
PEFO 26709	PFV 279 Dinosaur Wash E	Cervical vertebra	Azendohsauridae (Poposauroidea)	Blue Mesa Member (upper part)
Various (this paper)	PFV 217 Dinosaur Wash	Bonebed	*Puercosuchus traverorum*	Blue Mesa Member (upper part)
PEFO 38890	PFV 445 *Doswellia* Quarry	Humerus, distal end	Azendohsauridae (Aetosauria)	Blue Mesa Member (upper part)
PEFO 40724	PFV 448 Matt's Happy Place	Tooth	*Trilophosaurus buettneri*	Blue Mesa Member (upper part)
Various (e.g., PEFO 44764, PEFO 46652, PEFO 44780, PEFO 44770)	PFV 456 Thunderstorm Ridge	Limbs, dentary	Allokotosauria, *Trilophosaurus buettneri*, and Malerisaurinae	Blue Mesa Member (upper part)
Various (e.g., PEFO 37204, PEFO 41632)	PFV 396 Billings Gap Tank E1	Teeth	*Trilophosaurus buettneri* and Malerisaurinae	Blue Mesa Member (upper part)
PEFO 31165	PFV 191 Flag Canyon	Maxilla and dentary	*Trilophosaurus dornorum*	Sonsela Member (Camp Butte beds)
PEFO 31174	PFV 161 Agate Bridge N	Fragmentary skeleton	Azendohsauridae (*Trilophosaurus*, *Malerisaurus*, Prolacertiformes)	Sonsela Member (Camp Butte beds)
PEFO 44391	PFV 100 Wizard Wash E	Ilium	Allokotosauria (N/A)	Sonsela Member (Kellogg Butte bed)
Various (e.g., PEFO 39376/UWBM VP 108382, PEFO 42365/UWBM 116791	PFV 410 Kaye Quarry	Maxilla, cranial and postcranial elements	Allokotosauria, *Trilophosaurus dornorum*, Malerisaurinae	Sonsela Member (Jim Camp Wash beds)
Various (e.g., PEFO 42082)	PFV 089 Bowman Site	Teeth	*Trilophosaurus phasmalophos*	Sonsela Member (Jim Camp Wash beds)

allokotosaur specimens at PEFO (Table 1) (i.e., indeterminate Allokotosauria, *Trilophosaurus* spp., Azendohsauridae, Malerisaurinae, *Puercosuchus traverorum* n. gen. n. sp.). The re-identification of some of these specimens that were formerly published as 'plateosaurid' sauropodomorphs (PEFO 16733; Fig. 1.5; Hunt and Wright, 1999) or catalogued as 'poposauroids' (PEFO 26709) further demonstrates how additional comparative skeletal material from the Triassic around the world and a better understanding of convergence among apomorphies (and the resulting taxonomy) provide evidence for more robust biostratigraphic hypotheses.

Allokotosaurs are currently known from 11 different localities in the Adamanian-aged upper part of the Blue Mesa Member (Table 1). These include isolated teeth from microsites (e.g., PFV 396 and PFV 456) and postcranial remains, such as two humeri (PEFO 38268; Fig. 18.15, 18.16; PEFO 50111) and associated pubes (PEFO 34852), found associated with a phytosaur (*Smilosuchus adamanensis* Camp, 1930) at PFV 150 (not PFV 148 as listed by Griffin et al., 2017) similar to the robust holotype specimen of the malerisaurine '*Otischalkia elderae*' (TMM 31025-262) from the older Colorado City Formation (Otischalkian) of the Dockum Group of western Texas (Long and Murry, 1995; Nesbitt et al., 2021). Other Adamanian sites at PEFO with allokotosaurs include four sites in the lower part of the Sonsela Member (Camp Butte beds, Lot's Wife beds, Kellogg Butte beds, lower part of Jim Camp Wash beds; Martz and Parker, 2010; Parker and Martz, 2010; Sidor et al., 2018). Even with the recognition of malerisaurine azendohsaurids (Nesbitt et al., 2021) and the ability to identify isolated teeth to malerisaurines (this paper), only one allokotosaur taxon is known from Revueltian-aged strata in the park (and correlative strata nearby; Kligman et al., 2020), which may represent the youngest unambiguous allokotosaur in North America: *Trilophosaurus phasmalophos* Kligman et al., 2020 (but see Chambi-Trowell et al., 2022, for even younger Rhaetian-aged trilophosaurids from the United Kingdom). In New Mexico, Spielmann et al. (2013a) reported allokotosaur humeral fragments from the Bull Canyon Formation. At least one of these specimens (NMMNH P-4686) is from the main Revuelto Creek locality (NMMNH locality 1), which is the 'type assemblage locality' of the Revueltian holochronozone (Hunt, 2001). The only diagnostic phytosaur specimen from this site is a single, isolated 'juvenile' mystriosuchine squamosal (NMMNH P-16507; Hunt, 2001), which at face value would make the site Revueltian, as defined by Martz and Parker (2017). However, isolated squamosals often occur as float, and thus might not make the best biostratigraphic vouchers for Triassic localities. Further, the extensive vertebrate localities in the Revuelto Creek area have never been placed in stratigraphic order (e.g., Hunt, 2001), and thus the base of the Revueltian teilzone is presently undefined for east-central New Mexico (Martz and Parker, 2017). Simply assuming that all localities in the Bull Canyon

https://doi.org/10.1017/jpa.2022.49 Published online by Cambridge University Press

Formation are Revueltian (e.g., Spielmann et al., 2013a) is circular, especially given our current understanding of vertebrate biostratigraphy in the Late Triassic of Arizona and Texas (e.g., Parker and Martz, 2010; Martz et al., 2013; Martz and Parker, 2017). Other taxa from NMMNH Locality 1 (e.g., *Typothorax coccinarum* Cope, 1875; *Shuvosaurus inexpectatus* Chatterjee, 1993; *Revueltosaurus callenderi* Hunt, 1989; Hunt, 1989, 2001) have been recovered from upper Adamanian rock units in Arizona and Texas (Parker and Martz, 2010; Martz et al., 2013; Parker et al., 2021), and the presence of allokotosaurs in the assemblage may actually support an Adamanian age for this locality. Thus, it seems that the allokotosaur record in northeastern Arizona reflects at least a localized extinction event for this clade near the end of the Norian, where the group was relatively diverse and abundant during the Adamanian, but only a single trilophosaurid taxon is present above the Adamanian-Revueltian boundary (Parker and Martz, 2010; Kligman et al., 2020, fig. 3).

Conclusions

The allokotosaurs *Trilophosaurus buettneri* (Gregory, 1945; Spielmann et al., 2008), *Trilophosaurus jacobsi* Murry, 1987 (= ?*Spinosuchus caseanus* Huene, 1932; Nesbitt et al., 2015) (Heckert et al., 2001b, 2006; Spielmann et al., 2008), *Azendohsaurus madagaskarensis* (Flynn et al., 2010; Nesbitt et al., 2015), *Azendohsaurus laaroussii* (Cubo and Jalil, 2019), *Shringasaurus indicus* (Sengupta et al., 2017; Sengupta and Sengupta, 2021), and now *Puercosuchus traverorum* n. gen. n. sp. are all known from monodominant bonebeds. Whether members of this clade are often found in this kind of bonebed is the result of behavior (Sengupta and Sengupta, 2021) or simple abundance remains to be investigated, given that the respective occurrences vary significantly in taxonomy (i.e., trilophosaurids, azendohsaurids) and paleobiogeography. PFV 217, NMMNH L-3764, and the hundreds of bones of *Puercosuchus traverorum* n. gen. n. sp. preserved within those sites provide an opportunity to better understand the character states found in malerisaurine azendohsaurids, including dentition capable of carnivory (Nesbitt et al., 2021).

Prior to the discovery of the malerisaurine bonebed at PFV 217 in 2014, the only unambiguous allokotosaurs (a group that itself was not even named until a year later; Nesbitt et al., 2015) known from Petrified Forest National Park (Table 1) were (1) isolated teeth of *Trilophosaurus buettneri* or a closely related species from microvertebrate collections at PFV 122/PFV 188 (Long and Murry, 1995; Heckert, 2004) and PFV 396 (Kligman et al., 2020); (2) a skeleton referred to as cf. *Malerisaurus* (PEFO 31174; Parker and Martz, 2010) from the Camp Butte beds; and (3) the holotype specimen of *Trilophosaurus dornorum* Parker and Mueller, 2006, from the Lot's Wife beds of the Sonsela Member (Fig. 1.3). At the time (2010), *Trilophosaurus dornorum* was the highest stratigraphic occurrence of any allokotosaur in the park (Parker and Irmis, 2005; Parker and Mueller, 2006; Parker and Martz, 2010). The identification and collection of allokotosaurians has increased considerably in the American Southwest (Sidor et al., 2018; Kligman et al., 2020; Mellett et al., 2020; Nesbitt et al., 2021), and it is clear that these taxa played an important role in Late Triassic ecosystems, especially during the Adamanian (Kligman et al., 2020). As a member of the Malerisaurinae, *Puercosuchus traverorum* n. gen. n. sp. is a member of an early-diverging (Nesbitt et al., 2021) but relatively late-surviving allokotosaur group (Kligman et al., 2020), which suggests that more bonebeds like PFV 217 and NMMNH L-3764 may be discovered in other Late Triassic terrestrial strata worldwide.

Acknowledgments

We thank C. Sagebiel and M. Brown (TMM), C. Sidor (UWBM), and D. and J. Gillette (MNA) for access to collections in their care. We are especially indebted to N. Volden (NMMNH) who granted us unrestricted access to the specimens from L-3764. Thanks to A. Pritchard, M. Ezcurra, S. Werning, and A. Heckert for discussion, and to E. Lessner, L. Carter, and S. Matsuoka for help excavating the quarry at PFV 217. C. Lash, M. Smith, M. Brown, S. Egberts, D. Wagner, D. Boudreau, and P. Varela prepared the PEFO specimens. We also thank the late B. Mueller for many helpful conversations about the azendohsaurid fossils he collected for MOTT. Thanks to M. Ezcurra for providing comparative photographs of *Malerisaurus robinsonae*. We thank A. Heckert and S. Spiekman for constructive reviews that greatly improved the manuscript. Thanks to J. Nair for pointing out an error in the original phylogenetic definition of Malerisaurinae. SJN was funded by the National Science Foundation CAREER program (NSF EAR 1943286). This is PEFO contribution number 84. The conclusions presented here are those of the authors and do not represent the views of the United States Government.

Declaration of competing interests

The authors declare none.

Data availability statement

Data available from the Dryad Digital Repository: https://doi.org/10.5061/dryad.6djh9w13j.

References

Atchley, S.C., Nordt, L.C., Dworkin, S.I., Ramezani, J., Parker, W.G., Ash, S.R., and Bowring, S.A., 2013, A linkage among Pangean tectonism, cyclic alluviation, climate change, and biologic turnover in the Late Triassic: the record from the Chinle Formation, southwestern United States: Journal of Sedimentary Research, v. 83, p. 1147–1161.

Bassani, F., 1886, Sui fossili e sull'eta degli schisti bituminosi triasici di Besano in Lombardia: Atti Societa Italiana di Scienze Naturali, Milano, v. 29, p. 15–72.

Benton, M.J., and Allen, J.L., 1997, *Boreopricea* from the Lower Triassic of Russia, and the relationships of the prolacertiform reptiles: Palaeontology, v. 40, p. 931–953.

Broom, R., 1903, On a new reptile (*Proterosuchus fergusi*) from the Karroo beds of Tarkastad, South Africa: Annals of the South African Museum, v. 4, p. 159–164.

Camp, C.L., 1930, A study of the phytosaurs with description of new material from western North America: Memoirs of the University of California, v. 10, p. 1–174.

Carroll, R.L., 1981, Plesiosaur ancestors from the upper Permian of Madagascar: Philosophical Transactions of the Royal Society of London, v. 293, p. 315–383.

Case, E.C., 1928, A cotylosaur from the Upper Triassic of western Texas: Journal of the Washington Academy of Science, v. 18, p. 177–178.

https://doi.org/10.1017/jpa.2022.49 Published online by Cambridge University Press

Chambi-Trowell, S.A.V., Whiteside, D.I., Skinner, M., Benton, M.J., and Rayfield, E.J., 2022, Phylogenetic relationships of the European trilophosaurids *Tricuspisaurus thomasi* and *Variodens inopinatus*: Journal of Vertebrate Paleontology, v. 41, 1999250. https://doi.org/10.1080/02724634.2021.1999250.

Chatterjee, S., 1980, *Malerisaurus*, a new eosuchian reptile from the Late Triassic of India: Philosophical Transactions of the Royal Society of London, Series B, v. 291, p. 163–200.

Chatterjee, S., 1986, *Malerisaurus langstoni*, a new diapsid reptile from the Triassic of Texas: Journal of Vertebrate Paleontology, v. 6, p. 297–312.

Chatterjee, S., 1993, *Shuvosaurus*, a new theropod: an unusual theropod dinosaur from the Triassic of Texas: National Geographic Research and Exploration, v. 9, p. 274–285.

Colbert, E.H., 1970, The Triassic gliding reptile *Icarosaurus*: Bulletin of the American Museum of Natural History, v. 1423, p. 1–142.

Cope, E.D., 1875, The geology of New Mexico: Philadelphia Academy of Natural Sciences Proceedings, v. 27, p. 263–267.

Cubo, J., and Jalil, N.-D., 2019, Bone histology of *Azendohsaurus laaroussii*: implications for the evolution of thermometabolism in Archosauromorpha: Paleobiology, v. 45, p. 317–330.

Dilkes, D.W., 1998, The Early Triassic rhynchosaur *Mesosuchus browni* and the interrelationships of basal archosauromorph reptiles: Philosophical Transactions of the Royal Society of London, Series B: Biological Sciences, v. 353, p. 501–541.

Dutuit, J.M., 1972, Découverte d'un dinosaure ornithischien dans le Trias supérieur de l'Atlas occidental marocain: Comptes Rendus de l'Académie des Sciences de Paris, v. 275, p. 2841–2844.

Eberth, D.A., Shannon, M., and Noland, B.G., 2007, A bonebeds database: classification, biases, and patterns of occurrence, *in* Rogers, R.R., Eberth, D.A., and Fiorillo, A.R., eds., Bonebeds: Genesis, Analysis, and Paleobiological Significance: Chicago, University of Chicago Press, p. 103–219.

Evans, S.E., 2009, An early kuehneosaurid reptile from the Early Triassic of Poland: Palaeontologia Polonica, v. 65, p. 145–178.

Ezcurra, M.D., 2016, The phylogenetic relationships of basal archosauromorphs, with an emphasis on the systematics of proterosuchian archosauriforms: PeerJ, v. 4, e1778. https://doi.org/10.7717/peerj.1778.

Ezcurra, M.D., and Butler, R.J., 2015, Taxonomy of the proterosuchid archosauriforms (Diapsida: Archosauromorpha) from the earliest Triassic of South Africa, and implications for the early archosauriform radiation: Palaeontology, v. 58, p. 141–170.

Flynn, J.J., Nesbitt, S.J., Parrish, M.J., Ranivoharimanana, L., and Wyss, A.R., 2010, A new species of *Azendohsaurus* (Diapsida: Archosauromorpha) from the Triassic Isalo Group of southwestern Madagascar: cranium and mandible: Palaeontology, v. 53, p. 669–688.

Gauffre, F.-X., 1993, The prosauropod dinosaur *Azendohsaurus laaroussii* from the Upper Triassic of Morocco: Palaeontology, v. 36, p. 897–908.

Gill, F.B., Slikas, B., and Sheldon, F.H., 2005, Phylogeny of titmice (Paridae): II. Species relationships based on sequences of the mitochondrial cytochrome-B gene: The Auk, v. 122, p. 121–143.

Gottmann-Quesada, A., and Sander, P.M., 2009, A redescription of the early archosauromorph *Protorosaurus speneri* Meyer, 1832, and its phylogenetic relationships: Palaeontographica Abteilung A, v. 287, p. 123–220.

Gow, C.E., 1975, The morphology and relationships of *Youngina capensis* Broom and *Prolacerta broomi* Parrington: Palaeontologia Africana, v. 18, p. 89–131.

Gower, D.J., 1996, The tarsus of erythrosuchid archosaurs, and implications for early diapsid phylogeny: Zoological Journal of the Linnean Society, v. 116, p. 347–375.

Gregory, J.T., 1945, Osteology and relationships of *Trilophosaurus*: University of Texas Publication, v. 4401, p. 273–359.

Griffin, C.T., 2018, Developmental patterns and variation among early theropods: Journal of Anatomy, v. 232, p. 604–640.

Griffin, C.T., and Nesbitt, S.J., 2016, The femoral ontogeny and long bon histology of the Middle Triassic (?late Anisian) dinosauriform *Asilisaurus kongwe* and implications for the growth of early dinosaurs: Journal of Vertebrate Paleontology, v. 36, e1111224. https://doi.org/10.1080/02724634.2016.1111224.

Griffin, C.T., Stefanic, C.M., Parker, W.G., Hungerbühler, A., and Stocker, M.R., 2017, Sacral anatomy of the phytosaur *Smilosuchus adamanensis*, with implications for pelvic girdle evolution among Archosauriformes: Journal of Anatomy, v. 231, p. 886–905.

Griffin, C.T., Stocker, M.R., Colleary, C., Stefanic, C.M., Lessner, E.J., Riegler, M., Formoso, K., Koeller, K., and Nesbitt, S.J., 2020, Assessing ontogenetic maturity in extinct saurian reptiles: Biological Reviews, v. 96, p. 470–525.

Heckert, A.B., 2004, Late Triassic microvertebrates from the lower Chinle Group (Otischalkian–Adamanian: Carnian), southwestern U.S.A.: New Mexico Museum of Natural History and Science Bulletin, v. 27, p. 1–170.

Heckert, A.B., Lucas, S.G., and Hunt, A.P., 2001a, Stratigraphy, biostratigraphy and biochronology of lower Chinle Group (Adamanian: latest Carnian) vertebrate fossil assemblages in the vicinity of St. Johns, Arizona: Mesa Southwest Museum Bulletin, v. 8, p. 9–15.

Heckert, A.B, Lucas, S.G., Kahle, R., and Zeigler, K., 2001b, New occurrence of *Trilophosaurus* (Reptilia: Archosauromorpha) from the Upper Triassic of West Texas and its biochronological significance: New Mexico Geological Society Guidebook, v. 52, p. 115–122.

Heckert, A.B., Rinehart, L.F., Krzyzanowski, S.E., Lucas, S.G., and Harris, S.K., 2004, The Krzyzanowski bonebed: an Upper Triassic (Adamanian: latest Carnian) vertebrate fauna and its implications for microvertebrate studies: New Mexico Geology, v. 26, p. 64.

Heckert, A.B., Lucas, S.G., and Hunt, A.P., 2005, Triassic vertebrate fossils in Arizona: New Mexico Museum of Natural History and Science Bulletin, v. 29, p. 16–44.

Heckert, A.B., Lucas, S.G., Rinehart, L.F., Spielmann, J.A., Hunt, A.P., and Kahle, R., 2006, Revision of the archosauromorph reptile *Trilophosaurus*, with a description of the first skull of *Trilophosaurus jacobsi*, from the Upper Triassic Chinle Group, West Texas, USA: Palaeontology, v. 49, p. 621–640.

Hégron, A., Stocker, M.R., Marsh, A.D., and Nesbitt, S.J., 2020, Archosauromorphs (Reptilia: Diapsida) from the Lamy Quarry, Garita Creek Formation (Adamanian, Late Triassic), New Mexico, USA: Palaeodiversity, v. 13, p. 135–149.

Hoffman, A.C., 1965, On the discovery of a new thecodont from the Middle Beaufort Beds: Navorsinge van die Nasionale Museum Bloemfontein, v. 2, p. 33–40.

Holliday, C.M., and Nesbitt, S.J., 2013, Morphology and diversity of the mandibular symphysis of archosauriforms: Geological Society of London Special Publication, v. 379, p. 555–571.

Huene, F. von, 1932, Die fossile Reptil-Ordnung Saurischia, ihte Entwicklung und Geschichte: Monographien zur Geologie und Palaeontologie, v. 4, p. 1–361.

Huene, F. von, 1946, Die grossen Stämme der Tetrapoden in den geologischen Zeiten: Biologisches Zentralblatt, v. 65, p. 268–275.

Hunt, A.P., 1989, A new ?ornithischian dinosaur from the Bull Canyon Formation (Upper Triassic) of east-central New Mexico, *in* Lucas, S.G., and Hunt, A.P., eds., Dawn of the Age of Dinosaurs in the American Southwest: New Mexico Museum of Natural History and Science, p. 355–358.

Hunt, A.P., 2001, The vertebrate fauna, biostratigraphy and biochronology of the type Revueltian land-vertebrate faunachron, Bull Canyon Formation (Upper Triassic), east-central New Mexico: New Mexico Geological Society Guidebook, v. 52, p. 123–151.

Hunt, A.P., and Lucas, S.G., 1991, A new rhynchosaur from the Upper Triassic of West Texas, and the biochronology of Late Triassic rhynchosaurs: Palaeontology, v. 34, p. 927–938.

Hunt, A.P., and Lucas, S.G., 1994, Ornithischian dinosaurs from the Upper Triassic of the United States, *in* Fraser, N.C., Sues, H.-D., eds., In the Shadow of the Dinosaurs: Early Mesozoic Tetrapods: Cambridge, Cambridge University Press, p. 227–241.

Hunt, A.P., and Wright, J., 1999. New discoveries of Late Triassic dinosaurs from Petrified Forest National Park, Arizona, *in* Santucci, V.L., and McClellan, L., eds., National Park Service Paleontological Research: National Park Service Geological Resources Division Technical Report NPS/NRGRD/GRDTR-99/03, p. 96–99.

Irmis, R.B., Parker, W.G., Nesbitt, S.J., and Liu, J., 2007, Early ornithischian dinosaurs: the Triassic record: Historical Biology, v. 19, p. 3–22.

Jaquier, V.P., and Scheyer, T.M., 2017, Bone histology of the Middle Triassic long-necked reptiles *Tanystropheus* and *Macrocnemus* (Archosauromorpha, Protorosauria): Journal of Vertebrate Paleontology, v. 37, e1296456. https://doi.org/10.1080/02724634.2017.1296456.

Jaquier, V.P., Fraser, N.C., Furrer, H., and Scheyer, T.M., 2017, Osteology of a new specimen of *Macrocnemus* aff. *M. fuyuanensis* (Archosauromorpha, Protorosauria) from the Middle Triassic of Europe: potential implications for species recognition and paleogeography of tanystropheid protorosaurs: Frontiers in Earth Science, v. 5. https://doi.org/10.3389/feart.2017.00091.

Kligman, B.T., Marsh, A.D., Nesbitt, S.J., Parker, W.G., and Stocker, M.R., 2020, New trilophosaurid species demonstrates a decline in allokotosaur diversity across the Adamanian-Revueltian boundary in the Late Triassic of western North America: Palaeodiversity, v. 13, p. 25–37.

Lane, H.H., 1945, New mid-Pennsylvanian reptiles from Kansas: Transactions of the Kansas Academy of Sciences, v. 47, p. 381–390.

Langer, M.C., Abdala, F., Richter, M., and Benton, M., 1999, A sauropodomorph dinosaur from the Upper Triassic (Carnian) of southern Brazil: Comptes Rendus de l'Académie des Sciences, v. 329, p. 511–517.

Langer, M.C., França, M.A.G., and Gabriel, S., 2007, The pectoral girdle and forelimb anatomy of the stem-sauropodomorph *Saturnalia tupiniquim* (Upper Triassic, Brazil): Special Papers in Paleontology, v. 77, p. 113–137.

Lessner, E.J., Parker, W.G., Marsh, A.D., Nesbitt, S.J., Irmis, R.B., and Mueller, B.D., 2018, New insights into Late Triassic dinosauromorph-bearing assemblages from Texas using apomorphy-based identifications: PaleoBios, v. 35. https://doi.org/10.5070/P9351039960.

https://doi.org/10.1017/jpa.2022.49 Published online by Cambridge University Press

Li, C., Zhao, L.-J., and Wang, L.-T., 2007, A new species of *Macrocnemus* (Reptilia: Protosauria) from the Middle Triassic of southwestern China and its palaeogeographical implication: Earth Sciences, v. 50, p. 1601–1605.
Linnaeus, C., 1758, Systema Naturae Per Regna Tria Naturae, Secondum Classes, Ordines, Genera, Species, Cum Characteribus, Differentiis, Synonymis, Locis: Holmius, Laurentius Salvius, 824 p.
Long, R.A., and Murry, P.A., 1995, Late Triassic (Carnian and Norian) tetrapods from the southwestern United States: New Mexico Museum of Natural History and Science, v. 4, p. 1–254.
Lucas, S.G., 1993, The Chinle Group revised stratigraphy and chronology of Upper Triassic marine strata in the western United States: Museum of Northern Arizona Bulletin, v. 59, p. 27–50.
Marsh, A.D., and Parker, W.G., 2020, New dinosauromorph specimens from Petrified Forest National Park and a global biostratigraphic review of Triassic dinosauromorph body fossils: PaleoBios, v. 37. https://doi.org/10.5070/P9371050859.
Marsh, A.D., Parker, W.G., Kligman, B.T., and Lessner, E.J., 2017, Bonebed of a carnivorous archosauromorph from the Chinle Formation (Late Triassic: Norian) from Petrified Forest National Park: Geological Society of America Abstracts with Programs, v. 2017, p. 244.
Martz, J.W., and Parker, W.G., 2010, Revised lithostratigraphy of the Sonsela Member (Chinle Formation, Upper Triassic) in the southern part of Petrified Forest National Park, Arizona: PLoS ONE, v. 5, e9329. https://doi.org/10.1371/journal.pone.0009329.
Martz, J.W., and Parker, W.G., 2017, Revised formulation of the Late Triassic Land Vertebrate "Faunachrons" of western North America: recommendations for codifying nascent systems of vertebrate biochronology, *in* Zeigler, K.E., and Parker, W.G., eds., Terrestrial Depositional Systems: Deciphering Complexities through Multiple Stratigraphic Methods: Amsterdam, Elsevier, p. 39–124.
Martz, J.W., Mueller, B., Nesbitt, S.J., Stocker, M.R., Parker, W.G., Atanassov, M., Fraser, N., Weinbaum, J.C., and Lehane, J.R., 2013, A taxonomic and biostratigraphic re-evaluation of the Post Quarry vertebrate assemblage from the Cooper Canyon Formation (Dockum Group, Upper Triassic) of southern Garza County, western Texas: Earth and Environmental Science Transactions of the Royal Society of Edinburgh, v. 103, p. 339–364.
Mellett, M.P., Kligman, B.T., Marsh, A.D., Parker, W.G., Nesbitt, S.J., and Stocker, M.R., 2020, Dental microwear analysis of two new species of trilophosaurid from the Chinle Formation (Arizona) reveals diversity of herbivorous diets within the clade: Journal of Vertebrate Paleontology, The Society of Vertebrate Paleontology 80th Annual Meeting, Virtual 2020, October, 12–16, 2020, Meeting Program and Abstracts, p. 241–242.
Miall, A.D., 1996, The Geology of Fluvial Deposits: Sedimentary Facies, Basin Analysis, and Petroleum Geology: Berlin, Springer, 582 p.
Miall, A.D., 2010, Alluvial deposits, *in* James, N.P., and Dalrymple, R.W., eds., Facies Models 4: St. John's, Geological Association of Canada, 105–138.
Miedema, F., Spiekman, S.N.F., Fernandez, V., Reumer, J.W.F., and Scheyer, T.M., 2020, Cranial morphology of the tanystropheid *Macrocnemus bassanii* unveiled using synchrotron microtomography: Scientific Reports, v. 10, 12412. https://doi.org/10.1038/s41598-020-68912-4.
Mukherjee, D., 2015, New insights from bone microanatomy of the Late Triassic *Hyperodapedon* (Archosauromorpha, Rhynchosauria): implications for archosauromorphs growth strategy: Palaeontology, v. 58, p. 313–339.
Müller, R.T., Langer, M.C., Pacheco, C.P., and Dias-da-Silva, S., 2019, The role of ontogeny on character polarization in early dinosaurs: a new specimen from the Late Triassic of southern Brazil and its implications: Historical Biology, v. 31, p. 794–805.
Murry, P.A., 1987, New reptiles from the Upper Triassic Chinle Formation of Arizona: Journal of Vertebrate Paleontology, v. 61, p. 773–786.
Nesbitt, S.J., 2011, The early evolution of archosaurs: relationships and origin of major clades: Bulletin of the American Museum of Natural History, v. 352, p. 1–292.
Nesbitt, S.J., and Stocker, M.R., 2008, The vertebrate assemblage of the Late Triassic Canjilon Quarry (northern New Mexico, USA) and the importance of apomorphy-based assemblage comparisons: Journal of Vertebrate Paleontology, v. 28, p. 1063–1072.
Nesbitt, S.J., Irmis, R.B., and Parker, W.G., 2007, A critical re-evaluation of the Late Triassic dinosaur taxa of North America: Journal of Systematic Palaeontology, v. 5, p. 209–243.
Nesbitt, S.J., Flynn, J.J., Pritchard, A.C., Parrish, J.M., Ranivoharumanana, L., and Wyss, A.R., 2015, Postcranial osteology of *Azendohsaurus madagaskarensis* (?Middle to Upper Triassic, Isalo Group of Madagascar) and its systematic position among stem archosaurs: Bulletin of the American Museum of Natural History, v. 398, p. 1–126.
Nesbitt, S.J., Stocker, M.R., Ezcurra, M.D., Fraser, N.C, Heckert, A.B., Parker, W.G., Mueller, B., Sengupta, S., Bandyopadhyay, S., Pritchard, A.C., and Marsh, A.D., 2021, Widespread azendohsaurids (Archosauromorpha: Allokotosauria) from the Late Triassic of the western United States and India: Papers in Palaeontology, v. 8, p. e1413. https://doi.org/10.1002/spp2.1413.
Nopsca, F., 1930, Notizen über *Machrochemus bassanii* nov. gen. et spec.: Centralblatt für Mineralogie, Geologie und Paläontologie, Abteilung B, p. 252–255.
Nosotti, S., 2007, *Tanystropheus longobardicus* (Reptilia, Protorosauria): re-interpretations of the anatomy based on new specimens from the Middle Triassic of Besano (Lombardy, Northern Italy): Memorie della Societa Italiana di Scienze Naturali e del Museo Civico di Storia Naturale di Milano, v. 35, p. 1–88.
Owen, R., 1842, Report on British fossil reptiles, part II: Report of the British Association of the Advancement of Science, v. 11, p. 60–104.
Parker, W.G., 2006, The stratigraphic distribution of major fossil localities in Petrified Forest National Park, Arizona: Museum of Northern Arizona Bulletin, v. 62, p. 46–61.
Parker, W.G., 2018, Redescription of *Calyptosuchus* (*Stagonolepis*) *wellesi* (Archosauria: Pseudosuchia: Aetosauria) from the Late Triassic of the southwestern United States with a discussion of genera in vertebrate paleontology: PeerJ, v. 6, e4291. https://doi.org/10.7717/peerj.4291.
Parker, W.G., and Irmis, R.B., 2005, Advances in Late Triassic vertebrate paleontology based on new material from Petrified Forest National Park, Arizona: New Mexico Museum of Natural History and Science Bulletin, v. 29, p. 45–58.
Parker, W.G., and Martz, J.W., 2010, The Late Triassic (Norian) Adamanian-Revueltian tetrapod faunal transition in the Chinle Formation of Petrified Forest National Park: Earth and Environmental Science Transactions of The Royal Society of Edinburgh, v. 101, p. 231–260.
Parker, W.G., and Mueller, B., 2006, A new species of *Trilophosaurus* (Diapsida: Archosauromorpha) from the Sonsela Member (Chinle Formation) of Petrified Forest National Park, Arizona: Museum of Northern Arizona Bulletin, v. 62, p. 119–125.
Parker, W.G., Irmis, R.B., Nesbitt, S.J., Martz, J.W., and Browne, L.S., 2005, The Late Triassic pseudosuchian *Revueltosaurus callenderi* and its implications for the diversity of early ornithischian dinosaurs: Proceedings of the Royal Society B: Biological Sciences, v. 272, p. 963–969.
Parker, W.G. Nesbitt, S.J., Irmis, R.B., Martz, J.W., Marsh, A.D., Brown, M.A., Stocker, M.R., and Werning, S., 2021, Osteology, Histology, and Relationships of *Revueltosaurus callenderi* (Archosauria: Suchia) from the Upper Triassic (Norian) Chinle Formation of Petrified Forest National Park, Arizona, USA: The Anatomical Record. https://doi.org/10.1002/ar.24757.
Parrington, F.R., 1935, On *Prolacerta broomi*, gen. et sp. n. and the origin of lizards: Annals and Magazine of Natural History, v. 16, p. 197–205.
Peabody, F.E., 1952, *Petrolacosaurus kansensis* Lane, a Pennsylvanian reptile from Kansas: University of Kansas Paleontological Contributions, Vertebrata, v. 1, p. 1–41.
Pritchard, A.C., and Nesbitt, S.J., 2017, A bird-like skull in a Triassic diapsid reptile increases heterogeneity of the morphological and phylogenetic radiation of Diapsida: Royal Society Open Science, v. 4, 170499. http://doi.org/10.1098/rsos.170499.
Pritchard, A.C., and Sues, H.-D., 2019, Postcranial remains of *Teraterpeton hrynewichorum* (Reptilia: Archosauromopha) and the mosaic evolution of the saurian postcranial skeleton: Journal of Systematic Palaeontology, v. 17, p. 1745–1765.
Pritchard, A.C., Turner, A.H., Nesbitt, S.J., Irmis, R.B., and Smith, N.D., 2015, Late Triassic tanystropheids (Reptilia, Archosauromorpha) from northern New Mexico (Petrified Forest Member, Chinle Formation) and the biogeography, functional morphology, and evolution of Tanystropheidae: Journal of Vertebrate Paleontology, v. 35, e911186. https://doi.org/10.1080/02724634.2014.911186.
Pritchard, A.C., Gauthier, J.A., Hanson, M., Bever, G.S., and Bhullar, B.-A., 2018, A tiny Triassic saurian from Connecticut and the early evolution of the diapsid feeding apparatus: Nature Communications, v. 9 1213. https://doi.org/10.1038/s41467-018-03508-1.
Pritchard, A.C., Sues, H.-D., Scott, D., and Reisz, R.R., 2021, Osteology, relationships and functional morphology of *Weigeltisaurus jaekeli* (Diapsida, Weigeltisauridae) based on a complete skeleton from the Upper Permian Kupferschiefer of Germany: PeerJ, v. 9, e11413. https://doi.org/10.7717/peerj.11413.
Ramezani, J., Hoke, G.D., Fastovsky, D.E., Bowring, S.A., Therrien, F., Dworkin, S.I., Atchley, S.C., and Nordt, L.C., 2011, High-precision U-Pb zircon geochronology of the Late Triassic Chinle Formation, Petrified Forest National Park (Arizona, USA): temporal constraints on the early evolution of dinosaurs: Geological Society of America Bulletin, v. 123, p. 2142–2159.
Rasmussen, C., Mundil, R., Irmis, R.B., Geisler, D., Gehrels, G.E., Olsen, P.E., Kent, D.V., Lepre, C., Kinney, S.T., Geissman, J.W., and Parker, W.G., 2020, U-Pb zircon geochronology and depositional age models for the Upper Triassic Chinle Formation (Petrified Forest National Park, Arizona, USA): implications for Late Triassic paleoecological and paleoenvironmental change: Geological Society of America Bulletin, v. 133, p. 539–558.

Reisz, R.R., Modesto, S.P., and Scott, D.M., 2011, A new early Permian reptile and its significance in early diapsid evolution: Proceedings of the Royal Society B: Biological Sciences, v. 278, p. 3731–3737.
Rieppel, O., 1989, The hind limb of *Macrocnemus bassanii* (Nopsca) (Reptilia, Diapsida): development and functional anatomy: Journal of Vertebrate Paleontology, v. 9, p. 373–387.
Robinson, P.L., 1962, Gliding lizards from the Upper Keuper of Great Britain: Proceedings of the Geologic Society of London, v. 1001, p. 137–146.
Sarigül, V., 2017, New archosauromorph fragments from the Dockum Group of Texas and the assessment of earliest dinosaurs in North America: Historical Biology, v. 30, p. 1059–1075.
Sen, K., 2003, *Pamelaria dolichotrachela*, a new prolacertid reptile from the Middle Triassic of India: Journal of Asian Earth Sciences, v. 21, p. 663–681.
Sengupta, S., and Bandyopadhyay, S., 2022, The osteology of *Shringasaurus indicus*, an archosauromorph from the Middle Triassic Denwa Formation, Satpura Gondwana Basin, central India: Journal of Vertebrate Paleontology, v. 41, e2010740. https://doi.org/10.1080/02724634.2021.2010740.
Sengupta, S., and Sengupta, D.P., 2021, Taphonomy and depositional setting of the *Shringasaurus indicus* (Archosauromorpha: Allokotosauria) bonebed from the Middle Triassic Denwa Formation, Satpura Gondwana Basin: Palaios, v. 36, p. 339–351.
Sengupta, S., Ezcurra, M.D., and Bandyopadhyay, S., 2017, A new horned and long-necked herbivorous stem-archosaur from the Middle Triassic of India: Scientific Reports, v. 7, 8366. https://doi.org/10.1038/s41598-017-08658-8.
Sereno, P.C., 1999, The evolution of dinosaurs: Science, v. 284, p. 2137–2147.
Sidor, C.A., Peecook, B.R., Beightol, C.V., Kaye, T., and Livingston, G., 2018, A multitaxic bonebed featuring a new shuvosaurid (Archosauria: Poposauroidea) from the Sonsela Member of the Chinle Formation at Petrified Forest National Park: 78th Annual Meeting, Meeting Program and Abstracts, Journal of Vertebrate Paleontology, v. 38, p. 216.
Spiekman, S.N.F., Neenan, J.M., Fraser, N.C., Fernandez, V., Rieppel, O., Nosotti, S., and Scheyer, T.M., 2020a, Aquatic habitats and niche partitioning in the extraordinarily long-necked Triassic reptile *Tanystropheus*: Current Biology, v. 30, p. 3889–3895.
Spiekman S.N.F., Neenan, J.M., Fraser, N.C., Fernandez, V., Rieppel, O., Nosotti, S., and Scheyer, T.M., 2020b, The cranial morphology of *Tanystropheus hydroides* (Tanystropheidae, Archosauromorpha) as revealed by synchrotron microtomography: PeerJ, v. 8, e10299. https://doi.org/10.7717/peerj.10299.
Spiekman, S.N.F., Fraser, N.C., and Scheyer, T.M., 2021, A new phylogenetic hypothesis of Tanystropheidae (Diapsida, Archosauromorpha) and other "protorosaurs", and its implications for the early evolution of stem archosaurs: PeerJ, v. 9, e11143. https://doi.org/10.7717/peerj.11143.
Spielmann, J.A., Lucas, S.G., Rinehart, L.F., and Heckert, A.B., 2008, The Late Triassic archosauromorph *Trilophosaurus*: New Mexico Museum of Natural History and Science Bulletin, v. 43, p. 1–177.
Spielmann, J.A., Lucas, S.G., and Hunt, A.P., 2013a, The first Norian (Revueltian) rhynchosaur: Bull Canyon Formation, New Mexico, U.S.A.: New Mexico Museum of Natural History and Science Bulletin, v. 61, p. 562–566.
Spielmann, J.A., Lucas, S.G., Heckert, A.B., and Krzyzanowski, S.T., 2013b, *Trilophosaurus* (Archosauromorpha: Trilophosauridae) postcrania from the Upper Triassic Blue Mesa Member of the Petrified Forest Formation (Carnian: Adamanian), Arizona, USA: New Mexico Museum of Natural History and Science Bulletin, v. 61, p. 567–572.
Tabor, N.J., Myers, T.S., and Michel, L.A., 2017, Sedimentologist's guide for recognition, description, and classification of paleosols, *in* Ziegler, K.E., and Parker, W.G., eds., Terrestrial Depositional Ecosystems: Deciphering Complexities through Multiple Stratigraphic Methods: Amsterdam, Elsevier, p. 165–208.
Tatarinov, L.P., 1978, Triassic prolacertilians of the USSR: Paleontological Journal, v. 12, p. 505–514.
Vences, M., Guayasamin, J.M., Miralles, A., and de la Riva, I., 2013, To name or not to name: criteria to promote economy of change in Linnaean classification schemes: Zootaxa, v. 3636, p. 201–244.
von Meyer, H., 1832, Palaeologica zur Geschichte der Erde und ihrer Geschöpfe: Frankfurt, Verlag Siegmund Schmerber, 560 p.
Watson, D.M., 1912, *Mesosuchus browni*, gen. et spec. nov.: Records of the Albany Museum, v. 2, p. 296–297.
Welman, J., 1998, The taxonomy of the South African proterosuchids (Reptilia, Archosauromorpha): Journal of Vertebrate Paleontology, v. 18, p. 340–347.
Werning, S., and Irmis, R.B., 2010, Reconstructing the ontogeny of the Triassic basal archosauromorph *Trilophosaurus* using bone histology and limb bone morphometrics: Journal of Vertebrate Paleontology, v. 30, Program and Abstracts, 2010, 185A–186A.
Werning, S., and Nesbitt, S.J., 2016, Bone histology and growth in *Stenaulorhynchus stockleyi* (Archosauromorpha: Rhynchosauria) from the Middle Triassic of the Ruhuhu Basin of Tanzania: Comptes Rendus Palevol, v. 15, p. 163–175.
Wilson, J.A., 1999, A nomenclature for vertebral laminae in sauropods and other saurischian dinosaurs: Journal of Vertebrate Paleontology, v. 19, p. 639–653.
Wilson, J.A., D'Emic, M.D., Ikejiri, T., Moacdieh, E.M., and Whitlock, J.A., 2011, A nomenclature for vertebral fossae in sauropods and other saurischian dinosaurs: PLOS One, v. 6, p. e17114.
Woody, D.T., 2006, Revised stratigraphy of the lower Chinle Formation (Upper Triassic) of Petrified Forest National Park, Arizona: Museum of Northern Arizona Bulletin, v. 62, p. 17–45.

Accepted: 1 May 2022